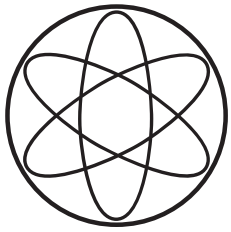

The Littlest Higgs and its Phenomenological Implications for Flavor Changing Neutral Currents and Lepton Flavor Violating Processes

Dissertation

von

Anton Poschenrieder

Technische Universität München
Physik Department T31
James Franck Straße
D-85748 Garching
Email: aposchen@ph.tum.de

Technische Universität
München
Physik-Department

Physik-Department
Technische Universität München
Institut für Theoretische Physik
Lehrstuhl T31 Univ.-Prof. Dr. Andrzej J. Buras

The Littlest Higgs and its Phenomenological Implications for Flavor Changing Neutral Currents and Lepton Flavor Violating Processes

Anton Poschenrieder

Vollständiger Abdruck der von der Fakultät für Physik der Technischen Universität München zur Erlangung des akademischen Grades eines

Doktors der Naturwissenschaften (Dr. rer. nat.)

genehmigten Dissertation.

Vorsitzender:		Univ.-Prof. Dr. Franz von Feilitzsch
Prüfer der Dissertation:	1.	Univ.-Prof. Dr. Andrzej J. Buras
	2.	Hon.-Prof. Dr. Wolfgang Hollik

Die Dissertation wurde am 29.08.2007 bei der Technischen Universität München eingereicht und durch die Fakultät für Physik am 08.10.2007 angenommen.

Gewidmet meinem Vater Karl-Heinz Poschenrieder
(1943 - 2005)

Kurzfassung

Das Ziel dieser vorliegenden Arbeit ist es, eine Untersuchung wichtiger flavor verletzender neutraler Ströme und lepton flavor verletzender Zerfälle im Littlest Higgs Modell ohne T-Parität und mit T-Parität vorzustellen.

Nach einer kurzen Einführung in das Standardmodell der Teilchenphysik diskutieren wir eine damit verbundene, wohlbekannte Schwierigkeit: das little hierarchy problem. Um dieses Problem zu beheben, stellen wir die grundlegenden Konzepte von Little Higgs Modellen vor, welche ursprünglich aus Ideen zur Dekonstruktion von Eichfeldtheorien hervorgegangen sind. Anschließend konzentrieren wir uns auf die ökonomischste Umsetzung dieser Idee und führen deshalb das Littlest Higgs Modell ohne T-Parität ein. Um seine Auswirkungen auf flavor verletzende neutrale Ströme zu untersuchen, leiten wir zunächst die Feynman-Regeln für das Littlest Higgs Modell ab, wobei wir Korrekturen bis zur Ordnung v^2/f^2 berücksichtigen. Mit Hilfe dieser Feynman-Regeln ist es uns möglich die Funktionen X und Y zu berechnen, welche für die Beschreibung der seltenen Zerfälle $K^+ \to \pi^+\nu\bar{\nu}$, $K_L \to \pi^0\nu\bar{\nu}$ und $B_{s,d} \to \mu^+\mu^-$ benötigt werden.

Aufgrund von elektroschwachen Präzisionsmessungen konnte jedoch bald gezeigt werden, dass die Skala für neue Physik f in diesem Modell in der Größenordnung $f \sim 2 - 3\,\mathrm{TeV}$ liegen muss und damit das fine-tuning Problem wieder eingeführt wird. Aus diesem Grund erweitern wir unsere Analyse auf ein realistischeres Modell, das Littlest Higgs Modell mit T-Parität, in welchem die Skala f auf $f \gtrsim 500\,\mathrm{GeV}$ gesenkt werden kann. Nachdem wir für dieses Modell die Feynman-Regeln abgeleitet haben, ermitteln wir erneut die Auswirkung auf die Funktionen X_i, Y_i und Z_i, welche für die Ermittlung der flavor verletzenden neutralen Ströme $K^+ \to \pi^+\nu\bar{\nu}$, $K_L \to \pi^0\nu\bar{\nu}$, $B_{s,d} \to \mu^+\mu^-$ und $K_L \to \pi^0\ell^+\ell^-$ erforderlich sind. Ferner präsentieren wir für die oben erwähnten Zerfälle eine numerische Analyse, wobei wir uns auf nicht-minimal flavor verletzende Beiträge konzentrieren. Schließlich erweitern wir unsere Analyse noch auf die Betrachtung lepton flavor verletzender Prozesse. Nach einer expliziten Berechnung mehrerer Prozesse wie $\ell_i \to \ell_j\gamma$, $\ell_i \to \ell_j\ell_k\ell_l$ und $\tau \to \pi\ell_i$ präsentieren wir eine numerische Analyse in verschiedenen Vergleichsszenarien. Dabei widmen wir uns vor allem Korrelationen zwischen verschiedenen Verzweigungsverhältnissen und beobachten Korrelationsmuster im Littlest Higgs Model mit T-Parität, welche sich grundlegend von denen des minimal supersymmetrischen Standardmodells unterscheiden. Wir beschließen diese Arbeit mit den wichtigsten Aussagen und geben einen kurzen Ausblick.

Abstract

Throughout this work we study several prominent flavor changing neutral current (FCNC) processes and lepton flavor violating (LFV) decays in the Littlest Higgs model without T-parity and with T-parity.

Beginning with a brief introduction to the Standard Model (SM) we discuss a well-known problem associated to it: the little hierarchy problem. In order to ameliorate this problem we present the basic concepts of Little Higgs models, which were originally inspired by the ideas of deconstructed gauge field theories. Subsequently we concentrate on the most economical implementation of this idea and thus present the Littlest Higgs without T-parity. In order to analyze its impact on FCNC processes we first derive the Feynman rules for the LH model, including the v^2/f^2 corrections. Having at hand the Feynman rules for this model the short distance functions X and Y are calculated, which are required to describe the rare decays $K^+ \to \pi^+\nu\bar{\nu}$, $K_L \to \pi^0\nu\bar{\nu}$ and $B_{s,d} \to \mu^+\mu^-$.

However, electroweak precision tests soon showed that the new physics scale f in this model should be of the order $2 - 3\,\text{TeV}$, thus re-introducing the fine-tuning problem. Therefore we extend our analysis to a more realistic model, the Littlest Higgs model with T-parity, in which the scale f can be lowered down to $f \gtrsim 500\,\text{GeV}$. After having derived the Feynman rules for this model we determine again the impact on the short distance functions X_i, Y_i and Z_i, $i = s, d, K$, which are relevant for the calculation of the FCNC processes like $K^+ \to \pi^+\nu\bar{\nu}$, $K_L \to \pi^0\nu\bar{\nu}$, $B_{s,d} \to \mu^+\mu^-$ and $K_L \to \pi^0\ell^+\ell^-$. This is followed by a numerical analysis of the decays mentioned above, focusing on effects from non-minimal flavor violating contributions. Finally we extend our analysis by considering LFV processes. After the explicit calculation of several processes, like $\ell_i \to \ell_j\gamma$, $\ell_i \to \ell_j\ell_k\ell_l$ and $\tau \to \pi\ell_i$ we present a numerical analysis in several benchmark scenarios. In doing so we turn our attention to correlations between branching ratios of several decays and observe correlation patterns in the LHT that are completely different from those in the Minimal Supersymmetric Standard Model. We conclude this work with the main messages and give a brief outlook.

Contents

Chapter 1

Introduction and Motivation

Particle physics and cosmology are the two fundamental fields in physics whose aims consist in explaining the origin of our universe. While cosmology tries to describe the evolution of the universe to its present state, particle physics is concerned with the understanding of the interactions of its basic constituents. During the last decades much progress has been made in establishing an understanding of these fundamental constituents. This finally led to the development of the *Standard Model (SM)* of particle physics.

The SM itself is a quantum field theory which exhibits a broken $SU(3)_C \otimes SU(2)_L \otimes U(1)_Y$ gauge symmetry and therewith is able to describe the strong, weak and electromagnetic forces. So far it has been extremely successful in explaining most experimental results and indeed there has been no confirmed experimental evidence that contradicts its predictions. In spite of its tremendous success and its remarkable agreement with experiment, the SM suffers from a number of limitations and is therefore considered an incomplete theory.

One of the most convincing reasons why the SM is only an effective field theory is the fact that it does not include the fourth elementary interaction, gravity, and so far all attempts to construct a theory of quantum gravitation have resulted in non-renormalizable theories. Apart from this there are many other theoretical questions that are not answered by the SM, e.g. it fails to account for the baryon asymmetry of the universe. Also, it does not explain why the observed pattern of masses of both quarks and leptons shows such a large hierarchy. A further shortcoming concerns the Higgs particle, which has not been found so far and thus leaves the mechanism of *electroweak symmetry breaking (EWSB)* unverified. Since the mass of the Higgs particle is not protected by any symmetry, radiative corrections yield contributions to the Higgs mass which are quadratically dependent on the cut-off of the theory. Therefore some unnatural adjustment between the bare mass and the one-loop corrections is needed to obtain a Higgs mass of the order of the weak scale.

To ameliorate this fine-tuning problem, particle theorists have been led to develop extensions of the SM, of which the most promising candidates are supersymmetric theories, grand unified theories or theories with extra space-time dimensions. Unfortunately, none of these

possible scenarios could be either confirmed or ruled out so far. However, the Large Hadron Collider (LHC) will be able to reach energies that are large enough to prove or disprove several extensions of the SM.

In [1, 2, 3] a new natural scheme for electroweak symmetry breaking has been proposed by *Arkani-Hamed et al.*, in which the little hierarchy problem is ameliorated. In these *Little Higgs* models the SM Higgs is protected by an approximate global symmetry and can thus be realized as a pseudo-Goldstone boson. Starting point of all these models is a non-linear sigma model G/H, where the global symmetry G is spontaneously broken down to its subgroup H and contains a set of gauge symmetries. In this process of symmetry breaking a number of Goldstone bosons arise, where one of them can be identified with the SM Higgs boson. However, the gauge groups are embedded in such a way that G is explicitly broken only in the presence of all gauge couplings and any diagram which contributes to the Higgs mass has to involve all these couplings. This new mechanism, known as collective symmetry breaking, prevents the Higgs mass from acquiring quadratic divergences at the one-loop level. In a specific model, the *Littlest Higgs model without T-parity (LH)* [4], the Higgs boson results from an approximate global $SU(5)$ symmetry, which is broken down to an $SO(5)$. Due to the existence of new heavy vector bosons $W_H^{\pm}$, Z_H and A_H with a mass $f = \mathcal{O}(1\,\text{TeV})$ the number of gauge bosons is doubled compared to the SM, while the fermion sector is enlarged only by one additional heavy top quark (T) which cancels the quadratic divergences coming from the usual SM top quark. The details of this model have been elaborated in [5, 6, 7], whereas constraints on the parameters of the Littlest Higgs model coming from direct searches and *electroweak precision tests (EWPT)* have been discussed in [8]. However, in addition to the constraints from EWPT, physics beyond the SM can also be detected in indirect searches via *flavor changing neutral currents (FCNC)*, i.e. by processes that only occur at the loop level in the SM. Thus, when looking for physics beyond the SM, FCNC offer an interesting alternative to the direct searches at colliders. In this thesis, we dedicate ourselves to the impact of the Littlest Higgs model on FCNC.

After the introduction of the Littlest Higgs model it was soon realized that EWPT require the relevant scale f of new physics to be at least $2 - 3\,\text{TeV}$, which would re-introduce a considerable fine-tuning. Since this strong constraint is due to the violation of the custodial $SU(2)$ symmetry at tree-level, physicists started to construct a more attractive model in which a discrete symmetry forbids tree-level corrections to electroweak observables. Such a discrete symmetry was introduced into the Littlest Higgs model by *Cheng* and *Low* [9] leading to the *Littlest Higgs model with T-parity (LHT)*, where the electroweak precision constraints [10] are weakened. In this model, the new gauge bosons, fermions and scalars are sufficiently light to be discovered at LHC and T-parity also provides a dark matter candidate [11]. Moreover, the flavor structure of the LHT model is richer than the one of the Standard Model (SM), mainly due to the presence of three doublets of mirror quarks as well as mirror leptons and their weak interactions with the ordinary quarks and leptons.

In first FCNC analyses the authors of [6, 7, 12, 13, 14] discussed the impact of the LH model without T-parity on particle-antiparticle mixing and other FCNC processes, like $K_L \to \pi^0\nu\bar{\nu}$, $K^+ \to \pi^+\nu\bar{\nu}$ and $B \to X_s\gamma$. It turns out that in the LH model the effects coming from new particles are rather small since the scale f is required to be above $2-3\,\text{TeV}$ in order to satisfy the EWPT, as already mentioned before. Moreover, due to these small effects it is very difficult to distinguish the LH model without T-parity from the SM. As pointed out in [7] one should also be aware of the fact that the LH model is an effective theory with an unspecified *ultraviolet (UV)* completion which is reflected in a number of left-over logarithmic divergences.

In the LHT model, $\Delta F = 2$ and $\Delta F = 1$ FCNC processes, like particle-antiparticle mixings, $B \to X_s\gamma$, $B \to X_s\ell^+\ell^-$ and rare K and B decays have been discussed in [15, 16] and [17], respectively. In this model, which is not stringently constrained by EWPT and contains new flavor and CP-violating interactions, large departures from the SM predictions are found, in particular for CP-violating observables that are strongly suppressed in the SM. These deviations from the SM can first of all be seen in the branching ratio for $K_L \to \pi^0\nu\bar{\nu}$ and the CP asymmetry $S_{\psi\phi}$ in the $B_s \to \psi\phi$ decay, but also in $Br(K_L \to \pi^0\ell^+\ell^-)$ and $Br(K^+ \to \pi^+\nu\bar{\nu})$. Smaller, but still significant effects have been found in rare $B_{s,d}$ decays and $\Delta M_{s,d}$. The presence of left-over divergences in $\Delta F = 1$ processes, that signals some sensitivity to the UV completion of the theory, introduces some theoretical uncertainty in the evaluation of the relevant branching ratios both in the LH model [7] and the LHT model [17]. On the other hand, $\Delta F = 2$ processes and the $B \to X_s\gamma$ decay are free from these divergences.

In the LHT model the effects of new particles on lepton flavor violating processes are expected to be much larger, since the presence of new flavor violating interactions and mirror leptons with masses of order $1\,\text{TeV}$ can change the SM expectations up to many orders of magnitude. While in the SM FCNC processes in the lepton sector, like $\ell_i \to \ell_j\gamma$ and $\mu^- \to e^-e^+e^-$, are very strongly suppressed due to tiny neutrino masses, these new effects can bring the relevant branching ratios for *lepton flavor violating (LFV)* processes close to the bounds available presently or in the near future. A further aim of this analysis also consists in finding patterns of LFV in this model and to constrain the mass spectrum of mirror leptons and the new weak mixing matrix in the lepton sector, $V_{H\ell}$, that in addition to three mixing angles contains three CP-violating phases. Moreover, we have calculated the $\mu - e$ conversion rate in nuclei as well as $(g-2)_\mu$ that has also been considered in [18, 19]. One of the most important results of the present thesis is the identification of correlations between various branching ratios that are less parameter dependent and differ significantly from corresponding correlations in the *Minimal Supersymmetric Standard Model (MSSM)* discussed in [20, 21, 22, 23, 24, 25]. The reason for this difference is that the dominance of the dipole operator in the decays in question present in the MSSM is substituted in the LHT model by the dominance of Z^0-penguin and box diagram contributions with the dipole

operator playing now a negligible role. Consequently, LFV processes provide a formidable possibility to distinguish these two models.

The remainder of this thesis is organized as follows. After a review of the main ingredients of the SM in Chapter 2 we will briefly summarize the main ideas of dimensional deconstruction in Chapter 3, which inspired physicists to construct Little Higgs models. Chapter 4 is then devoted to the introduction of the LH model, in which we also present a short analysis of the rare decays $K_L \to \pi^0\nu\bar{\nu}$, $K^+ \to \pi^+\nu\bar{\nu}$ and $B_{s,d} \to \mu^+\mu^-$. Next, in Chapter 5 of this work we continue with the description of the Littlest Higgs model with T-parity. Finally in Chapter 6 we study the implications of the LHT on rare decays and lepton flavor violating processes like $\ell_i \to \ell_j\gamma$ with particular attention paid to $\mu \to e\gamma$, for which a new stringent experimental upper bound should be available in the coming year. Furthermore we calculate $(g-2)_\mu$. For all these processes we present a detailed numerical analysis. In Chapter 7 we conclude this thesis with a list of messages from our analysis and with a brief outlook.

Chapter 2

The Standard Model

The SM is a very successful theory describing the electroweak and strong interactions of quarks and leptons at energies up to about a few hundred GeV. The theory of strong interactions, known as *Quantum Chromodynamics (QCD)* [26], is a non-abelian gauge theory based on an $SU(3)_C$ gauge group, while the standard theory of electroweak interactions is the Glashow-Weinberg-Salam model relying on an $SU(2)_L \otimes U(1)_Y$ gauge group. In [27] *Glashow* originally proposed how the weak and the electromagnetic interactions can be unified into this gauge group, and *Weinberg* and *Salam* showed [28, 29] how the weak gauge bosons receive a mass without spoiling the renormalizability of the theory.

2.1 Review of the Standard Model

2.1.1 Quantum Chromodynamics

From experiments we know that quarks possess an internal degree of freedom, called color. To describe the interactions between quarks and gluons, *Gell-Mann et al.* chose a local $SU(3)_C$ symmetry with the gluons sitting in the adjoint representation, which induced them to define the following covariant derivative

$$D_\mu = \partial_\mu + i g_s G_\mu^a \frac{\lambda_a}{2}, \quad a = 1, ..., 8 \tag{2.1.1}$$

with $\lambda_a/2$ being the generators of the $SU(3)_C$ group. Disregarding the strong CP problem the most general renormalizable kinetic term for the gauge fields reads:

$$\mathcal{L}_{\text{QCD}} = -\frac{1}{4} G_{\mu\nu}^a G_a^{\mu\nu}, \tag{2.1.2}$$

with the non-abelian field-strength tensor $G_{\mu\nu}^a$ given by

$$G_{\mu\nu}^a = \partial_\mu G_\nu^a - \partial_\nu G_\mu^a - g_s f_{abc} G_\mu^b G_\nu^c. \tag{2.1.3}$$

In contrast to abelian field-strength tensors, the non-abelian field-strength tensor (2.1.3) contains both linear and quadratic terms in the gauge fields, such that the theory is non-trivial even in the absence of matter fields. These self-interactions are an important aspect of non-abelian gauge theories and are in particular responsible for the asymptotic freedom of QCD [30].

2.1.2 The Electroweak Sector of the Standard Model

As mentioned before, the standard theory of electroweak interactions is based on the gauge group $SU(2)_L \otimes U(1)_Y$. This gauge group has four vector fields, where three of them, denoted by W^i_μ, are related to the adjoint representation of $SU(2)_L$ and one to the $U(1)_Y$, denoted by B_μ. In order to make the Lagrangian invariant under local gauge transformations, the partial derivative ∂_μ has to be substituted by the covariant derivative D_μ, i.e.

$$\partial_\mu \to D_\mu \equiv \partial_\mu + ig\frac{\tau_a}{2}W^a_\mu + ig'\frac{Y}{2}B_\mu, \quad a = 1,2,3, \tag{2.1.4}$$

where $T_a = \tau_a/2$ and $\frac{1}{2}Y$ are the group generators of $SU(2)_L$ and $U(1)_Y$, and g, g' their corresponding coupling constants.

In order to allow for parity violation in the electroweak theory we need to embed the left- and right-handed components of the fermions into different group representations. Motivated by neutral weak currents, all the left-handed fermions are taken to transform as doublets, while the right-handed fermions are singlets under $SU(2)_L$.

The fermions appear in three generations: Each generation consists of a neutrino ν'_i, a charged lepton e'_i with electric charge $Q_e = -1$, and the up- and down-type quarks u'_i and d'_i with charge $Q_u = 2/3$ and $Q_d = -1/3$. The lepton and quark doublets are given by

$$E'^i_L = P_L \begin{pmatrix} \nu'_i \\ e'_i \end{pmatrix} = \left(\begin{pmatrix} \nu'_e \\ e' \end{pmatrix}_L, \quad \begin{pmatrix} \nu'_\mu \\ \mu' \end{pmatrix}_L, \quad \begin{pmatrix} \nu'_\tau \\ \tau' \end{pmatrix}_L \right), \tag{2.1.5}$$

$$Q'^i_L = P_L \begin{pmatrix} u'_i \\ d'_i \end{pmatrix} = \left(\begin{pmatrix} u' \\ d' \end{pmatrix}_L, \quad \begin{pmatrix} c' \\ s' \end{pmatrix}_L, \quad \begin{pmatrix} t' \\ b' \end{pmatrix}_L \right), \tag{2.1.6}$$

while the singlets consist of

$$e'^i_R = P_R e'^i = \left(e'_R, \mu'_R, \tau'_R\right), \tag{2.1.7}$$

$$u'^i_R = P_R u'^i = \left(u'_R, c'_R, t'_R\right), \tag{2.1.8}$$

$$d'^i_R = P_R d'^i = \left(d'_R, s'_R, b'_R\right), \tag{2.1.9}$$

where $P_{L,R} = (1 \mp \gamma^5)/2$ are left- and right-handed projectors of the fermion fields and $i = 1, ..., 3$ denotes the generation index. Additionally, we assign to each of them the hypercharge Y and weak isospin T_3 quantum numbers, which can be found in Table 2.1. The primes at the

Lepton	T_3	Q	Y	*Quark*	T_3	Q	Y
ν_e	$\frac{1}{2}$	0	-1	u_L	$\frac{1}{2}$	$\frac{2}{3}$	$\frac{1}{3}$
e_L^-	$-\frac{1}{2}$	-1	-1	d_L	$-\frac{1}{2}$	$-\frac{1}{3}$	$\frac{1}{3}$
	$-$	$-$	$-$	u_R	0	$\frac{2}{3}$	$\frac{4}{3}$
e_R^-	0	-1	-2	d_R	0	$-\frac{1}{3}$	$-\frac{2}{3}$

Table 2.1: *Weak isospin and hypercharge quantum numbers of the first generation of leptons and quarks*

fermion fields indicate eigenstates of the electroweak interaction, which are not necessarily identical to the mass eigenstates.

Applying this notation, we can then write down the fermionic part of the Lagrangian describing massless spinor fields,

$$\mathcal{L}_F = \sum_{i=1}^{3} \left(\bar{E}_L'^i i \not{D} E_L'^i + \bar{Q}_L'^i i \not{D} Q_L'^i + \bar{e}_R'^i i \not{D} e_R'^i + \bar{u}_R'^i i \not{D} u_R'^i + \bar{d}_R'^i i \not{D} d_R'^i \right). \tag{2.1.10}$$

In the limit of vanishing fermion masses one can see from (2.1.10) that the fermionic part of the Lagrangian has a high degree of symmetry. We can see that this Lagrangian is invariant under the separate groups of unitary transformations $U(3)_E \times U(3)_Q \times U(3)_e \times U(3)_u \times U(3)_d$, that is a $U(3)$ symmetry for each of the multiplets $E_L'^i$, $Q_L'^i$, $e_R'^i$, $u_R'^i$ and $d_R'^i$.

Including again the gauge kinetic terms leaves us with the $SU(2)_L \otimes U(1)_Y$-invariant Lagrangian, which can be written as

$$\begin{aligned} \mathcal{L} \;=\; & \sum_{f_L, f_R} \left[\bar{f}_L \gamma^\mu \left(i\partial_\mu - g\frac{\tau_a}{2} W_\mu^a - g'\frac{Y}{2} B_\mu \right) f_L + \bar{f}_R \gamma^\mu \left(i\partial_\mu - g'\frac{Y}{2} B_\mu \right) f_R \right] \\ & -\frac{1}{4} W_{\mu\nu}^i W_i^{\mu\nu} - \frac{1}{4} B_{\mu\nu} B^{\mu\nu}, \end{aligned} \tag{2.1.11}$$

where a summation over all left- and right-handed fermion fields f_L and f_R is understood. In contrast to the abelian field-strength tensor $B_{\mu\nu}$, the non-abelian field-strength tensor $W_{\mu\nu}^i$ contains both linear and quadratic terms in the gauge fields.

2.1.3 The Higgs Sector and Spontaneous Symmetry Breaking in the Standard Model

The Lagrangian in (2.1.11) describes massless gauge bosons interacting with massless fermions. But with gauge fields and fermions being massless the SM is incomplete, since it does not accommodate the observed non-zero masses of the charged leptons, quarks, and weak gauge

bosons. However, gauge theories do not allow for massive gauge bosons, since mass terms of the type $m_A^2 A_\mu^a A_a^\mu$ are not gauge-invariant. A mass term for the fermions of the form $-m\bar{f}f = -m\left(\bar{f}_L f_R + \bar{f}_R f_L\right)$ is also forbidden, since left- and right-handed fermion fields transform according to different representations of the gauge group $SU(2)_L$.

According to these arguments we have to include masses for gauge bosons and fermions in the theory without violating gauge invariance and without destroying the renormalizability, which critically depends on the gauge symmetry of the interactions. To fulfill these requirements another possibility, denoted as the *Higgs mechanism*, was introduced, which relies on the phenomenon of *spontaneous symmetry breaking*. In this process we introduce an elementary scalar field ϕ, that is coupled to gauge and matter fields. Due to its self-interactions this scalar field acquires a non-zero *vacuum expectation value (vev)*, which is responsible for the masses of the gauge and matter fields. This scalar field is also necessary to guarantee unitarity in a theory with massive vector bosons.

The idea of this mechanism consists in assuming that the classical Lagrangian of a theory possesses either a global or local symmetry, which, however, is not respected by the vacuum state. Since the symmetry is not broken explicitly by non-symmetric terms in the Lagrangian, this is usually denoted as a *spontaneously broken* symmetry. In the case of the spontaneous breaking of a (continuous) global symmetry the Goldstone theorem [31] holds and predicts massless particles, called *Goldstone bosons*, corresponding to every broken symmetry generator. However, if the global symmetry of the classical Lagrangian is explicitly broken by small terms, the broken symmetry generators are not related to massless particles anymore, but to particles with a small mass. These particles are then denoted as pseudo-Goldstone bosons. An example for an explicit global symmetry breaking is the chiral symmetry breaking in QCD with two or three quark flavors due to quark mass terms. In such a scenario the pseudo-Goldstone bosons, arising from the chiral symmetry breaking, can be identified with the pions, $\pi^\pm$, π^0 and $K^\pm$, K^0, $\bar{K}^0$, η_8, respectively. In the case of a broken *local* symmetry Goldstone bosons arise as well, however, these Goldstone boson fields can be eliminated from the theory with the help of gauge transformations. They are "eaten" by the corresponding gauge fields, which in turn become massive. In the SM this is the way how vector and fermion fields acquire a mass.

In the particular case of the SM, spontaneous symmetry breaking is achieved by means of a single complex scalar field ϕ that transforms as a doublet of $SU(2)_L$,

$$\phi = \begin{pmatrix} \phi^+ \\ \phi^0 \end{pmatrix} = \begin{pmatrix} \frac{\phi_1 + i\phi_2}{\sqrt{2}} \\ \frac{\phi_3 + i\phi_4}{\sqrt{2}} \end{pmatrix}, \tag{2.1.12}$$

with the ϕ_i, $i = 1, 2, 3, 4$ being real. As we will see later the superscript denotes the electric charge of the corresponding components and thus fixes the hypercharge of ϕ to be 1 according to (2.1.23). Using (2.1.12) we can now write down the most general renormalizable and

$SU(2)_L$-invariant Lagrangian for the scalar doublet,

$$\mathcal{L}_H = \left(D_\mu \phi\right)^\dagger \left(D_\mu \phi\right) + \mu^2 \phi^\dagger \phi - \lambda \left(\phi^\dagger \phi\right)^2. \tag{2.1.13}$$

As before the covariant derivative is given by

$$D_\mu \to \partial_\mu + igT_a W_\mu^a + ig' \frac{Y}{2} B_\mu. \tag{2.1.14}$$

The Lagrangian (2.1.13) also contains self-interactions between the Higgs fields due to the potential $V(\phi)$

$$V(\phi) = -\mu^2 \left(\phi^\dagger \phi\right) + \lambda \left(\phi^\dagger \phi\right)^2, \tag{2.1.15}$$

where λ and μ are two new real parameters. In order to obtain a stable vacuum, the potential has to be bounded from below so that the quartic coupling λ has to be positive. With μ^2 and λ positive the Higgs potential $V(\phi)$ has a minimum at

$$\langle \phi^\dagger \phi \rangle = \frac{\mu^2}{2\lambda}. \tag{2.1.16}$$

This ground state corresponds to an infinite number of degenerate minima. In choosing one of them, the symmetry is spontaneously broken, since the Lagrangian (2.1.13) still respects the $SU(2)_L \times U(1)_Y$, but the vacuum state does not. Without loss of generality we choose the vacuum expectation values

$$\langle |\phi_i| \rangle = 0, \quad i = 1, 2, 4, \tag{2.1.17}$$

$$\langle |\phi_3| \rangle = v = \sqrt{\frac{\mu^2}{\lambda}}. \tag{2.1.18}$$

Expanding ϕ around this vacuum and making the substitution

$$h(x) = \phi_3(x) - v, \tag{2.1.19}$$

we can re-express the Lagrangian in terms of physical particles. By choosing the expectation value of the neutral component to be nonzero we ensure that the vacuum is invariant under $U(1)_Q$ of QED, and the photon remains massless. This yields

$$\langle \phi \rangle = \langle 0 | \begin{pmatrix} \phi^+ \\ \phi^0 \end{pmatrix} |0\rangle = \frac{1}{\sqrt{2}} \begin{pmatrix} 0 \\ v \end{pmatrix}. \tag{2.1.20}$$

Because

$$\tau_a \langle \phi \rangle \neq 0, \quad Y \langle \phi \rangle \neq 0, \tag{2.1.21}$$

both $SU(2)_L$ and $U(1)_Y$ are broken, but

$$Q\langle \phi \rangle = \left(\frac{\tau_3}{2} + \frac{Y}{2}\right) \langle \phi \rangle = \frac{1}{\sqrt{2}} \begin{pmatrix} 1 & 0 \\ 0 & 0 \end{pmatrix} \begin{pmatrix} 0 \\ v \end{pmatrix} = 0. \tag{2.1.22}$$

Thus, the linear combination

$$Q = T_3 + \frac{Y}{2}, \tag{2.1.23}$$

may be identified with the generator of the unbroken residual electromagnetic $U(1)_Q$ symmetry. Hence, we expect three gauge bosons to be massive while one remains massless.

To find the masses of the gauge bosons we substitute (2.1.20) into (2.1.13) which contains

$$\begin{aligned} & \left| ig\frac{\tau_a}{2}W_\mu^a\langle\phi\rangle + i\frac{g'}{2}YB_\mu\langle\phi\rangle \right|^2 \\ = & \frac{1}{8}\left| \begin{pmatrix} gW_\mu^3 + g'B_\mu & g\left(W_\mu^1 - iW_\mu^2\right) \\ g\left(W_\mu^1 + iW_\mu^2\right) & -gW_\mu^3 + g'B_\mu \end{pmatrix} \begin{pmatrix} 0 \\ v \end{pmatrix} \right|^2 \\ = & \frac{1}{8}v^2\left(gW_\mu^3 - g'B_\mu\right)^2 + 0\left(g'W_\mu^3 + gB_\mu\right)^2 + \left(\frac{1}{2}vg\right)^2 W_\mu^+ W^{-\mu}, \end{aligned} \tag{2.1.24}$$

where

$$W^\pm = \left(W^1 \mp iW^2\right)/\sqrt{2}. \tag{2.1.25}$$

From (2.1.24) we can see that the mass matrix of the neutral fields is off-diagonal in the (W_μ^3, B_μ) basis and, as expected, one of the mass eigenvalues is zero. We have displayed this in (2.1.24) where the combination of fields in the second term is orthogonal to that in the first one. This allows us to define

$$\begin{aligned} Z_\mu &= \frac{gW_\mu^3 - g'B_\mu}{\sqrt{g^2 + g'^2}} = W_\mu^3\cos\theta_W - B_\mu\sin\theta_W, \\ A_\mu &= \frac{g'W_\mu^3 + gB_\mu}{\sqrt{g^2 + g'^2}} = W_\mu^3\sin\theta_W + B_\mu\cos\theta_W, \end{aligned} \tag{2.1.26}$$

with the Weinberg angle θ_W defined by

$$\sin\theta_W = \frac{g'}{\sqrt{g^2 + g'^2}}, \quad \cos\theta_W = \frac{g}{\sqrt{g^2 + g'^2}}. \tag{2.1.27}$$

Therefore (2.1.24) can now be written in terms of the physical mass eigenstates $W_\mu^\pm$, Z_μ and the photon A_μ as

$$M_W^2 W_\mu^+ W^{-\mu} + \frac{1}{2}M_Z^2 Z_\mu^2 + \frac{1}{2}M_\gamma^2 A_\mu^2, \tag{2.1.28}$$

where the masses are given by

$$M_W = \frac{1}{2}vg, \quad M_Z = \frac{1}{2}v\left(g^2 + g'^2\right)^{1/2}, \quad M_\gamma = 0, \tag{2.1.29}$$

and hence

$$\frac{M_W}{M_Z} = \cos\theta_W. \tag{2.1.30}$$

2.1.4 Yukawa Sector

In the previous subsection we have seen how the Higgs mechanism generates masses for the electroweak gauge bosons. We can now invoke the same mechanism to give masses to the various fermions via Yukawa interactions. In order to allow for fermion masses of the up- and down-type right-handed quark fields, an additional scalar doublet with weak hypercharge -1 is necessary. In the SM this can be achieved by defining the conjugate of the scalar doublet by

$$\tilde{\phi} = i\tau_2\phi^* = \begin{pmatrix} \bar{\phi}^0 \\ -\phi^- \end{pmatrix}. \tag{2.1.31}$$

Following these conventions we can write down the most general renormalizable and gauge-invariant Lagrangian relating the fermion fields to the scalar doublets,

$$\mathcal{L}_Y = -\sum_{i,j=1}^{3} \left(\lambda_e'^{ij} \bar{E}_L'^i \phi e_R'^j + \lambda_u'^{ij} \bar{Q}_L'^i \tilde{\phi} u_R'^j + \lambda_d'^{ij} \bar{Q}_L'^i \phi d_R'^j + \text{h.c.} \right), \tag{2.1.32}$$

where the Yukawa couplings λ_e', λ_u' and λ_d' are general complex 3×3 matrices. As one can see from Table 2.1, the Yukawa Lagrangian is invariant under $SU(2)_L \otimes U(1)_Y$.

As already mentioned in Subsection 2.1.2, the largest group of unitary field transformations that commutes with the gauge group is $U(3)^5$ and can be decomposed into

$$\begin{aligned} &SU(3)_{Q_L} \otimes SU(3)_{U_R} \otimes SU(3)_{D_R} \otimes SU(3)_{L_L} \otimes SU(3)_{E_R} \otimes \\ &\quad U(1)_B \otimes U(1)_L \otimes U(1)_Y \otimes U(1)_{PQ} \otimes U(1)_{E_R}. \end{aligned} \tag{2.1.33}$$

In order to diagonalize the Yukawa matrices we can exploit this symmetry and rotate the left-handed fermion fields via unitary matrices related to the corresponding symmetry group. Such a transformation rotates the eigenstates $E_L'^i$ and $Q_L'^i$ as

$$E_L'^i \to \sum_{j=1}^{3} U_{e,L}^{ij} E_L'^j, \qquad Q_L'^i \to \sum_{j=1}^{3} U_{u,L}^{ij} Q_L'^j. \tag{2.1.34}$$

Similarly the analogous transformations of the right-handed chiral fields read

$$e_R'^i \to \sum U_{e,R}^{ij} e_R'^j, \quad u_R'^i \to \sum_{j=1}^{3} U_{u,R}^{ij} u_R'^j, \quad d_R'^i \to \sum_{j=1}^{3} U_{d,R}^{ij} d_R'^j. \tag{2.1.35}$$

In (2.1.34) and (2.1.35) the different rotation matrices correspond to the symmetry groups in (2.1.33). According to these rotations the Yukawa matrices then have to transform as

$$\lambda_e = U_{e,L} \lambda_e' U_{e,R}^\dagger, \quad \lambda_u = U_{u,L} \lambda_u' U_{u,R}^\dagger, \quad \lambda_d = U_{d,L} \lambda_d' U_{d,R}^\dagger, \tag{2.1.36}$$

which means that either λ_e' and λ_u' or λ_e' and λ_d' can be diagonalized simultaneously. In choosing the first possibility, namely the simultaneous diagonalization of λ_e' and λ_u', we are

left with a Yukawa coupling λ'_d which is neither real nor diagonal. However, we can decompose λ_d in such a way that it can be written as the product of a diagonal, real and non-negative matrix $D_d = U_{d,L}\lambda'_d U^\dagger_{d,R}$ and a unitary matrix $V = U_{u,L}U^\dagger_{d,L}$ via

$$VD_d = U_{u,L}\lambda'_d U^\dagger_{d,R}. \tag{2.1.37}$$

The matrix V in (2.1.37) is the famous Cabibbo-Kobayashi-Maskawa (CKM) matrix, which describes the mixing between the different quark generation in the SM.

By rotating the fermionic fields as given in (2.1.34) and (2.1.35) we are able to diagonalize the Yukawa matrices by choosing a different basis, in which the mass matrices are diagonal. Such a basis is therefore called mass eigenstate basis in contrast to the weak eigenstate basis and can be denoted by

$$\begin{aligned} \nu^i_L = \sum_{j=1}^{3} U^{ij}_{e,L}\nu'^j_L, \quad e^i_L = \sum_{j=1}^{3} U^{ij}_{e,L}e'^j_L, \quad u^i_L = \sum_{j=1}^{3} U^{ij}_{u,L}u'^j_L, \quad d^i_L = \sum_{j=1}^{3} U^{ij}_{d,L}d'^j_L, \\ e^i_R = \sum_{j=1}^{3} U^{ij}_{e,R}e'^j_R, \quad u^i_R = \sum_{j=1}^{3} U^{ij}_{u,R}u'^j_R, \quad d^i_R = \sum_{j=1}^{3} U^{ij}_{d,R}d'^j_R. \end{aligned} \tag{2.1.38}$$

In contrast to the lepton sector, where the two components of the isospin doublet feel the same rotation matrix, u'^i_L and d'^i_L transform differently under the unitary transformations (2.1.38), which leads to flavor mixing in the quark sector due to the CKM mixing matrix V.

Finally we can rewrite the Lagrangian (2.1.32) in terms of mass eigenstates (2.1.38), where the masses of the charged leptons, up- and down-type quarks are related to the diagonal elements of the Yukawa couplings by

$$m^i_e = \frac{v}{\sqrt{2}}D^{ii}_e, \quad m^i_u = \frac{v}{\sqrt{2}}D^{ii}_u, \quad m^i_d = \frac{v}{\sqrt{2}}D^{ii}_d, \tag{2.1.39}$$

with D_e, D_u and D_d being diagonal, real and non-negative.

2.2 Why Go Beyond the Standard Model

2.2.1 The Standard Model as an Effective Field Theory

Despite the fact that the SM is extremely successful in describing the fundamental interactions of particles and despite the fact that there have been no confirmed experimental results that contradict its predictions, it suffers from several conceptual problems.

One of the most obvious indications for the incompleteness of the SM is the fact that it does not include gravity and since the gravitational interactions become strong at the Planck scale, $M_{Pl} \sim 10^{19}\,\text{GeV}$, the SM cannot be the underlying theory to describe all physical laws. So far, all attempts to quantize general relativity result in non-renormalizable field theories. Therefore these theories can predict correct results at lowest order, but they do not allow for a precise calculation of experimental quantities at the quantum level.

Apart from the question of how to incorporate gravity, the SM itself has several unnatural features. As already discussed in previous chapters the gauge group of the SM consists of three gauge factors $SU(3)_C$, $SU(2)_L$ and $U(1)_Y$ with three independent coupling constants. Although the SM can unify the weak and electromagnetic force utilizing the idea of the symmetry breaking mechanism $SU(2)_L \otimes U(1)_Y \rightarrow U(1)_Q$, it cannot provide a unification of all three forces. It is also surprising that the $SU(2)_L \otimes U(1)_Y$ gauge factor distinguishes between left and right handed states, while the $SU(3)_C$ does not. Another important, so far undiscovered sector of the SM is the Higgs sector, which is responsible for the generation of masses and the spontaneous symmetry breakdown. Besides, it requires an inelegant addition of parameters to the Lagrangian, since it does not provide an explanation for the values of the particles' masses.

A further question which still remains unanswered is that the theory does not give any arguments why there are exactly three generations of matter. Together with the unknown origin of the parameters in the mass matrix, mentioned above, this is the reason why there are 19 free parameters in the SM. These are the three coupling parameters (α, θ_W, Λ_{QCD}), the two Higgs parameters (M_H and λ), the nine fermion masses (m_e, m_u, m_d; m_μ, m_c, m_s; m_τ, m_t, m_b), the three mixing angles and one phase angle in the CKM matrix, and the strong QCD phase parameter θ. There are even more parameters if neutrino masses and mixings are included.

Thus, due to these shortcomings, the SM cannot be the complete theory of nature, and some new understanding is needed in order for these questions to be answered properly.

2.2.2 Unitarity

As already stated in the last subsection, at least above the Planck scale of $M_{Pl} \sim 10^{19}\,\text{GeV}$, the SM has to be replaced by a more general theory that includes quantum gravity. Thus an upper bound for the cut-off is given by the Planck scale M_{Pl}. However, there are further reasons like the high-energy scattering of weak gauge bosons why the SM can only be valid up to a much lower cut-off.

A fundamental motivation to generate the masses of W and Z bosons by the Higgs mechanism is that the Higgs boson is needed as an extra degree of freedom to soften the UV behavior of massive gauge bosons. When we look at the scattering of longitudinal polarizations of massive spin-1 particles we obtain a tree level amplitude which possesses a E^4 dependence

$$\mathcal{A} = \mathcal{A}^{(4)} \left(\frac{E}{M}\right)^4 + \mathcal{A}^{(2)} \left(\frac{E}{M}\right)^2 + ..., \tag{2.2.40}$$

where M is the mass of the massive gauge boson. From (2.2.40) we can see that $\mathcal{A}$ becomes larger than 1 and would spoil the unitarity of the S-matrix when the energy scale E is of the order of the gauge boson masses. In the absence of any other fundamental degrees of freedom the theory would therefore enter a strongly coupled regime and we would not be

able to apply perturbative methods. The Higgs particle as a new degree of freedom can now give an additional contribution to the scattering amplitude (2.2.40) which exactly cancels that part of the amplitude growing with energy. Including the Higgs particle we obtain an amplitude $\mathcal{A} = g^2 M_H^2/(4M_W^2)$, which is finite at arbitrarily high energies. However, to preserve perturbative unitarity the Higgs particle should not be too heavy. We can get a rough upper bound for the Higgs mass from the decomposition of the amplitudes into partial waves [32]

$$\mathcal{A} = 16\pi \sum_{l=0}^{\infty} (2l+1)\, P_l\,(\cos\theta)\, a_l, \tag{2.2.41}$$

where the P_l are the Legendre polynomials.

Using this decomposition we get for the coefficient a_0 in the SM without a Higgs boson

$$a_0 = \frac{g^2 E^2}{16\pi M_W^2}, \tag{2.2.42}$$

which tells us that perturbative unitarity cannot be maintained above $\sim 620\,\mathrm{GeV}$. Including the Higgs boson, the coefficient a_0 becomes

$$a_0 = \frac{g^2 M_H}{64\pi M_W^2}, \tag{2.2.43}$$

which yields the upper bound $M_H \leq 1.2\,\mathrm{TeV}$ for the Higgs mass. Considering a different channel one can even get the more stringent upper bound $M_H \leq 780\,\mathrm{GeV}$ [32].

A further bound on the Higgs mass can be derived from the study of radiative corrections to the Higgs potential. At the quantum level, the coefficient λ in the Higgs potential (2.1.15) run with energy as given in [33],

$$16\pi^2 \frac{d\lambda}{d\ln Q} = 24\lambda^2 - \left(3g'^2 + 9g^2 - 12y_t^2\right)\lambda + \frac{3}{8}g'^4 + \frac{3}{4}g'^2 g^2 + \frac{9}{8}g^4 - 6y_t^4 + \ldots \tag{2.2.44}$$

Solving (2.2.44) in the large Higgs mass limit, where the first term on the right hand side in (2.2.44) dominates, yields the solution

$$\lambda\,(Q) = \frac{M_H^2}{2v^2 - \frac{3}{2\pi^2} M_H^2 \ln\frac{Q}{v}}, \tag{2.2.45}$$

which shows a Landau pole at

$$Q = v e^{4\pi^2 v^2/3M_H^2}. \tag{2.2.46}$$

To prevent this instability new physics has to appear below that scale and thus we obtain a relation between the cut-off of the SM and the Higgs mass

$$\ln\frac{\Lambda}{v} \leq \frac{16\pi^2 m_W^2}{3g^2 m_H^2}, \tag{2.2.47}$$

from which an upper bound on the Higgs mass for a fixed cut-off scale can be derived.

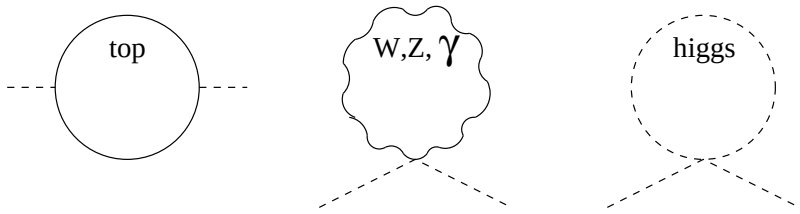

Figure 2.1: *Most important, quadratically divergent contributions to the Higgs mass, making the Higgs UV sensitive (taken from M. Schmaltz et al. [3]).*

2.2.3 Naturalness and Hierarchy Problem

Generally, in particle physics it should be possible to deduce a low-energy theory from a high-energy theory without carefully adjusting its parameters. This means that no fine-tuning of the high-energy parameters should be necessary to derive the low-energy effective theory. A definition of naturalness has been given by 't Hooft in the following version [34]: *at any energy scale Q, a physical parameter $\alpha(Q)$ or set of parameters $\alpha_i(Q)$ is allowed to be very small only if the replacement $\alpha_i(Q) = 0$ increases the symmetry of the theory.*

So far we have looked at the running of the Higgs quartic coupling to derive upper bounds on the Higgs mass. However, radiative corrections are even more important when we consider the mass term of the Higgs, since it is highly dependent on the UV physics. To determine the one-loop corrections to the Higgs mass M_H^2 we assume the SM to be valid up to a cut-off Λ and calculate the one-loop corrections of Figure 2.1, which yields the following result

$$\delta M_H^2 = \left(\frac{1}{4}\left(9g^2 + 3g'^2\right) - 6y_t^2 + 6\lambda\right)\frac{\Lambda^2}{32\pi^2}. \tag{2.2.48}$$

Assuming a cut-off of 10 TeV we can see from (2.2.48) that the contributions coming from the gauge, top and Higgs contributions to the Higgs mass are of the order of $(600\,\mathrm{GeV})^2$, $-(1.5\,\mathrm{TeV})^2$ and $(600\,\mathrm{GeV})^2$, respectively. Thus all these particles give unnaturally large corrections to the Higgs mass and some precise adjustment, i.e. fine-tuning, between the bare mass and the one-loop correction is needed to preserve the *vev* of the Higgs at the weak scale. From the contributions to the Higgs mass mentioned above we can see that a fine-tuning of one part in 100 among the tree level parameters is necessary in order to keep the mass of the Higgs in the range of a few hundred GeV. Such a precise adjustment of parameters strongly contradicts 't Hooft's definition, since setting $M_H = 0$ does not lead to any new symmetry and therefore a fine-tuning of parameters will be necessary. This is considered as unnatural and is usually denoted as the hierarchy problem.

According to these arguments the cut-off of the theory should not be much higher than the Higgs boson mass and future colliders like the LHC should be able to uncover a more fundamental theory soon. However, indirect searches through precision data from LEP did not show any signals so far that points towards new physics at this scale. These analyses

seem to favor a light Higgs with a mass of $100 - 200\,\mathrm{GeV}$, but require the scale of new physics to be at least $5\,\mathrm{TeV}$. This hierarchy between these two different scales is often referred to as the little hierarchy problem [35].

However, assuming that physics beyond the SM already appears at the TeV scale, we are able to regulate the Higgs mass and restore naturalness by newly introduced particles. In the following we want to sketch some of the most popular theories, which serve as possible candidates to explain the physics beyond the SM.

2.2.4 Supersymmetry

One of the most popular candidate theories beyond the SM is weak scale supersymmetry. In this model the superpartners of the SM particles possess a different statistics and contribute to the radiative corrections to the Higgs mass with the opposite sign and in the limit of exact supersymmetry, all corrections to M_H cancel. However, exact supersymmetry requires the superpartners to have exactly the same masses as their SM partners, which has not been observed in nature and therefore supersymmetry must be broken. Due to a broken supersymmetry, there is a remnant logarithmic divergence dominated by the negative contribution of the top quark. Then, assuming a soft supersymmetry breaking scale at around $1\,\mathrm{TeV}$, the Higgs becomes tachyonic and the electroweak symmetry is radiatively broken. In its simplest version, denoted as the MSSM, such a scenario is considerably constrained to live in a fraction of its parameter space. In the MSSM the main constraint comes from the experimental lower bound on the Higgs mass M_H, which is typically light and hardly above $120\,\mathrm{GeV}$.

2.2.5 Extra Dimensions

A different solution to the hierarchy problem is proposed by extra dimensional models, among which the model of *Randall* and *Sundrum* [36, 37] is one of the most popular. In their $5D$ model they assume the extra space dimension not to be flat but to have a nontrivial geometry. More precisely, they consider a setup with a bulk geometry of the form

$$ds^2 = a^2(y)\, dx^\mu dx_\mu - dy^2, \quad y \in [0, \pi R]\,. \tag{2.2.49}$$

with two branes, where matter can be localized. To realize such a setup *Randall* and *Sundrum* choose a negative cosmological constant in the bulk and opposite signs for those on the branes. In the original works the SM particles are confined to one of the branes, which is denoted as the visible brane. On the remaining brane, the hidden one, $4D$ gravity is strong with a fundamental scale M_*. However, due to the exponential factor in the metric, the fundamental scale of gravity on the visible brane is much larger

$$M_{Pl}^{vis} = e^{k\pi R} M_* \tag{2.2.50}$$

and one can easily obtain a fundamental scale M_* in the TeV region, therefore avoiding the hierarchy problem.

Chapter 3

From Extra Dimensions to the Little Higgs

Gauge theories in more than four space-time dimensions are non-renormalizable and various quantum problems cannot be solved consistently. However, it has been demonstrated [1, 38] that the physics of higher dimensional gauge theories can alternatively be described by certain four dimensional theories which possess an enlarged gauge symmetry. For example, there is a correspondence between five dimensional gauge theories with the gauge group G and four dimensional gauge theories whose gauge group is a direct product of the gauge group G replicated N times, $G \times G \times \cdots \times G$. The resulting four dimensional theory is then referred to as deconstructed and each copy of G may be interpreted as the gauge group located at a particular point along a new, discretized, "deconstructed" dimension. The spectrum of matter fields is a set of bifundamental representations expressed by a moose or quiver diagram that has its analogy in lattice gauge theory. This setup can be considered as an alternative description of the higher dimensional theory, but has the property of being renormalizable. Phenomenologically interesting theories of this kind are for example Little Higgs theories, which will be discussed later.

3.1 Basics of Deconstruction

3.1.1 Moose-Diagrams and Deconstruction

In this subsection we focus on the four dimensional model of [1, 38], which contains both gauge fields and Weyl-fermions. These are conveniently accommodated in so-called "moose" [39] or "quiver" [40] diagrams. In these diagrams the N gauge groups $\mathbb{G}$ and $\mathbb{G}_s$ are symbolized by circles and fermions by directed links between the sites i and $i+1$. The moose diagram we want to consider is shown in Fig. 3.2 and describes a 4D field theory with a $\mathbb{G}^N \times \mathbb{G}_s^N$ gauge group, where we will choose $\mathbb{G} = SU(m)$ and $\mathbb{G}_s = SU(n)$. Furthermore, we require

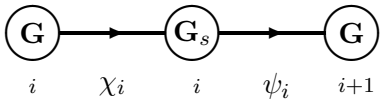

Figure 3.1: *A side of the polygon (taken from Arkani-Hamed et al. [1]).*

all gauge couplings of the $SU(m)$ groups to be set equal to a common value g, while all the $SU(n)$ couplings are set to g_s.

As shown in Fig. 3.1, the sides of the polygon each represent two types of fermions, which transform under the corresponding gauge groups as

$$\chi_i \quad \text{transforming as} \quad (\mathbf{m}, \bar{\mathbf{n}}, \mathbf{1}) \quad \text{under} \quad SU_i(m) \times SU_i(n) \times SU_{i+1}(m), \tag{3.1.1}$$

$$\psi_i \quad \text{transforming as} \quad (\mathbf{1}, \mathbf{n}, \bar{\mathbf{m}}) \quad \text{under} \quad SU_i(m) \times SU_i(n) \times SU_{i+1}(m). \tag{3.1.2}$$

At energies much higher than Λ_s and Λ this theory can be described by N sets of massless and weakly interacting fermions and gauge bosons. However, at lower energies one of the gauge interactions can become strongly coupled and without loss of generality, we assume $\Lambda_s \gg \Lambda$. Thus, around the scale Λ_s, $\mathbb{G}_s = SU(n)$ becomes strongly coupled, while $\mathbb{G}$ can still be treated perturbatively. At this scale a pair of fermions condenses similar to quark confinement leading to ordinary glueballs and baryons in QCD. For each pair of fermions we thus assume a non-zero vacuum expectation value,

$$\langle \chi_i \psi_i \rangle \sim 4\pi f_s^3 U_i, \tag{3.1.3}$$

with $f_s \sim \Lambda_s/(4\pi)$ and U_i being a unitary $m \times m$ matrix parameterizing the direction of the condensate in $SU(m)$ space. The moose diagram of Fig. 3.2 then turns into a condensed moose diagram as depicted in Fig. 3.3. Below the scale Λ_s the theory of this condensed moose diagram can be described as a $\prod_{i=1}^{N} SU(m)_i$ gauge theory connected by a set of *non-linear sigma model (NLSM)* fields, denoted by U_i. Each of these link fields contains the corresponding Goldstone boson fields arising from the symmetry breakdown and can be parameterized by

$$U_i = \exp\left\{ \frac{i}{f_s} \sum_{a=1}^{m^2-1} \pi_i^a T_a \right\}, \tag{3.1.4}$$

where the T_a correspond to the $SU(m)$ generators. The transformation property of the Goldstone boson fields under $SU(m)_i \times SU(m)_{i+1}$ is then given by those of the U_i which transform as $(\mathbf{m}, \bar{\mathbf{m}})$, or explicitly

$$U_i \to g_i^{-1}(x) U_i g_{i+1}(x), \tag{3.1.5}$$

where $g_i \in SU(m)_i$. Moreover, the U_i are singlets under the strong $SU(n)$ gauge group.

Suppressing higher dimensional operators, that are irrelevant for the low energy theory, we can write the effective action for the Goldstone bosons as

$$S_{\text{eff}} = \int d^4x \sum_{i=1}^{N} \left\{ f_s^2 \text{Tr}\left[(D_\mu U_i)^\dagger D^\mu U_i \right] - \frac{1}{2g^2} \text{Tr}\left(F^i_{\mu\nu} F_i^{\mu\nu} \right) + ... \right\}, \tag{3.1.6}$$

where the covariant derivative is defined by

$$D_\mu U_i = \partial_\mu U_i - igA^i_\mu U_i + igU_i A^{i+1}_\mu, \quad A^i_\mu = A^{i,a}_\mu T^a. \tag{3.1.7}$$

The action (3.1.6) connects the gauge fields at neighboring sites and the different Goldstone bosons are linked by a local "nearest neighbor" interaction. As pointed out in [1, 38], the action (3.1.6), corresponding to the condensed moose diagram in Fig. 3.3, can be interpreted as the discretized action for a five dimensional theory with a gauge group $SU(m)$, where the fifth dimension has been latticized. For further details the reader is referred to [1, 38].

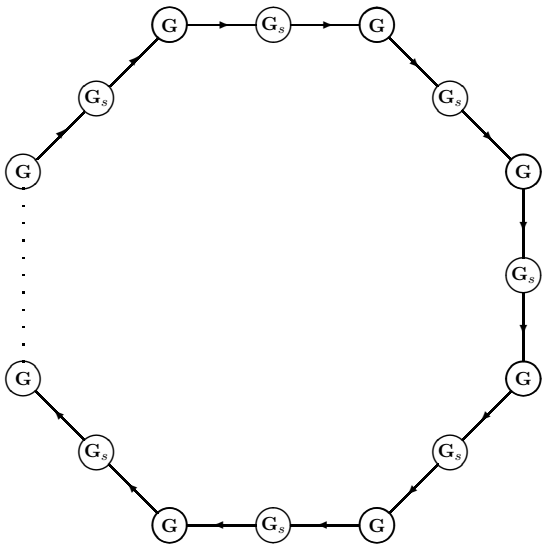

Figure 3.2: *A moose diagram (taken from ArkaniHamed et al. [1]).*

3.1.2 Symmetry Breaking

According to the previous subsection it is obvious by construction that the low energy Lagrangian of (3.1.6) possesses a local $SU(m)^N$ symmetry. Considering just one side of the condensed moose diagram, i.e. the Goldstone boson matrix U_i and its corresponding gauge groups $SU(m)_i$ and $SU(m)_{i+1}$ in Fig. 3.1, we can see that U_i transforms under the two gauge groups independently. Thus the symmetry group of each side of the polygon is given by $SU(m)_i \times SU(m)_{i+1}$. However, they are related by the gauge couplings, which explicitly break this accidental symmetry.

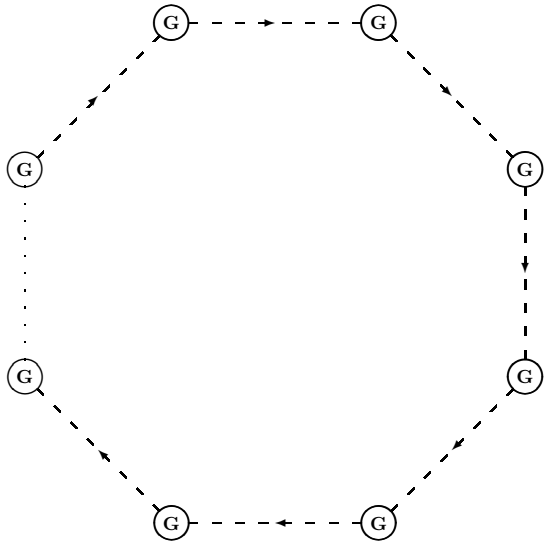

Figure 3.3: *A condensed moose diagram (taken from ArkaniHamed et al. [1]).*

Switching off the $SU(m)$ gauge couplings, the polygon breaks up, (3.1.6) simplifies significantly and the low energy Lagrangian reduces to

$$\mathcal{L}_{g=0} = \sum_{i=1}^{N} f_s^2 \mathrm{Tr}\left(\partial_\mu U_i^\dagger \partial^\mu U_i\right). \tag{3.1.8}$$

From (3.1.8) one can see that the different NLSM fields U_i decouple and can be transformed globally

$$U_i(x) \to L_i U_i(x) R_i^\dagger, \tag{3.1.9}$$

where the L_i, $R_i^\dagger$ are independent $SU(m)$ matrices and can for example be associated with the transformations of the left-handed $\chi^\dagger$ and right-handed ψ, respectively. Thus, in the absence of gauge interactions, such a theory has an accidental "chiral" global $[SU(m)_L \times SU(m)_R]^N$ symmetry, where the global symmetry groups of each side are now denoted with

$$\mathbb{G}_i \to \mathbb{G}_{L_i} \quad \text{and} \quad \mathbb{G}_{i+1} \to \mathbb{G}_{R_i}. \tag{3.1.10}$$

Still assuming vanishing couplings g, the accidental global symmetry, in analogy to spontaneous chiral symmetry breaking in QCD, is spontaneously broken down to its diagonal subgroup via vacuum expectation values of the NLSM fields,

$$SU(m)_{L_i} \times SU(m)_{R_i} \xrightarrow{SSB} SU(m)_{L_i=R_i}, \tag{3.1.11}$$

where the NLSM fields can be expressed as in (3.1.4). Concerning the symmetry of the total moose diagram this implies a symmetry breakdown

$$[SU(m)_{L_i} \times SU(m)_{R_i}]^N \xrightarrow{SSB} [SU(m)_{L_i=R_i}]^N, \tag{3.1.12}$$

with the index L and R denoting the left and right gauge group belonging to the same side of the polygon.

In contrast to the spontaneous symmetry breakdown described above, the global accidental symmetry can also be broken explicitly via the gauge couplings. Considering the transformation properties both of the gauge bosons

$$A_{i\mu} \to g_i A_{i\mu} g_i^\dagger \tag{3.1.13}$$

and Goldstone bosons (3.1.9) one can see [2] that, in the presence of the gauge couplings, only a $\left[SU(m)_{L_i=R_{i-1}}\right]^N$ is preserved, as soon as $L_i = g_i = R_{i-1}$. That is, it is necessary for the right gauge group of a side to be equal to the left gauge group of the neighboring side. Thus the global symmetry $[SU(m)_{L_i} \times SU(m)_{R_i}]^N$ is explicitly broken to $\left[SU(m)_{L_i=R_{i-1}}\right]^N$ by the presence of gauge couplings at the level of the classical Lagrangian.

As depicted in the following diagram the explicit symmetry breaking arises from the presence of gauge couplings and connects each single side of the condensed moose diagram while the spontaneous symmetry breakdown leaves the diagonal subgroup of each single side unbroken.

$$\begin{array}{ccc} [SU(m)_{L_i} \times SU(m)_{R_i}]^N & \xrightarrow{SSB} & [SU(m)_{L_i=R_i}]^N \\ \Big\downarrow g & & \Big\downarrow g \\ \left[SU(m)_{L_i=R_{i-1}}\right]^N & \xrightarrow{SSB} & SU(m)_{\text{diag}} \end{array} \tag{3.1.14}$$

Using the gauge freedom, almost all U_i can be gauged to unity by an appropriate choice of gauge transformations. As discussed in [2], in unitary gauge it is possible to set $N-1$ of the N NLSM fields to unity, where one Nambu-Goldstone field remains and is associated with the product $U_1 U_2 \cdots U_N$. This field contains the pseudo Goldstone boson describing the low energy limit of the theory and can be parameterized as

$$U = \exp\left\{\frac{i}{f_s}\phi\right\}, \quad \phi = \frac{1}{\sqrt{N}}\left(\pi_1 + ... + \pi_N\right). \tag{3.1.15}$$

Since the global accidental symmetry $[SU(m)_L \times SU(m)_R]^N$ is broken at the classical level only by the gauge couplings, ϕ remains massless at tree level and receives its mass by quantum corrections. However, these quantum corrections include only diagrams which involve all gauge couplings at the same time.

In [2] this is demonstrated by introducing spurion fields q_i, which transform as

$$U_i \to L_i U_i R_{i+1}^\dagger, \tag{3.1.16}$$

$$A_i \to L_i A_i L_i^\dagger, \tag{3.1.17}$$

$$q_i \to R_{i+1} q_i L_{i+1}^\dagger. \tag{3.1.18}$$

This guarantees the modified covariant derivative

$$D_\mu^q U_i = \partial_\mu U_i + igA_{i\mu}U_i - igU_i q_i A_{i+1\mu} q_i^\dagger \tag{3.1.19}$$

to be invariant under a global $SU(m)^{2N}$. Since U is defined as the product of all U_i, the potential containing a mass term for ϕ must be a function of $\prod_i U_i$ and the leading nontrivial operator involving only the U_i is given by [2]

$$\mathcal{O} = \left|\mathrm{Tr}\left(U_1 q_1 \cdots U_N q_N\right)\right|^2, \tag{3.1.20}$$

with a natural size for the coefficient of this operator given by $(4\pi f)^2 f^2 (g^2/16\pi^2)^N$ [41]. From this one can see that all couplings must be involved to generate such an operator. Metaphorically speaking, ϕ is distributed over the whole condensed moose diagram, thus being a non-local object, while the gauge couplings, which connect the sides of nearest neighbors of the polygon, are local objects in theory space. Thus it is not possible to generate quantum corrections depending on ϕ involving only a single gauge coupling, which leads to the fact that ϕ can be realized as a light pseudo-Goldstone boson. In the later Subsection 3.1.5 we will see that this mechanism of generating scalar fields with natural small masses can be embedded in physically more viable model, which will lead to Little Higgs models.

3.1.3 Relation to Lattice Gauge Theory

In the original works [1, 2, 38] *Arkani-Hamed et al.* have pointed out that theories as described in the previous subsection can actually be interpreted as higher dimensional field theories in the low energy limit. In particular, the theory described by the moose diagram in Figure 3.3 corresponds to a $5D$ gauge theory with one dimension compactified on a circle. In contrast to many other theories, this dimension is not continuous, but discretized [42] on a lattice with N sites. To see this correspondence, we briefly demonstrate how gauge theory is formulated on a spacetime lattice [43]. Usually in lattice gauge theory the gauge fields are replaced by so-called link fields U, that implement a parallel transport along the path $\mathcal{C}$:

$$U\left(\mathcal{C}\right) = P \exp\left(-ig \int_{\mathcal{C}} A_N \mathrm{d}x^N\right) \tag{3.1.21}$$

with P denoting the path-ordering operator.

Since we want to discretize only one dimension, while the remaining four dimensions shall remain continuous, a link field is introduced only for A_5. Denoting the lattice points by i and the lattice spacing by a, the link fields between two lattice points i and $i+1$ can be approximated by

$$U_i = \exp\left(-igaA_5\left(\left(i+1/2\right)a\right)\right). \tag{3.1.22}$$

Introducing the corresponding covariant derivatives for the U_i,

$$D_\mu U_i = \partial_\mu U_i - igA_\mu\left(ia\right)U_i + igA_\mu\left(\left(i+1\right)a\right)U_i, \tag{3.1.23}$$

and expanding it in terms of the lattice spacing a, we find that at order $\mathcal{O}(a)$,

$$D_\mu U_i = -iagF_{\mu 5}\left(ai\right) + \mathcal{O}\left(a^2\right). \tag{3.1.24}$$

Performing the sum over a finite number of points 0 to N and identifying $i = 0$ with $i = N$ we obtain a compactified and discretized interval of size $L = Na$ with the topology of a circle. To see the analogy to a 5D continuum theory the gauge fields have to be rescaled and the sum has to be substituted by an integral

$$a\sum_p \to \int dx^5 \tag{3.1.25}$$

with the gauge coupling constant of the 5D EFT given by $g_5^2 = ag^2$. By comparing (3.1.22) with (3.1.4) one can the see the correspondence of the NLSM to a latticized version of a 5D non-abelian gauge theory with the lattice spacing a and the circumference R of the fifth dimension,

$$\pi_a^i T^a / f_s = -agA_5^i, \quad a = \frac{1}{gf_s}, \quad R = Na. \tag{3.1.26}$$

3.1.4 Non-Renormalizability and Chiral Perturbation Theory

As we have seen in the previous subsections the deconstructed theory is a NLSM, which is non-renormalizable and can make predictions only up to a cut-off scale Λ. Yet, we can write down the effective Lagrangian using a non-linear realization of the gauge symmetry, where we make use of the notation in [44]. In analogy to the established techniques of chiral perturbation theory for low energy QCD [41, 45] all the terms in the Lagrangian of a NLSM can be organized in a power series in small momenta $p \ll \Lambda \sim 4\pi f$,

$$\mathcal{L}_{eff} = \mathcal{L}_2 + \mathcal{L}_4 + ..., \tag{3.1.27}$$

where the terms in $\mathcal{L}_2$ are of order $\mathcal{O}(p^2)$, the terms in $\mathcal{L}_4$ of order $\mathcal{O}(p^4)$.

Having expanded the Lagrangian of a NLSM into a series in p/Λ we can see that the higher dimensional terms, which are suppressed by inverse powers of Λ, destroy the renormalizability of the NLSM. Yet, renormalizability does not pose a problem here, since in an *effective field theories (EFT)* it is always possible to remove all divergences at a fixed order in the momentum expansion.

In Chiral Perturbation Theory, for example, the most general effective Lagrangian at the order $\mathcal{O}(p^4)$ has to include both the tree-level graphs originating from $\mathcal{L}_4$, the one-loop graphs associated with the lowest-order Lagrangian $\mathcal{O}(p^2)$ and the Wess-Zumino-Witten functional to account for the chiral anomaly. The complete effective Lagrangian at order $\mathcal{O}(p^4)$ is given in [45, 46] and needs to be renormalized due to divergent Goldstone loops. These divergences can be absorbed in the renormalization of the coupling constants. Schematically, the Lagrangian

can be written as a sum of operators multiplied by bare low-energy constants $\mathcal{L}_4 = \sum_i L_i \mathcal{O}_i$, where the L_i are given by [44]

$$L_i = L_i^r(\mu) + \Gamma_i \lambda, \qquad \lambda = \frac{\mu^{d-4}}{16\pi^2}\left\{\frac{1}{d-4} - \frac{1}{2}\left[\log(4\pi) + \Gamma'(1) + 1\right]\right\}. \tag{3.1.28}$$

From (3.1.28) we can see the constants L_i absorbing the divergences from divergent loops of $\mathcal{L}_2$ so that the scheme- and scale-dependent renormalized constants $L_i^r(\mu)$ are finite. The remaining coefficient Γ_i of the divergent term can explicitly be calculated from the one-loop generating functional and are given in [45, 46]. Finally, one has to perform a matching between effective and full theory at low energies to determine these low-energy constants. However, for strongly interacting theories case they cannot be calculated and have to be determined from experiment.

3.1.5 The Minimal Moose Model

To derive a realistic Little Higgs model, where the SM Higgs is realized as a pseudo Goldstone boson, it was proposed by *Arkani-Hamed et al.* in [47] to start with a deconstructed theory that has at least two "compactified dimensions". In the minimal version such a model consists of two sites and four link fields, where one site corresponds to the gauge group $G_1 = SU(3)$, while the other site is $G_2 = SU(2) \times U(1)$. These sites are connected by 4 link fields X_i, $i = 1, ..., 4$, which are 3×3 NLSM fields describing the Goldstone fields. In the absence of any gauge interactions the theory has a large, approximate $SU(3)^8$ global symmetry, which is spontaneously broken to $SU(3)^4$. Denoting the Goldstone fields by x_i and the global $SU(3)$ transformations by L_i, R_i, the NLSM fields $X_i = \exp(2ix_i/f)$ transform as

$$X_i \to L_i X_i R_i^\dagger, \quad i = 1, 2, 3, 4. \tag{3.1.29}$$

Below the cut-off $\Lambda \sim 4\pi f \sim 10\,\text{TeV}$ of this model the theory can be described by the effective Lagrangian

$$\mathcal{L} = \mathcal{L}_G + \mathcal{L}_X + \mathcal{L}_t + \mathcal{L}_\psi, \tag{3.1.30}$$

where $\mathcal{L}_G$ represents the conventional kinetic terms and gauge interactions of the NLSM and $\mathcal{L}_X$, $\mathcal{L}_t$, $\mathcal{L}_\psi$ will be explained in turn. As some modes of the Goldstone bosons will serve as a Higgs boson and should therefore couple to fermions, a coupling between the four fields X_j is introduced. Additionally, we have to generate a Higgs potential to trigger the electroweak symmetry breaking, which will be achieved by introducing $\mathcal{L}_X$ containing so-called "plaquette" couplings between the X_j. These consist of gauge invariant objects similar to Wilson loops in lattice gauge theory and are added in an ad hoc way:

$$\mathcal{L}_\text{X} = f^4 \text{Tr}(A X_1 X_2^\dagger X_3 X_4^\dagger) + f^4 \text{Tr}\left(A' X_1 X_4^\dagger X_3 X_2^\dagger\right) + \text{h.c.}. \tag{3.1.31}$$

In (3.1.31), A, A' denote the matrices $A = \kappa \mathbf{1} + \varepsilon \mathbf{T_8}$ and $A' = \kappa' \mathbf{1} + \varepsilon' \mathbf{T_8}$. Each of these ε, ε' terms preserves enough of the global symmetry to leave some of the Goldstone bosons

massless, i.e. these ε, ε' respect an $SU(2) \times U(1)$ symmetry, but break the global $SU(3)$ to generate pseudo Goldstone bosons.

To generate the SM Yukawa couplings, the NLSM is coupled to the SM quark fields by the two remaining terms $\mathcal{L}_t$ and $\mathcal{L}_\psi$. In doing so, the top Yukawa sector is modified in a peculiar way. To avoid quadratic divergences coming from the top sector we introduce a pair of additional vectorlike quarks U and U^c, which have the same statistics as the SM quarks and will cancel the dangerous divergences to the Higgs boson mass at the one-loop order. In order to achieve this the Yukawa interaction for the top quark is chosen to be

$$\mathcal{L}_t = \lambda f \left(0\ 0\ u_3^{c\prime}\right) X_1 X_2^\dagger \begin{pmatrix} q_3 \\ U \end{pmatrix} + \lambda' f U U^c + \text{h.c.}. \tag{3.1.32}$$

Since the Yukawa couplings for the remaining quarks are much smaller than that of the top quark, the quadratic divergences related to them are negligible for a cut-off $\Lambda \sim 10\,\text{TeV}$, especially in view of the two-loop divergences coming from top quark loops which are present in the model anyway. Therefore the standard Yukawa interaction for light up-type quarks $\mathcal{L}_\psi$ has the same form as (3.1.32) but with U, U^c removed, while for the down and charged lepton sector $\mathcal{L}_\psi$ contains

$$\mathcal{L}_\psi = \lambda_\text{D} \left(q\ \ 0\right) X_1 X_2^\dagger f \begin{pmatrix} 0 \\ 0 \\ d^c \end{pmatrix} + \lambda_\text{E} \left(l\ \ 0\right) X_1 X_2^\dagger f \begin{pmatrix} 0 \\ 0 \\ e^c \end{pmatrix}, \tag{3.1.33}$$

which finalizes the construction of the model. However, one should be aware of the shortcomings of this construction. The most striking one is the fact that the terms included in the Lagrangian were not selected by any symmetry principle. This means that all the terms that were neglected will be generated radiatively at higher loop level. To forbid certain terms in the low energy Lagrangian it is necessary to construct an appropriate UV completion of the model and it is unclear whether such a completion exists in a satisfactory form. Besides, the Little Higgs mechanism alone cannot explain the hierarchy between the cut-off of the low energy theory and the GUT or Planck scale. To do so, again some kind of UV completion is needed [48]. For detailed informations about this model and its interactions the reader is referred to the original work [47] by *Arkani-Hamed et al.*.

Chapter 4

The Littlest Higgs Model without T-Parity

Little Higgs models [2, 4, 47, 49, 50, 51], as an alternative to supersymmetric models, have been invented to stabilize the Higgs boson mass against large radiative corrections by introducing new gauge bosons, scalars and quarks. In contrast to supersymmetric models, the cancellation of quadratic divergences is realized between particles of the same spin statistics. In these models the physics below the TeV scale can be approximately described by the SM, while for energies higher than 1 TeV new particles emerge. However, one should be aware of the fact that the Little Higgs is not the end of the story and the ultraviolet completion of the theory must still be explored.

Based on the Little Higgs idea, a model named *Littlest Higgs Model without T-Parity (LH)* has been constructed [4] and its explicit interactions have been presented in [5, 6, 7]. Numerous phenomenological studies in this model have been performed, see e.g. [5, 8]. In this chapter, we will concentrate on the effects of new particles on rare decays like $K_L \to \pi^0\nu\bar{\nu}$, $K^+ \to \pi^+\nu\bar{\nu}$ and $B_{s,d} \to \mu^+\mu^-$, which are known to be ideal probes for physics beyond the SM.

4.1 The Structure of the Littlest Higgs Model

In the LH model, the starting point is a global symmetry group G which is spontaneously broken down to a subgroup H. This symmetry breaking occurs at a scale f of the order of 1 TeV. Since this model realizes the Higgs as a pseudo-Goldstone boson, the unbroken symmetry group H should contain $SU(2)_L \otimes U(1)_Y$ as a subgroup. Similarly to the SM, one would expect that the gauge interactions will again induce one-loop quadratically divergent contributions to the Higgs mass. In order to avoid this, we assume that G contains a gauged subgroup including *two copies* of $SU(2)_L \otimes U(1)_Y$: $G \supset G_1 \otimes G_2 = [SU(2)_1 \otimes U(1)_1] \otimes [SU(2)_2 \otimes U(1)_2]$. These two copies are now arranged in such a way that each G_i commutes

with a different subgroup X_i of G, and hence preserves a different global symmetry. This is sufficient to forbid a Higgs mass term. Only when both gauge groups come into play, the symmetry is broken and a mass term for the Higgs boson is allowed. We will see that at one-loop level one can therefore only get logarithmically divergent contributions, and quadratic divergences first appear at two-loop level.

The full exposition of the model can be found in the original paper [4] and in [5]. We will follow the notations of [5] as far as possible. References to comprehensive reviews can be found in [3].

4.1.1 Symmetry Breaking Pattern

In the LH model the electroweak sector of the SM is embedded in an $SU(5)/SO(5)$ NLSM, which means that the global symmetry group $G = SU(5)$ is spontaneously broken down to its subgroup $H = SO(5)$. The symmetry groups protecting the Higgs mass are chosen to be $X_i = SU(3)_i$, $i = 1, 2$. Moreover, each X_i contains a gauged $SU(2)_i \otimes U(1)_i$ subgroup and should not lie entirely inside H, since they shall explicitly break the symmetry protecting the Higgs mass.

The symmetry breaking $SU(5) \to SO(5)$ is induced by a vacuum condensate of a scalar field transforming in the symmetric tensor representation of $SU(5)$. A vacuum expectation value proportional to the unit matrix then breaks $SU(5) \to SO(5)$. However, it is convenient to choose the vacuum expectation value in the direction of Σ_0 given by the 5×5 symmetric matrix [4]

$$\Sigma_0 = \begin{pmatrix} & & \mathbf{1}_{2\times 2} \\ & 1 & \\ \mathbf{1}_{2\times 2} & & \end{pmatrix}, \tag{4.1.1}$$

where $\mathbf{1}_{2\times 2}$ represents a 2×2 unit matrix.

In order to see that Σ_0 yields the right symmetry breaking pattern, we have to transform the standard generators of $SU(5)$, λ_a, by a similarity transformation. The generators λ_a are either symmetric or antisymmetric, where the 10 antisymmetric generators are identified with the $SO(5)$ subgroup generators. Introducing S as

$$S = \frac{1}{2}\begin{pmatrix} 1+i & 0 & 0 & 1-i & 0 \\ 0 & 1+i & 0 & 0 & 1-i \\ 0 & 0 & 1 & 0 & 0 \\ 1-i & 0 & 0 & 1+i & 0 \\ 0 & 1-i & 0 & 0 & 1+i \end{pmatrix}, \tag{4.1.2}$$

we can then define new generators by a similarity transformation $\tilde{\lambda}_a := S\lambda_a S^{-1}$. Furthermore, the symmetric and unitary matrix S is related to Σ_0 by $\Sigma_0 = S^2 = S^T S$. Using these relations we can then immediately see that the new generators $\tilde{\lambda}_a$ satisfy

$$\tilde{\lambda}_a \Sigma_0 = (S\lambda_a S^{-1})(S^2) = \pm(S\lambda_a S)^T = \pm\Sigma_0 \tilde{\lambda}_a^T, \tag{4.1.3}$$

where the plus sign corresponds to symmetric generators and the minus sign to antisymmetric generators of $SU(5)$. From (4.1.3) it is evident that the unbroken $SO(5)$ generators, denoted by T_a, fulfill

$$T_a\Sigma_0 + \Sigma_0 T_a^T = 0, \tag{4.1.4}$$

while the broken generators, denoted by X_a, obey

$$X_a\Sigma_0 - \Sigma_0 X_a^T = 0. \tag{4.1.5}$$

This can easily be seen by observing that an unbroken symmetry preserves the vacuum and therefore the relation $O\Sigma_0 O^T = \Sigma_0$, with $O = \exp\left(i\alpha^a T_a\right)$, must hold. Expanding the latter in terms of α leads to

$$\Sigma_0 = \left(1 + i\alpha^a T_a\right)\Sigma_0\left(1 + i\alpha^a T_a^T\right) = \Sigma_0 + i\alpha^a\left(T_a\Sigma_0 + \Sigma_0 T_a^T\right) + \mathcal{O}\left(\alpha^2\right), \tag{4.1.6}$$

yielding condition (4.1.4) for the unbroken generators of $SO(5)$. Consequently, the remaining 14 symmetric generators are broken and obey $X_a\Sigma_0 - \Sigma_0 X_a^T = 0$.

Thus, from the breaking $SU(5) \to SO(5)$, we obtain 14 Goldstone bosons corresponding to the 14 broken generators. Under the unbroken $SU(2)_L \otimes U(1)_Y$, these transform as

$$\mathbf{1}_0 \oplus \mathbf{3}_0 \oplus \mathbf{2}_{\pm\frac{1}{2}} \oplus \mathbf{3}_{\pm 1}. \tag{4.1.7}$$

The first two sets are eaten by the gauge bosons corresponding to the broken $G_1 \otimes G_2$ generators, thereby giving a TeV scale mass to them. The third set is a complex doublet, identified with the Higgs boson while the last set is an additional complex triplet.

Similarly to the QCD chiral Lagrangian for pions, the dynamics of the theory at low energy scales below $4\pi f$ can be described in terms of the massless Nambu-Goldstone degrees of freedom, each of them corresponding to one of the broken generators X_a. Thus we can parameterize all the 14 Nambu-Goldstone bosons from the breaking of $SU(5)/SO(5)$ by a NLSM, whose Lagrangian contains all possible Lorentz-invariant, local operators built out of the field

$$\Sigma(x) = e^{i\Pi/f}\Sigma_0 e^{i\Pi^T/f} = e^{2i\Pi/f}\Sigma_0. \tag{4.1.8}$$

For the second equality in (4.1.8) we used the relation $X^a\Sigma_0 = \Sigma_0 X^{aT}$, obeyed by the broken generators. Moreover, f is the Goldstone boson decay constant of the order 1 TeV, and $\Pi = \pi^a X_a$. Using (4.1.7) and ignoring the Goldstone bosons that are eaten by the heavy gauge bosons, the Goldstone boson matrix Π can be written in terms of fields with definite electroweak quantum numbers as

$$\Pi = \begin{pmatrix} & \frac{h^\dagger}{\sqrt{2}} & \phi^\dagger \\ \frac{h}{\sqrt{2}} & & \frac{h^*}{\sqrt{2}} \\ \phi & \frac{h^T}{\sqrt{2}} & \end{pmatrix}. \tag{4.1.9}$$

Here h is the Higgs doublet and ϕ is a complex triplet under the unbroken $SU(2)_L \otimes U(1)_Y$. They can be represented by

$$h = \left(h^+, h^0\right), \quad \phi = \begin{pmatrix} \phi^{++} & \frac{\phi^+}{\sqrt{2}} \\ \frac{\phi^+}{\sqrt{2}} & \phi^0 \end{pmatrix}. \tag{4.1.10}$$

As already mentioned earlier, the condensate Σ_0 does not only break the global symmetry group $G = SU(5)$ down to $SO(5)$, but also breaks the gauge group $[SU(2)_1 \otimes U(1)_1] \otimes [SU(2)_2 \otimes U(1)_2]$ to its "diagonal" subgroup $SU(2) \times U(1)$, which then is identified with the SM electroweak gauge group. To summarize the pattern of symmetry breaking discussed in the last paragraphs we illustrate it in the following cartoon.

$$\begin{array}{ccc} SU(5) & \xrightarrow{SSB} & SO(5) \\ {\scriptstyle g_1}\big\downarrow{\scriptstyle g_2} & & {\scriptstyle g_1}\big\downarrow{\scriptstyle g_2} \\ [SU(2) \times U(1)]^2 & \xrightarrow{SSB} & [SU(2) \times U(1)]_{\text{diag}} \end{array} \tag{4.1.11}$$

The first $SU(2)_1 \times U(1)_1$ subgroup is embedded in the $SU(5)$ in such a way as to preserve a global $SU(3)$ symmetry in the lower-right 3×3 block, while the second $SU(2)_2 \times U(1)_2$ preserves an $SU(3)$ symmetry in the upper-left 3×3 block. Thus, we define the generators of $G_1 = SU(2)_1 \times U(1)_1$ as

$$Q_1^a = \begin{pmatrix} \frac{\sigma^a}{2} & & \\ & & \\ & & \mathbf{0}_{3\times 3} \end{pmatrix}, \qquad Y_1 = \frac{1}{10}\begin{pmatrix} -3 & & & & \\ & -3 & & & \\ & & 2 & & \\ & & & 2 & \\ & & & & 2 \end{pmatrix}, \tag{4.1.12}$$

and the ones of $G_2 = SU(2)_2 \times U(1)_2$ as

$$Q_2^a = \begin{pmatrix} \mathbf{0}_{3\times 3} & & \\ & & \\ & & -\frac{\sigma^{a*}}{2} \end{pmatrix}, \qquad Y_2 = \frac{1}{10}\begin{pmatrix} -2 & & & & \\ & -2 & & & \\ & & -2 & & \\ & & & 3 & \\ & & & & 3 \end{pmatrix}. \tag{4.1.13}$$

The diagonal $SU(2) \times U(1)$ generators

$$Q^a = \frac{1}{\sqrt{2}}\left(Q_1^a + Q_2^a\right), \qquad Y = Y_1 + Y_2 \tag{4.1.14}$$

are unbroken, since

$$Q^a\Sigma_0 + \Sigma_0 Q^{aT} = \begin{pmatrix} \mathbf{0}_{2\times 2} & & \sigma_a/2 \\ & 0 & \\ \mathbf{0}_{2\times 2} & & -\sigma_a^*/2 \end{pmatrix} + \begin{pmatrix} \mathbf{0}_{2\times 2} & & -\sigma_a^{*T}/2 \\ & 0 & \\ \mathbf{0}_{2\times 2} & & \sigma_a^T/2 \end{pmatrix} = 0, \tag{4.1.15}$$

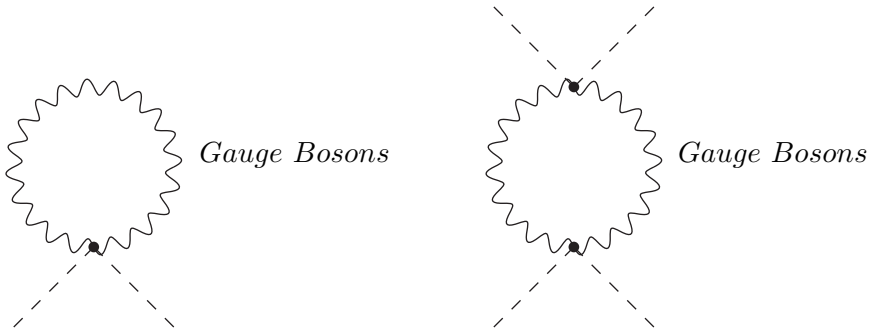

Figure 4.1: *Gauge boson contributions to the Higgs mass. Diagram (a) is the quadratically divergent contribution to the Higgs mass in the SM, while Diagram (b) denotes the logarithmically contribution to the Higgs mass in the LH model (continuous lines correspond to the* Σ *field, while wiggly lines denote gauge bosons).*

where in the last step we used the hermiticity of the Pauli matrices. Analogously we can proceed in the case of $Y\Sigma_0 + \Sigma_0 Y^T = 0$.

At the end of this subsection we want to recall once more that all gauge couplings of G_1 leave a global $SU(3)_2$ symmetry in the lower-right 3×3 block invariant. Assuming further on the gauge couplings of G_2 to be switched off, the enlarged symmetry forbids the radiative generation of a Higgs mass, i.e. a mass term $hh^\dagger$ is forbidden by symmetry. The situation is similar when the G_1 gauge couplings are turned off and only G_2 is active. Only when both couplings are turned on at the same time, the symmetry is sufficiently broken and allows the appearance of a Higgs mass. This mechanism is known as *collective symmetry breaking* and eliminates all quadratically divergent one-loop contributions to the Higgs mass. From Fig. 4.1 we can see that Diagram (a) contains only a single gauge coupling in it, and hence cannot contribute to the Higgs mass. In the SM this is the diagram, which is responsible for the hierarchy problem. Diagram (b) is again a one-loop diagram, however is only logarithmically divergent, since both couplings are involved. Therefore it does not generate large radiative corrections to the Higgs mass. Moreover, there are possible two-loop diagrams that are quadratically divergent, but their value is suppressed by a an additional loop factor of $1/(4\pi)$ and thus is sufficiently small to prevent the little hierarchy problem from being re-introduced at the TeV scale.

4.1.2 The Gauge Boson Sector

As seen in the last section, the effective field theory of the LH model can be parameterized by an $SU(5)/SO(5)$ NLSM with a gauged subgroup

$$G_1 \otimes G_2 = [SU(2)_1 \otimes U(1)_1] \otimes [SU(2)_2 \otimes U(1)_2]\,, \tag{4.1.16}$$

which is spontaneously broken down to the SM gauge group. In particular, by the symmetry breaking of the NLSM, the Lagrangian still preserves the full $[SU(2) \otimes U(1)]^2$ gauge symmetry. The leading order dimension-two term in the NLSM, describing the Σ field, can be written for the scalar sector [4, 52] as

$$\mathcal{L}_\Sigma = \frac{1}{2}\frac{f^2}{4}\mathrm{Tr}\left(D_\mu\Sigma\right)\left(D^\mu\Sigma\right)^\dagger . \tag{4.1.17}$$

The numerical coefficients have been chosen such that the scalar kinetic terms are canonically normalized. (4.1.17) is manifestly gauge invariant under $G_1 \otimes G_2$ if the covariant derivative is defined as

$$D_\mu\Sigma = \partial_\mu\Sigma - i\sum_{j=1}^{2}\left\{g_j W_{\mu j}^a\left(Q_j^a\Sigma + \Sigma Q_j^{aT}\right) + ig_j' B_{\mu j}\left(Y_j\Sigma + \Sigma Y_j^T\right)\right\}, \tag{4.1.18}$$

where the $SU(2)_{j=1,2}$ gauge fields are given by $W_{\mu j}^a$, the $U(1)_{j=1,2}$ gauge fields by $B_{\mu j}$ and the corresponding generators $Q_{1,2}^a$, $Y_{1,2}$ are defined in (4.1.12) and (4.1.13).

In order to write the Lagrangian in terms of the scalar fields h, ϕ and the gauge bosons, respectively, we linearize (4.1.17) by expanding Σ in powers of $1/f$ around its vacuum expectation value Σ_0,

$$\Sigma = \Sigma_0 + \frac{2i}{f}\begin{pmatrix} \phi^\dagger & \frac{h^\dagger}{\sqrt{2}} & \mathbf{0}_{2\times 2} \\ \frac{h^*}{\sqrt{2}} & 0 & \frac{h}{\sqrt{2}} \\ \mathbf{0}_{2\times 2} & \frac{h^T}{\sqrt{2}} & \phi \end{pmatrix} - \frac{1}{f^2}\begin{pmatrix} h^\dagger h^* & \sqrt{2}\phi^\dagger h^T & h^\dagger h + 2\phi^\dagger\phi \\ \sqrt{2}h\phi^\dagger & 2hh^\dagger & \sqrt{2}h^*\phi \\ h^T h^* + 2\phi\phi^\dagger & \sqrt{2}\phi h^\dagger & h^T h \end{pmatrix} + \mathcal{O}(\frac{1}{f^3}). \tag{4.1.19}$$

In the process of spontaneous symmetry breaking the local gauge symmetry $G_1 \otimes G_2$ is broken down to the diagonal subgroup $[SU(2)_L \otimes U(1)_Y]$ identified with the electroweak SM gauge group. The corresponding unbroken generators of $[SU(2)_L \otimes U(1)_Y]$ are given in (4.1.14) while the broken generators are

$$Q'^a = \frac{1}{\sqrt{g_1^4 + g_2^4}}\left(g_1^2 Q_1^a - g_2^2 Q_2^a\right). \tag{4.1.20}$$

In this process 4 of the 14 Goldstone bosons of the $SU(5) \to SO(5)$ breaking are eaten to give mass to 4 particular linear combinations of the gauge fields. This gives rise to mass terms of order f for half of the gauge bosons (the heavy W' and B')

$$m_{W'} = \frac{f}{2}\sqrt{g_1^2 + g_2^2} = \frac{g}{2sc}f, \qquad m_{B'} = \frac{f}{2\sqrt{5}}\sqrt{g_1'^2 + g_2'^2} = \frac{g'}{2\sqrt{5}s'c'}f. \tag{4.1.21}$$

Here s, c, s' and c' are the sines and cosines of the angles that describe the mixing of the $[SU(2)_1 \times U(1)_1] \otimes [SU(2)_2 \times U(1)_2]$ gauge bosons

$$\begin{aligned} W &= sW_1 + cW_2, & W' &= -cW_1 + sW_2 \\ B &= s'B_1 + c'B_2, & B' &= -c'B_1 + s'B_2. \end{aligned} \tag{4.1.22}$$

In (4.1.22) W_1 and W_2 each represent the three gauge bosons of $SU(2)_1$ and $SU(2)_2$, respectively, while B_1 and B_2 are the corresponding gauge bosons of $U(1)_1$ and $U(1)_2$. The corresponding mixing angles are given by

$$s = \frac{g_2}{\sqrt{g_1^2 + g_2^2}}, \qquad c = \frac{g_1}{\sqrt{g_1^2 + g_2^2}}, \tag{4.1.23}$$

$$s' = \frac{g_2'}{\sqrt{g_1'^2 + g_2'^2}}, \qquad c' = \frac{g_1'}{\sqrt{g_1'^2 + g_2'^2}}, \tag{4.1.24}$$

where $g_{1,2}$ are $SU(2)_{1,2}$ coupling constants and $g'_{1,2}$ the ones of $U(1)_{1,2}$. The W and B remain massless at this stage and can be identified with the SM gauge bosons, with couplings

$$g = g_1 s = g_2 c, \qquad g' = g_1' s' = g_2' c'. \tag{4.1.25}$$

Finally, we can obtain the couplings of the gauge bosons to the two scalar degrees of freedom by re-expressing (4.1.17) in terms of the mass eigenstates W, W', B and B' and using the expansion (4.1.19) of Σ in powers of $1/f$.

In the second step of the gauge symmetry breaking the SM group is broken down to $U(1)_Q$. Since the details of this breakdown are already presented in [5, 7] we will summarize only the most important results. After having broken the SM group to $U(1)_Q$ the mass eigenstates of the gauge bosons can be obtained by diagonalizing

$$\begin{aligned}
\mathcal{L}_{masses} = {} & W_\mu^{'a} W^{'a\mu} \left(\frac{m_{W'}^2}{2} - \frac{1}{8} g^2 v^2 \right) + (W_\mu^1 W^{1\mu} + W_\mu^2 W^{2\mu}) \left(\frac{1}{8} g^2 v^2 \left(1 - \frac{1}{6} \frac{v^2}{f^2} \right) \right) \\
& + W_\mu^3 W^{3\mu} \left(\frac{1}{8} g^2 v^2 \left(1 - \frac{1}{6} \frac{v^2}{f^2} \right) \right) + W_\mu^a W^{'a\mu} \left(-\frac{1}{4} g^2 v^2 \frac{(c^2 - s^2)}{2sc} \right) \\
& + B'_\mu B^{'\mu} \left(\frac{m_{B'}^2}{2} - \frac{1}{8} g'^2 v^2 \right) + B_\mu B^\mu \left(\frac{1}{8} g'^2 v^2 \left(1 - \frac{1}{6} \frac{v^2}{f^2} \right) \right) \\
& + B_\mu B^{'\mu} \left(-\frac{1}{4} g'^2 v^2 \frac{(c'^2 - s'^2)}{2s'c'} \right) + W_\mu^3 B^\mu \left(\frac{1}{4} g g' v^2 \left(1 - \frac{1}{6} \frac{v^2}{f^2} \right) \right) \\
& + W_\mu^{'3} B^{'\mu} \left(-\frac{1}{8} g g' v^2 \left(\frac{cs'}{sc'} + \frac{sc'}{cs'} \right) \right) + W_\mu^3 B^{'\mu} \left(-\frac{1}{4} g g' v^2 \frac{(c'^2 - s'^2)}{2s'c'} \right) \\
& + W_\mu^{'3} B^\mu \left(-\frac{1}{4} g g' v^2 \frac{(c^2 - s^2)}{2sc} \right),
\end{aligned} \tag{4.1.26}$$

with v denoting the vev of the neutral components of the complex doublet. In our analysis we will set the vev of the complex triplet, v', to zero.

The final mass eigenstates of the charged gauge bosons are $W_L^\pm$ and $W_H^\pm$ where the indices L and H stand for "light" and "heavy". The mass eigenstates are given by

$$W_L = W + \frac{v^2}{2f^2} sc(c^2 - s^2) W', \qquad W_H = W' - \frac{v^2}{2f^2} sc(c^2 - s^2) W, \tag{4.1.27}$$

while the corresponding masses read

$$M^2_{W^\pm_L} = m^2_W\left(1-\frac{v^2}{f^2}\left(\frac{1}{6}+\frac{1}{4}(c^2-s^2)^2\right)\right), \tag{4.1.28}$$

$$M^2_{W^\pm_H} = m^2_W\left(\frac{f^2}{s^2c^2v^2}-1\right). \tag{4.1.29}$$

As one can see from (4.1.28) and (4.1.29), the mass of the $W^\pm_L$ boson approaches the SM value $m_W \equiv gv/2$ when $f \to \infty$.

The neutral gauge boson mass eigenstates A_L, Z_L, A_H and Z_H are given by

$$\begin{aligned}
A_L &= -s_W W^3 + c_W B,\\
Z_L &= c_W W^3 + s_W B + x_Z^{W'}\frac{v^2}{f^2}W'^3 + x_Z^{B'}\frac{v^2}{f^2}B',\\
A_H &= B' + x_H\frac{v^2}{f^2}W'^3 - x_Z^{B'}\frac{v^2}{f^2}(c_W W^3 + s_W B),\\
Z_H &= W'^3 - x_H\frac{v^2}{f^2}B' - x_Z^{W'}\frac{v^2}{f^2}(c_W W^3 + s_W B),
\end{aligned} \tag{4.1.30}$$

with

$$\begin{aligned}
x_H &= \frac{5}{2}gg'\frac{scs'c'(c^2s'^2+s^2c'^2)}{(5g^2s'^2c'^2-g'^2s^2c^2)},\\
x_Z^{W'} &= \frac{1}{2c_w}sc(c^2-s^2),\\
x_Z^{B'} &= \frac{5}{2s_w}s'c'(c'^2-s'^2).
\end{aligned} \tag{4.1.31}$$

Here

$$s_W = \frac{g'}{\sqrt{g^2+g'^2}}, \qquad c_W = \frac{g}{\sqrt{g^2+g'^2}} \tag{4.1.32}$$

are the sine and the cosine of the Weinberg angle describing the weak mixing in the SM.

A_L and Z_L are the SM photon and Z^0 boson and A_H and Z_H the new heavy photon and heavy Z^0 boson, respectively. Their masses are given by

$$M^2_{A_L} = 0, \tag{4.1.33}$$

$$M^2_{Z_L} = m^2_Z\left(1-\frac{v^2}{f^2}\left(\frac{1}{6}+\frac{1}{4}(c^2-s^2)^2+\frac{5}{4}(c'^2-s'^2)^2\right)\right), \tag{4.1.34}$$

$$M^2_{A_H} = m^2_Z s^2_W\left(\frac{f^2}{5s'^2c'^2v^2}-1\right), \tag{4.1.35}$$

$$M^2_{Z_H} = m^2_W\left(\frac{f^2}{s^2c^2v^2}-1\right), \tag{4.1.36}$$

where m_Z is the SM Z^0 boson mass with $m_Z \equiv gv/(2c_W)$.

It is evident from (4.1.28) and (4.1.34) that the tree level SM relation

$$\frac{m^2_W}{m^2_Z} = c^2_W \tag{4.1.37}$$

is not valid for the $W_L^\pm$ and Z_L^0 masses. To $\mathcal{O}(v^2/f^2)$ we have [5]

$$\frac{M^2_{W_L^\pm}}{M^2_{Z_L}} = c_W^2 \left(1 + \frac{v^2}{f^2}\frac{5}{4}(c'^2 - s'^2)^2\right) \tag{4.1.38}$$

which reflects the tree level breaking of the custodial $SU(2)$ in the LH model. Formula (4.1.38) will play an important role in our later analysis.
From (4.1.28) and (4.1.29) we find

$$M_{W_H^\pm} = \frac{f}{v}\frac{M_{W_L^\pm}}{sc}, \tag{4.1.39}$$

which is valid to order v^2/f^2.

The formulae given above have already been presented in [5] but at a few places the results shown here differ from the ones presented there. We would like to spell out these differences explicitly.

- In going from (4.1.26) to (4.1.30) no field redefinitions have been made as done in [5]. As a result of this, the formulae in (4.1.30) differ from (A34) in [5] by B replaced by $-B$. This difference is a matter of choice and has no impact on physical results.

- The results for $x_Z^{W'}$ and $x_Z^{B'}$ in (4.1.31) differ by sign from the ones given in (A35) of [5]. This difference is crucial for the removal of the divergences in the calculations in the unitary gauge.

- In contrast to (A37) of [5] the presence of terms proportional to x_H can not be confirmed at this order as seen in (4.1.35) and (4.1.36). Moreover, the result shown here is consistent with that of the LH model with T-parity [11, 16, 17] presented in the next chapter, where the terms proportional to x_H are also absent at this order.

4.1.3 Fermions and Their Interactions

In the SM fermions become massive due to their couplings to the Higgs via Yukawa interactions, and so far we have not included any fermions in the theory. However, due to its large Yukawa coupling to the Higgs the top quark induces a large quadratically divergent contribution to the Higgs mass. In the LH model this problem is solved by adding new fermions to the theory in order to precisely cancel these top loops. The quadratic divergences coming from the other fermions do not constitute any problem, since their Yukawa couplings are much smaller than the one of the top quark so that their contributions at a scale Λ of order 10 TeV are quite negligible and do not necessitate fine-tuning.

The newly introduced fermions are a pair of vector-like, colored Weyl fermions $\tilde{t}$ and $\tilde{t}'^c$ with quantum numbers $(\mathbf{3},\mathbf{1})$ and $(\overline{\mathbf{3}},\mathbf{1})$ under the two global $SU(3)$s. For convenience we accommodate the new particles in the row vector $\chi = (b_3, t_3, \tilde{t})$. The quantum numbers of

these new particles further allows us to write down a bare mass term for the new fields of order f. The coupling of the SM top quark and the new fermions to the Goldstone boson field Σ is given by

$$\mathcal{L}_t = \frac{1}{2}\lambda_1 f \varepsilon_{ijk}\varepsilon_{xy}\chi_i \Sigma_{jx}\Sigma_{ky} u_3'^c + \lambda_2 f \tilde{t}\tilde{t}'^c + \text{h.c.}, \tag{4.1.40}$$

where i, j, k are summed over $1, 2, 3$ while x, y are summed over $4, 5$ and $u_3'^c$ corresponds to the right-handed top quark of the SM. It can be seen that the first term in (4.1.40) is $SU(3)_1$-invariant but breaks $SU(3)_2$, while for the second term the converse is true. Hence to generate a contribution to the Higgs mass parameter from the extended top sector, both λ_1 and λ_2 need to be turned on. From this it follows that a quadratic divergence cannot be generated at the one-loop level.

To extract the coupling of the fermions to the Goldstone bosons from (4.1.40), we expand the Σ field as given in (4.1.19). From this we obtain the following couplings

$$\begin{aligned}
\mathcal{L}_t \;=\; & \lambda_2 f \tilde{t}\tilde{t}'^c + i\lambda_1 \left\{ -b_3 \left[\sqrt{2}h^+ + \frac{i}{f}\left(\sqrt{2}h^-\phi^{++} + h^{0*}\phi^+ \right) \right] u_3'^c \right. \\
& -t_3 \left[\sqrt{2}h^0 + \frac{i}{f}\left(h^-\phi^+ + \sqrt{2}h^{0*}\phi^0 \right) \right] u_3'^c \\
& \left. + \tilde{t} \left[-if + \frac{i}{f}\left(h^+h^- + h^0h^{0*} + 2\phi^{++}\phi^{--} + \phi^+\phi^- + 2\phi^0\phi^{0*} \right) \right] u_3'^c \right\} + h.c.,
\end{aligned} \tag{4.1.41}$$

The most important contributions of (4.1.41) are

$$\mathcal{L}_t = \lambda_2 f \tilde{t}\tilde{t}'^c - \frac{\lambda_1}{f}\tilde{t}h^0h^{0*}u_3'^c + \lambda_1 f \tilde{t}u_3'^c - i\lambda_1\sqrt{2}q_3h^0u_3'^c + h.c. + ..., \tag{4.1.42}$$

where the dots indicate terms involving the heavy scalar ϕ, and $q_3 = (b_3, t_3)$. From the interactions given in (4.1.42) one can explicitly see how the quadratically divergent top loop gets canceled at one loop order by the new heavy fermions t_3, $\tilde{t}$, $u_3'^c$.

The Lagrangian in (4.1.41) contains a fermion mass term of order f. Defining the mixtures of $\tilde{t}^c$ and $u_3'^c$ as

$$\tilde{t}^c = \frac{1}{\sqrt{\lambda_1^2+\lambda_2^2}}\left(\lambda_2\tilde{t}'^c + \lambda_1 u_3'^c\right), \quad u_3^c = \frac{1}{\sqrt{\lambda_1^2+\lambda_2^2}}\left(-\lambda_1\tilde{t}'^c + \lambda_2 u_3'^c\right), \tag{4.1.43}$$

(4.1.41) can be diagonalized and yields a mass term $f\sqrt{\lambda_1^2+\lambda_2^2}\tilde{t}\tilde{t}^c = m_{\tilde{t}}\tilde{t}\tilde{t}^c$ for the heavy fermion.

After electroweak symmetry breaking at the scale v additional mass terms for the fermions are generated and the Lagrangian, after diagonalization, reads

$$\mathcal{L}_{mass} = -m_t t_L t_R^c - M_T T_L T_R^c, \tag{4.1.44}$$

where the masses up to order v^2/f^2 are given by

$$\begin{aligned} m_t &= \frac{\lambda_1\lambda_2}{\sqrt{\lambda_1^2+\lambda_2^2}}v\left\{1+\frac{v^2}{f^2}\left[-\frac{1}{3}+\frac{fv'}{v^2}+\frac{1}{2}\frac{\lambda_1^2}{\lambda_1^2+\lambda_2^2}\left(1-\frac{\lambda_1^2}{\lambda_1^2+\lambda_2^2}\right)\right]\right\}, \\ M_T &= f\sqrt{\lambda_1^2+\lambda_2^2}\left[1+\mathcal{O}(v^2/f^2)\right]. \end{aligned} \tag{4.1.45}$$

Moreover, the physical mass eigenstates t_L, t_R^c, T_L, T_R^c, which correspond to the masses in (4.1.45), are given by the following rotation

$$t_L = c_L t_3 - s_L\tilde{t}, \quad t_R^c = c_R u_3'^c - s_R\tilde{t}'^c \tag{4.1.46}$$

$$T_L = s_L t_3 + c_L\tilde{t}, \quad T_R^c = s_R u_3'^c + s_R\tilde{t}'^c \tag{4.1.47}$$

with the rotation angles

$$\begin{aligned} s_L &= x_L\frac{v}{f}\left[1+\frac{v^2}{f^2}d_2\right], \\ c_L &= 1-\frac{x_L^2}{2}\frac{v^2}{f^2}, \\ s_R &= \sqrt{x_L}\left[1-\frac{v^2}{f^2}(1-x_L)\left(\frac{1}{2}-x_L\right)\right], \\ c_R &= \sqrt{1-x_L}\left[1+\frac{v^2}{f^2}x_L\left(\frac{1}{2}-x_L\right)\right]. \end{aligned} \tag{4.1.48}$$

Expressing M_T in terms of m_t we get the useful relation

$$M_T = \frac{f}{v}\frac{m_t}{\sqrt{x_L(1-x_L)}}\left(1+\frac{v^2}{f^2}\left(\frac{1}{3}-x_L(1-x_L)\right)\right), \qquad x_L = \frac{\lambda_1^2}{\lambda_1^2+\lambda_2^2}. \tag{4.1.49}$$

Following [5] λ_1 and λ_2 in (4.1.40) are expected to be $\mathcal{O}(1)$ with

$$\lambda_i \geq \frac{m_t}{v}, \qquad \text{or} \qquad \frac{1}{\lambda_1^2}+\frac{1}{\lambda_2^2} \approx \left(\frac{v}{m_t}\right)^2. \tag{4.1.50}$$

Thus, within a good approximation we can express in terms of the mass m_t and the mixing parameter x_L

$$\lambda_1 = \frac{m_t}{v}\frac{1}{\sqrt{1-x_L}}, \qquad \lambda_2 = \frac{m_t}{v}\frac{1}{\sqrt{x_L}}, \tag{4.1.51}$$

where x_L can in principle vary in the range $0 < x_L < 1$. As discussed in [5, 6, 13], the parameter x_L is crucial for the gauge interactions of the heavy T quark. For $x_L \approx 0$ and $x_L \approx 1$, the mass M_T becomes very large [13].

In summary we see that the Lagrangian (4.1.42) includes all desired features: the quadratic divergence due to the top loop is canceled, and the SM Yukawa coupling to the quark doublet

$$\lambda_t q_3 h^0 u_3^c, \quad \text{with} \quad \lambda_t = \frac{\lambda_1\lambda_2}{\sqrt{\lambda_1^2+\lambda_2^2}} \tag{4.1.52}$$

is reproduced at low energies by integrating out the heavy quark from the Lagrangian (4.1.42).

The scalar interactions of the up-type quarks of the first two generations can be chosen to take the same form as in (4.1.40), except that there is no need for the extra vector-like quarks $\tilde{t}, \tilde{t}'^c$. The interactions with the down-type quarks and leptons of the three generations are generated by a similar Lagrangian.

4.1.4 The Effective Higgs Potential and Electroweak Symmetry Breaking

In the LH model, the appearance of a Higgs potential is forbidden at tree level due to the global symmetries protecting the Lagrangian. However, a potential for the Higgs is generated by quantum effects at one- and higher-loop level since the Yukawa and gauge interactions explicitly break all the symmetries of the Lagrangian. Such radiative corrections by vector boson and fermion loops result in a Coleman-Weinberg potential which can be generically parameterized as

$$V = \lambda_{\phi^2} f^2 \mathrm{Tr}\left(\phi^\dagger \phi\right) + i\lambda_{h\phi h} f\left(h\phi^\dagger h^T - h^*\phi h^\dagger\right) - \mu^2 h h^\dagger + \lambda_{h^4}\left(h h^\dagger\right)^2, \tag{4.1.53}$$

where terms involving ϕ^4 and $h^2\phi^2$ have been neglected due to their small contributions to the vacuum expectation value of h.

First we are going to compute the quadratically divergent one-loop contributions to the Coleman-Weinberg potential coming from gauge bosons. This contribution is given by [53]

$$\frac{\Lambda^2}{(4\pi)^2}\mathrm{Tr}M_V^2(\Sigma), \tag{4.1.54}$$

where $M_V^2(\Sigma)$ is the gauge boson mass matrix in the presence of a background field Σ and can be determined from the covariant derivative (4.1.18). A calculation of this contributions then yields [4]

$$\mathcal{L}_a = \frac{1}{2} a f^4 \left\{ g_j^2 \sum_n \mathrm{Tr}\left[\left(Q_j^n \Sigma\right)\left(Q_j^n \Sigma\right)^*\right] + g_j'^2 \mathrm{Tr}\left[\left(Y_j \Sigma\right)\left(Y_j \Sigma\right)^*\right] \right\}. \tag{4.1.55}$$

Here we cut off the quadratically divergent contributions of the gauge bosons at a scale $\Lambda = 4\pi f$, and a is a $\mathcal{O}(1)$ coefficient, whose precise value depends on the unknown UV physics at Λ. Linearizing the Σ field in terms of the fields h and ϕ, we can rewrite the potential as

$$\begin{aligned}\mathcal{L}_a &= \frac{1}{2} a\left(g_1^2 + g_1'^2\right)\left[f^2 \mathrm{Tr}\left(\phi^\dagger\phi\right) - \frac{if}{2}\left(h\phi^\dagger h^T - h^*\phi h^\dagger\right) + \frac{1}{4}\left(h h^\dagger\right)^2 + ...\right] \\ &+ \frac{1}{2} a\left(g_2^2 + g_2'^2\right)\left[f^2 \mathrm{Tr}\left(\phi^\dagger\phi\right) + \frac{if}{2}\left(h\phi^\dagger h^T - h^*\phi h^\dagger\right) + \frac{1}{4}\left(h h^\dagger\right)^2 + ...\right].\end{aligned} \tag{4.1.56}$$

The last expression (4.1.56) can also be understood by looking at the $SU(3)$ transformation properties of h and ϕ. Following [4] these two fields transform under an $SU(3)_1$ according to

$$h_i \rightarrow h_i + f\varepsilon_i + ... \tag{4.1.57}$$

$$\phi_{ij} \rightarrow \phi_{ij} - i\left(\varepsilon_i h_j + \varepsilon_j h_i\right) + ... \tag{4.1.58}$$

while under an $SU(3)_2$ they transform as

$$h_i \rightarrow h_i + f\eta_i + ... \tag{4.1.59}$$

$$\phi_{ij} \rightarrow \phi_{ij} + i\left(\eta_i h_j + \eta_j h_i\right) + ... \ . \tag{4.1.60}$$

Then the invariant quantities are given by

$$\left|\phi_{ij} \pm \frac{i}{2f}\left(h_i h_j + h_j h_i\right)\right|^2 . \tag{4.1.61}$$

Upon expansion, this yields exactly the terms in square brackets in (4.1.56).

Similarly we calculate the quadratically divergent contribution to the Coleman-Weinberg potential arising from fermion loops [4],

$$\mathcal{L}_{a'} = -\frac{1}{2}a'\lambda_1^2 f^4 \varepsilon^{wx}\varepsilon_{yz}\varepsilon^{ijk}\varepsilon_{kmn}\Sigma_{iw}\Sigma_{jx}\Sigma^{*my}\Sigma^{*nz} + \text{h.c.} \ . \tag{4.1.62}$$

Since the fermion-Higgs interaction preserves the $SU(3)_1$ global symmetry in the upper 3×3 block of Σ, the contribution of fermions must have the same form as the term proportional to $g_2^2 + g_2'^2$ in (4.1.56) with a coefficient now given by $-\frac{1}{2}a'\lambda_1^2$.

Adding up these two contributions from gauge bosons and fermions we end up with the overall potential given by

$$\left(\frac{1}{2}a\left(g_1^2 + g_1'^2\right) - \frac{1}{2}a'\lambda_1^2\right) f^2 \left|\phi_{ij} + \frac{i}{2f}\left(h_i h_j + h_j h_i\right)\right|^2 \tag{4.1.63}$$

$$+\frac{1}{2}a\left(g_2^2 + g_2'^2\right) f^2 \left|\phi_{ij} - \frac{i}{2f}\left(h_i h_j + h_j h_i\right)\right|^2 \ . \tag{4.1.64}$$

In order to find the equation of motion for ϕ, we determine the minimum of the overall potential, which imposes the following condition on ϕ_{ij}

$$\left[a\left(g_1^2 + g_1'^2\right) - a'\lambda_1^2\right]\left(\phi_{ij} + \frac{i}{f}h_i h_j\right) + a\left(g_2^2 + g_2'^2\right)\left(\phi_{ij} - \frac{i}{f}h_i h_j\right) = 0. \tag{4.1.65}$$

Thus, at energies below the triplet mass, after having integrated out ϕ, we are left with a quartic potential for h

$$\lambda\left(hh^\dagger\right)^2, \quad \text{where} \quad \lambda = a\frac{\left(g_1^2 + g_1'^2 - a'/a\lambda_1^2\right)\left(g_2^2 + g_2'^2\right)}{g_1^2 + g_1'^2 - a'/a\lambda_1^2 + g_2^2 + g_2'^2}. \tag{4.1.66}$$

We can see from (4.1.66) that turning off the gauge couplings g_2 and g_2' restores the $SU(3)_2$ symmetry and indeed sets $\lambda = 0$. Similarly, turning off the $SU(3)_1$ breaking terms g_1, g_1' and λ_1 again yields $\lambda = 0$ and a Higgs potential is not generated.

One further remark is in order here. From (4.1.56) and (4.1.62) we can express the coefficients λ_{h^4}, $\lambda_{h\phi h}$ and λ_{ϕ^2} in terms of c, c', s, s' g, g' and λ_1. In particular, we find the relation

$$\lambda_{h^4} = \frac{1}{4}\lambda_{\phi^2}. \tag{4.1.67}$$

For further details the reader is referred to [5].

4.2 Feynman Rules in the Littlest Higgs Model

Charged Gauge Boson–Fermion Interactions

The Feynman rules for vertices involving the charged $W_L^\pm$ and $W_H^\pm$ gauge bosons and quarks in the notation $C\gamma_\mu(1-\gamma_5)$ [7] are given in Table 4.1. Here x_L is given in (4.1.49) while a, b and d_2 are defined by

$$a = \frac{1}{2}c^2(c^2-s^2), \qquad b = \frac{1}{2}s^2(c^2-s^2), \qquad d_2 = -\frac{5}{6}+\frac{1}{2}x_L^2+2x_L(1-x_L). \tag{4.2.68}$$

For leptons the Feynman rules can be obtained from the entries of the first line with $V_{ij}=1$. The V_{ij} are the usual CKM parameters. The issue of the violation of the CKM unitarity at $\mathcal{O}(v^2/f^2)$ has already been discussed in detail in [6] and will not be repeated here. Table 4.1 should be compared with Table VIII of [5]. Due to different phase conventions for the t and T fields, the rules for the vertices $W_L^\pm \bar{T} d_j$ and $W_H^\pm \bar{T} d_j$ differ by a crucial factor i as already discussed in [6].

Table 4.1: Feynman Rules in LH Model for $W_{L,H}$: $C\gamma_\mu(1-\gamma_5)$.

Vertex	C	Vertex	C
$W_L^+\bar{u}_i d_j$	$\frac{ig}{2\sqrt{2}}\, V_{ij}\left(1-\frac{v^2}{f^2}a\right)$	$W_H^+\bar{u}_i d_j$	$-\frac{ig}{2\sqrt{2}}\, V_{ij}\frac{c}{s}\left(1+b\frac{v^2}{f^2}\right)$
$W_L^+\bar{t} d_j$	$\frac{ig}{2\sqrt{2}}\, V_{tj}\left(1-\frac{v^2}{f^2}(\frac{1}{2}x_L^2+a)\right)$	$W_H^+\bar{t} d_j$	$-\frac{ig}{2\sqrt{2}}\, V_{tj}\frac{c}{s}\left(1-\frac{v^2}{f^2}(\frac{1}{2}x_L^2-b)\right)$
$W_L^+\bar{T} d_j$	$\frac{ig}{2\sqrt{2}}\, V_{tj}\, x_L\, \frac{v}{f}\left(1+\frac{v^2}{f^2}(d_2-a)\right)$	$W_H^+\bar{T} d_j$	$-\frac{ig}{2\sqrt{2}}\, V_{tj}\frac{c}{s}\, x_L\, \frac{v}{f}$

Neutral Gauge Boson–Fermion Interactions

The vertices involving quarks and leptons and the neutral gauge bosons Z_L^0, Z_H^0 and A_H^0, that are relevant for the decays considered in the next section, are presented in Table 4.2, where g_V and g_A universally parameterize the vertices as follows:

$$i\gamma_\mu(g_V+g_A\gamma_5), \tag{4.2.69}$$

and

$$u = (c'^2-s'^2), \qquad a' = \frac{1}{2}c'^2(c'^2-s'^2). \tag{4.2.70}$$

These rules follow from (A55) of [5] that we confirmed except for the signs in $x_Z^{W'}$ and $x_Z^{B'}$ in (4.1.31) as discussed above. In spite of agreeing with (A55) the rules presented in Table 4.2 differ surprisingly at various places from Table IX of [5]. The differences are found in the couplings $Z_L\bar{u}u$, $Z_L\bar{t}t$, $Z_L\bar{T}t$, $A_H\bar{T}T$ and $Z_H\bar{T}T$. They all are crucial for the cancellation of the divergences in the calculations discussed below. In order to make the comparison with

[5] as simple as possible, Table 4.2 has exactly the same form as table IX of [5]. Table 4.2 contains also higher order terms in v/f that were required in the calculation of diagrams in classes 4 and 5 discussed below and were not present in [5].

As discussed in [5], the gauge invariance of the Yukawa interactions alone cannot unambiguously fix all the $U(1)$ charge values. The two parameters y_e and y_u that enter the Feynman rules in Table 4.2 are undetermined. Requiring that the $U(1)$ charge assignments are anomaly free, they can be fixed to be

$$y_e = \frac{3}{5}, \qquad y_u = -\frac{2}{5}. \tag{4.2.71}$$

On the other hand, as emphasized in [5], in an effective field theory valid below a cutoff, it is unnecessary to be completely anomaly free as the anomalies could be canceled by some specific extra matter at the cutoff scale. In the rest of this thesis y_e and y_u are set to the values given in (4.2.71) in order to avoid additional sensitivity to the physics at the cut-off scale.

The rules for the triple gauge boson vertices can be found in Table VII of [5] and are not presented here.

Charged Scalar Interactions

Only the following Feynman rules given in [5] are of relevance in this thesis:

$$\Phi^+ \bar{u}_i d_j : \quad -\frac{i}{\sqrt{2}} \frac{g}{4} \frac{m_i}{M_{W_L}} (1-\gamma_5) \frac{v}{f} V_{ij} \tag{4.2.72}$$

$$\Phi^+ \bar{T} d_j : \quad -\frac{i}{\sqrt{2}} \frac{g}{4} \frac{m_t}{M_{W_L}} (1-\gamma_5) \frac{\lambda_1}{\lambda_2} \frac{v}{f} V_{tj} \tag{4.2.73}$$

$$\Phi^+ \Phi^- Z_L : \quad i \frac{g}{c_w} s_w^2 (p_+ - p_-)_\mu \tag{4.2.74}$$

with $p_\pm$ being the outgoing momenta of $\Phi^\pm$. For the $\Phi^- \bar{d}_j u_i$ vertex, $(1-\gamma_5)$ should be replaced by $(1+\gamma_5)$ and V_{ij} by V_{ij}^*. The case for $\Phi^- \bar{d}_j T$ is analogous.

4.3 Rare Decays in the Littlest Higgs Model

4.3.1 X and Y Functions

To describe the physics of rare decays it is convenient to use the framework of an effective field theory. In such an effective field theory it is possible to formulate the physics by a certain set of parameters without any reference to what is going on at arbitrarily small distances. With the help of the Operator Product Expansion the effective Hamiltonian can generally be written as

$$\mathcal{H}_{eff} = \mathcal{H}_{light} + \frac{G_F}{\sqrt{2}} \sum_i V_{CKM}^i C_i(\mu) \mathcal{O}_i, \tag{4.3.75}$$

Table 4.2: Feynman Rules in the LH Model for the gauge bosons Z_L, A_H and Z_H. g_V and g_A are defined through (4.2.69).

vertex	g_V	g_A
$A_L\bar{f}f$	$-eQ_f$	0
$Z_L\bar{u}u$	$-\frac{g}{2c_w}\left\{(\frac{1}{2}-\frac{4}{3}s_w^2)-\frac{v^2}{f^2}\left[c_w x_Z^{W'}c/2s+\frac{s_w x_Z^{B'}}{s'c'}\left(2y_u+\frac{17}{15}-\frac{5}{6}c'^2\right)\right]\right\}$	$-\frac{g}{2c_w}\left\{-\frac{1}{2}-\frac{v^2}{f^2}\left[-c_w x_Z^{W'}c/2s+\frac{s_w x_Z^{B'}}{s'c'}\left(\frac{1}{5}-\frac{1}{2}c'^2\right)\right]\right\}$
$Z_L\bar{d}d$	$-\frac{g}{2c_w}\left\{(-\frac{1}{2}+\frac{2}{3}s_w^2)-\frac{v^2}{f^2}\left[-c_w x_Z^{W'}c/2s+\frac{s_w x_Z^{B'}}{s'c'}\left(2y_u+\frac{11}{15}+\frac{1}{6}c'^2\right)\right]\right\}$	$-\frac{g}{2c_w}\left\{\frac{1}{2}-\frac{v^2}{f^2}\left[c_w x_Z^{W'}c/2s+\frac{s_w x_Z^{B'}}{s'c'}\left(-\frac{1}{5}+\frac{1}{2}c'^2\right)\right]\right\}$
$Z_L\bar{e}e$	$-\frac{g}{2c_w}\left\{(-\frac{1}{2}+2s_w^2)-\frac{v^2}{f^2}\left[-c_w x_Z^{W'}c/2s+\frac{s_w x_Z^{B'}}{s'c'}\left(2y_e-\frac{9}{5}+\frac{3}{2}c'^2\right)\right]\right\}$	$-\frac{g}{2c_w}\left\{\frac{1}{2}-\frac{v^2}{f^2}\left[c_w x_Z^{W'}c/2s+\frac{s_w x_Z^{B'}}{s'c'}\left(-\frac{1}{5}+\frac{1}{2}c'^2\right)\right]\right\}$
$Z_L\bar{\nu}\nu$	$-\frac{g}{2c_w}\left\{\frac{1}{2}-\frac{v^2}{f^2}\left[c_w x_Z^{W'}c/2s+\frac{s_w x_Z^{B'}}{s'c'}\left(y_e-\frac{4}{5}+\frac{1}{2}c'^2\right)\right]\right\}$	$-\frac{g}{2c_w}\left\{-\frac{1}{2}-\frac{v^2}{f^2}\left[-c_w x_Z^{W'}c/2s+\frac{s_w x_Z^{B'}}{s'c'}\left(-y_e+\frac{4}{5}-\frac{1}{2}c'^2\right)\right]\right\}$
$Z_L\bar{t}t$	$-\frac{g}{2c_w}\left\{(\frac{1}{2}-\frac{4}{3}s_w^2)-\frac{v^2}{f^2}\left[x_L^2/2+c_w x_Z^{W'}c/2s+\frac{s_w x_Z^{B'}}{s'c'}\left(2y_u+\frac{17}{15}-\frac{5}{6}c'^2-\frac{1}{5}\frac{\lambda_1^2}{\lambda_1^2+\lambda_2^2}\right)\right]\right\}$	$-\frac{g}{2c_w}\left\{-\frac{1}{2}-\frac{v^2}{f^2}\left[-x_L^2/2-c_w x_Z^{W'}c/2s+\frac{s_w x_Z^{B'}}{s'c'}\left(\frac{1}{5}-\frac{1}{2}c'^2-\frac{1}{5}\frac{\lambda_1^2}{\lambda_1^2+\lambda_2^2}\right)\right]\right\}$
$Z_L\bar{T}T$	$\frac{g}{2c_w}\left\{\frac{4}{3}s_w^2+\frac{v^2}{f^2}\left(-\frac{1}{2}x_L^2+\frac{s_w x_Z^{B'}}{s'c'}(2y_u+\frac{14}{15}-\frac{4}{3}c'^2+\frac{1}{5}x_L)\right)\right\}$	$\frac{g}{2c_w}\frac{v^2}{f^2}\left\{\frac{1}{2}x_L^2+\frac{s_w x_Z^{B'}}{s'c'}\frac{1}{5}x_L\right\}$
$Z_L\bar{T}t$	$\frac{g}{2c_w}\left\{-\frac{v}{f}\frac{1}{2}x_L+\frac{v^2}{f^2}\frac{s_w x_Z^{B'}}{c's'}\left(\frac{1}{5}x_L\frac{\lambda_2}{\lambda_1}\right)+\frac{v^3}{f^3}\left(\frac{1}{4}x_L^3-\frac{1}{2}x_L d_2+x_L(\frac{c'}{s'}\frac{s_w x_Z^{B'}}{2}+\frac{c}{s}\frac{c_w x_Z^{W'}}{2})\right)\right\}$	$\frac{g}{2c_w}\left\{\frac{v}{f}\frac{1}{2}x_L+\frac{v^2}{f^2}\frac{s_w x_Z^{B'}}{c's'}\left(\frac{1}{5}x_L\frac{\lambda_2}{\lambda_1}\right)+\frac{v^3}{f^3}\left(-\frac{1}{4}x_L^3+\frac{1}{2}x_L d_2-x_L(\frac{c'}{s'}\frac{s_w x_Z^{B'}}{2}+\frac{c}{s}\frac{c_w x_Z^{W'}}{2})\right)\right\}$
$A_H\bar{u}u$	$\frac{g'}{2s'c'}\left(2y_u+\frac{17}{15}-\frac{5}{6}c'^2\right)$	$\frac{g'}{2s'c'}\left(\frac{1}{5}-\frac{1}{2}c'^2\right)$
$A_H\bar{d}d$	$\frac{g'}{2s'c'}\left(2y_u+\frac{11}{15}+\frac{1}{6}c'^2\right)$	$\frac{g'}{2s'c'}\left(-\frac{1}{5}+\frac{1}{2}c'^2\right)$
$A_H\bar{e}e$	$\frac{g'}{2s'c'}\left(2y_e-\frac{9}{5}+\frac{3}{2}c'^2\right)$	$\frac{g'}{2s'c'}\left(-\frac{1}{5}+\frac{1}{2}c'^2\right)$
$A_H\bar{\nu}\nu$	$\frac{g'}{2s'c'}\left(y_e-\frac{4}{5}+\frac{1}{2}c'^2\right)$	$\frac{g'}{2s'c'}\left(-y_e+\frac{4}{5}-\frac{1}{2}c'^2\right)$
$A_H\bar{t}t$	$\frac{g'}{2s'c'}\left(2y_u+\frac{17}{15}-\frac{5}{6}c'^2-\frac{1}{5}\frac{\lambda_1^2}{\lambda_1^2+\lambda_2^2}\right)$	$\frac{g'}{2s'c'}\left(\frac{1}{5}-\frac{1}{2}c'^2-\frac{1}{5}\frac{\lambda_1^2}{\lambda_1^2+\lambda_2^2}\right)$
$A_H\bar{T}T$	$\frac{g'}{2s'c'}\left(2y_u+\frac{14}{15}-\frac{4}{3}c'^2+\frac{1}{5}\frac{\lambda_1^2}{\lambda_1^2+\lambda_2^2}\right)$	$\frac{g'}{2s'c'}\frac{1}{5}\frac{\lambda_1^2}{\lambda_1^2+\lambda_2^2}$
$A_H\bar{T}t$	$\frac{g'}{2s'c'}\left(\frac{1}{5}x_L\frac{\lambda_2}{\lambda_1}+\frac{v}{f}\frac{1}{2}c'^2x_L\right)$	$\frac{g'}{2s'c'}\left(\frac{1}{5}x_L\frac{\lambda_2}{\lambda_1}-\frac{v}{f}\frac{1}{2}c'^2x_L\right)$
$Z_H\bar{u}u$	$gc/4s$	$-gc/4s$
$Z_H\bar{d}d$	$-gc/4s$	$gc/4s$
$Z_H\bar{e}e$	$-gc/4s$	$gc/4s$
$Z_H\bar{\nu}\nu$	$gc/4s$	$-gc/4s$
$Z_H\bar{t}t$	$gc/4s$	$-gc/4s$
$Z_H\bar{T}T$	$\mathcal{O}(v^2/f^2)$	$\mathcal{O}(v^2/f^2)$
$Z_H\bar{T}t$	$gx_Lvc/4fs$	$-gx_Lvc/4fs$

where the $\mathcal{O}_i$ are the relevant local operators of the considered decay. In this sense the effective Hamiltonian $\mathcal{H}_{eff}$ in (4.3.75) can be regarded as a sum of effective vertices accompanied by effective coupling constants $C_i(\mu)$. Formally, the effective theory can be derived by integrating out the heavy particles within the path integral formalism.

In earlier papers [6, 12, 13] the effects of the Littlest Higgs model without T-Parity on particle-antiparticle mixing and other processes have been analyzed. In this section, however, we will be concerned with the impact of the LH on the rare decays $K^+ \to \pi^+ \nu\bar{\nu}$, $K_L \to \pi^0 \nu\bar{\nu}$ and $B_{s,d} \to \mu^+\mu^-$, where the effective Hamiltonian is governed by the functions X and Y. These functions can be determined from Z^0 penguins and the corresponding box contributions to the effective Hamiltonian with $\nu\bar{\nu}$ and $\mu\bar{\mu}$ in the final state, respectively. Adding these two contributions yields the final effective Hamiltonian which is then given by

$$\left(\mathcal{H}_{eff}^{\bar{\nu}\nu}\right)_{Z+Box} = \frac{g^4}{64\pi^2}\frac{1}{M_W^2}\underbrace{\left(C(v) + B^{\nu\bar{\nu}}(v)\right)}_{=X(v)}(\bar{s}d)_{V-A}(\bar{\nu}\nu)_{V-A}\,, \tag{4.3.76}$$

$$\left(\mathcal{H}_{eff}^{\mu\bar{\mu}}\right)_{Z+Box} = \frac{g^4}{64\pi^2}\frac{1}{M_W^2}\underbrace{\left(C(v) + B^{\mu\bar{\mu}}(v)\right)}_{=Y(v)}(\bar{s}d)_{V-A}(\bar{\mu}\mu)_{V-A}\,. \tag{4.3.77}$$

From (4.3.77) one can see that the gauge independent functions $X(v)$ and $Y(v)$ are defined through the linear combinations $C(v) + B^{\nu\bar{\nu}}(v)$ and $C(v) + B^{\mu\bar{\mu}}(v)$, respectively.

In the Littlest Higgs model the functions X and Y are modified through contributions coming from penguin and box diagrams involving the new heavy fields W_H, Z_H, A_H, T and $\Phi^{\pm}$. To determine these contributions it is useful to group the diagrams contributing at $\mathcal{O}(v^2/f^2)$ into six distinct classes, which are shown in Appendix A.1.

In class 1 we group all the diagrams with modifications of the SM vertices, where the circles around the vertices indicate the $\mathcal{O}(v^2/f^2)$ corrections *without* the x_L^2 terms. Additionally, we also include the $W_L W_H Z_L$ triple vertex and the (W_L,A_H) penguin diagrams in this class. The second class contains the contributions of the standard top quark in the (W_H,Z_L) and (W_L,Z_H) penguin diagrams, the (W_L,W_H) box diagram and the diagrams with the $W_L W_H Z_H$ and $W_H W_H Z_L$ triple vertices of order v^2/f^2. All diagrams involving the new heavy T quark and the modifications from the SM top quark proportional to x_L^2 are displayed in Fig. A.3 and belong to the third class. Further contributions containing the heavy top quark T are summarized in class 4 and 5. Although being suppressed by a factor v^4/f^4, these classes of diagrams have to be considered, since the mass of the heavy T is of order f and therefore leads to a relevant v^2/f^2 contribution. For completeness, in Figure A.6 we show class 6, which contains all the diagrams involving $\Phi^{\pm}$.

Apart from the diagrams given in Appendix A.1 we may also not forget that in the LH model the custodial $SU(2)$ symmetry is already broken at the v^2/f^2 level. Since we have to express the M_Z mass in the Z-penguin in terms of M_W, the breakdown of the custodial symmetry yields additional $\mathcal{O}(v^2/f^2)$ corrections. These corrections arise from diagrams of

class 1 and Z_L penguins with heavy top quark T of class 3 and are given by

$$\Delta X_{\text{Custodial 1}} = \Delta Y_{\text{Custodial 1}} = \frac{v^2}{f^2}\frac{5}{4}(c'^2 - s'^2)^2 C(x_t)_{\text{unitary}}, \tag{4.3.78}$$

$$\Delta X_{\text{Custodial 3}} = \Delta Y_{\text{Custodial 3}} = \frac{v^4}{f^4}\frac{5}{4}(c'^2 - s'^2)^2 x_L^2 C(x_T)_{\text{Class 3}}, \tag{4.3.79}$$

with

$$\begin{aligned} C(x_t)_{\text{unitary}} &= -\frac{x_t}{16}\left(\frac{1}{\varepsilon} + \ln\frac{\mu^2}{M_{W_L}^2}\right) - \frac{x_t^2 - 7x_t}{32(1-x_t)} + \frac{4x_t - 2x_t^2 + x_t^3}{16(1-x_t)^2}\log x_t, \\ C(x_T)_{\text{class 3}} &= -\frac{x_T}{16}\left(\frac{1}{\varepsilon} + \ln\frac{\mu^2}{M_{W_L}^2}\right) - \frac{3x_T}{32} + \frac{(-2+x_T)\log x_T}{16}. \end{aligned}$$

After the calculation of all diagrams coming from these 6 classes [7] we can see that the classes 2, 3 and 4 are free of divergences, whereas some divergences contained in class 1 and 5 can only cancel in the sum together with the inclusion of the singularities from (4.3.78) and (4.3.79) due to the breakdown of the custodial $SU(2)$ symmetry.

However, as already mentioned earlier we are left with some singularities coming from classes 1, 5 and charged Higgs diagrams of class 6. In summary, we obtain the final divergence

$$C_{\text{div}} = \frac{x_t}{64}\frac{1}{1-x_L}\frac{v^2}{f^2}\left(-\frac{S_1}{5} + S_2\right), \tag{4.3.80}$$

where we used the abbreviations S_1 resulting from classes 1 and 5 and S_2 from charged Higgs diagrams,

$$S_1 = \frac{1}{\varepsilon} + \ln\frac{\mu^2}{M_{W_L}^2} \qquad \text{and} \qquad S_2 = \frac{1}{\varepsilon} + \ln\frac{\mu^2}{M_\Phi^2}. \tag{4.3.81}$$

After these comments on our calculation we can now write down our results for X and Y in the LH model, that are necessary to describe the phenomenology of rare decays like $K_L \to \pi^0\nu\bar{\nu}$, $K^+ \to \pi^+\nu\bar{\nu}$ and $B_{s,d} \to \mu^+\mu^-$. From our calculation we find the following functions $X_{\text{LH}}(x_t, z)$ and $Y_{\text{LH}}(x_t, z)$

$$X_{\text{LH}}(x_t, z) = X_{\text{SM}}(x_t) + \Delta X_1 + \Delta X_2 + \Delta X_3 + \Delta X_4 + \Delta X_5 + \Delta X_6, \tag{4.3.82}$$

$$Y_{\text{LH}}(x_t, z) = Y_{\text{SM}}(x_t) + \Delta Y_1 + \Delta Y_2 + \Delta Y_3 + \Delta Y_4 + \Delta Y_5 + \Delta Y_6, \tag{4.3.83}$$

where the parameter z in (4.3.82) and (4.3.83) denotes collectively all the parameters in the LH model. As seen in Appendix A.3 the singularities mentioned in (4.3.80) are included in the contributions ΔX_1, ΔX_5, ΔX_6 and ΔY_1, ΔY_5, ΔY_6, respectively. In detail, we find for each contribution ΔX_i and ΔY_i

$$\Delta X_1 = \frac{v^2}{f^2}U_1, \qquad \Delta X_2 = c^4\frac{v^2}{f^2}U_2 = \frac{c^2}{s^2}\frac{1}{y}U_2, \tag{4.3.84}$$

$$\Delta X_3 = x_L^2\frac{v^2}{f^2}U_3, \qquad \Delta X_4 = x_L^2 c^4\frac{v^4}{f^4}U_4 = x_L^2\frac{c^2}{s^2}\frac{1}{y}\frac{v^2}{f^2}U_4, \tag{4.3.85}$$

$$\Delta X_5 = x_L^2\frac{v^4}{f^4}U_5, \qquad \Delta X_6 = \frac{v^2}{f^2}\frac{x_t}{128}\frac{1}{1-x_L}\left(1 - 2x_L U_6(\hat{x}_T)\right), \tag{4.3.86}$$

and

$$\Delta Y_1 = \frac{v^2}{f^2} V_1, \qquad \Delta Y_2 = c^4 \frac{v^2}{f^2} V_2 = \frac{c^2}{s^2} \frac{1}{y} V_2, \tag{4.3.87}$$

$$\Delta Y_3 = x_L^2 \frac{v^2}{f^2} V_3, \qquad \Delta Y_4 = x_L^2 c^4 \frac{v^4}{f^4} V_4 = x_L^2 \frac{c^2}{s^2} \frac{1}{y} \frac{v^2}{f^2} V_4, \tag{4.3.88}$$

$$\Delta Y_5 = x_L^2 \frac{v^4}{f^4} V_5, \qquad \Delta Y_6 = \Delta X_6, \tag{4.3.89}$$

where the different functions U_i and V_6 can be found in the Appendix A.3. Finally, after having included the finite parts of the two corrections due to the custodial relation given by (4.3.78) and (4.3.79) into the X and Y functions of class 1 and 5 the final results (4.3.82) and (4.3.83) turn out to be independent of s'.

4.3.2 The Issue of Leftover Singularities

It may seem surprising that FCNC amplitudes considered in the previous section contain residual ultraviolet divergences reflected by the non-cancellation of the $1/\varepsilon$ poles at $\mathcal{O}(v^2/f^2)$ in the unitary gauge calculation. Indeed due to the GIM mechanism [29] the FCNC processes considered here vanish at tree level both in the SM and in the LH model in question. Therefore within the particle content of the low energy representation of the LH model there seems to be no freedom to cancel the left-over divergences as the necessary tree level counter terms are absent.

At first sight then one could worry that the remaining divergence is an artifact of the unitary gauge calculation. However, the fact that the dominant divergence comes from the gauge independent charged triplet Higgs $\Phi^\pm$ contribution gives us a hint that the residual divergence is not an artifact of the unitary gauge but reflects the true sensitivity to the UV completion of the LH model and the presence of additional contributions to the NLSM used as the effective field theory at low energy.

In order to put this hypothesis onto a solid ground we have analyzed the divergent part of the amplitudes in the Feynman gauge. Then the box diagram contributions are finite and it is sufficient to concentrate on the penguin (vertex) contributions. In this context let us recall that in the SM the divergent contributions from penguin diagrams involving only quarks and gauge bosons are removed by the GIM mechanism as the divergent terms are mass independent. Some of the vertex diagrams with internal Goldstone bosons are also divergent and being proportional to $m_i^2, (i = u, c, t)$ these divergences cannot be removed by the GIM mechanism [29]. Within the SM they cancel, however, due to gauge invariance and renormalizability of the theory.

In the LH model in the Feynman gauge there are no divergences left from the pure gauge boson diagrams of classes 1 - 5 shown in Figs. A.1 – A.5 in the appendix. Note also that the divergence from the breakdown of the custodial symmetry is also absent as in the Feynman gauge the SM function C is finite. Thus the left-over divergences come only from the charged

triplet Higgs contribution in Fig. A.6 and two charged Goldstone bosons that now have to be included in the evaluation of the diagrams of classes 1-5. These are a charged vector Higgs boson which is responsible for the mass of W_H and the usual charged doublet Higgs boson which gives mass to W_L. We confirm that the left-over divergence coming from these Goldstone boson contributions to classes 1-5 exactly reproduces the divergence discovered in the corresponding unitary gauge calculation. Combined with the charged triplet Higgs contribution we reproduce, in the Feynman gauge, the full divergence of (4.3.80).

To understand the meaning of these ultraviolet divergences it is important to recall that the LH model is a NLSM, an effective field theory that describes the low energy behavior of a symmetric theory below the scale where the symmetry is dynamically broken. In this region the currents associated with the dynamically broken generators are conserved by a cancellation between the quark charge form factor current and the Goldstone current. Quark currents will remain conserved even when the charge form factor is renormalized as long as the Yukawa coupling of the Goldstone bosons to the fermions has a corresponding renormalization. It is easy to confirm that this is exactly what happens in the NLSM used above to describe the LH theory and the divergence may be identified as a renormalization of the quark charges associated with neutral current processes. The subsequent gauging of the Little Higgs theory only rearranges the infrared structure of the theory but cannot modify the ultraviolet behavior. The divergence in the charge form factors is not a true ultraviolet divergence but reflects sensitivity to the UV completion of the theory.

This same mechanism can be observed in the phenomenological description of dynamical chiral symmetry breaking in QCD using a non-linear realization of the pseudo-scalar mesons as Goldstone bosons. Here the axial charges are dynamically broken but the axial vector currents remain conserved due to the Goldstone currents of pions. To apply this theory to the physical baryons, the axial charge of the baryon is observed to be renormalized, $G_A \sim 1.26 \neq 1$. This renormalization is consistent with a conserved axial vector current as long as the Goldstone coupling of the pions to the baryons is modified according to the Goldberger-Treiman relation. In fact, the naive constituent quark model predicts an even larger value of 5/3 for the axial charge of the baryon where the axial charge of the quark is taken to be 1. This kind of divergence was already encountered by *Peris* [54] in a study of the constituent quark model for baryons. He calculates the corrections to the axial charge G_A of the baryon from the loop corrections of the chiral quark constituents. His calculation uses a linear sigma model of pions coupled to constituent quarks to regularize the nonlinear theory. In the broken phase, the pionic radiative corrections generate a logarithmically enhanced correction to the axial charge form factor. The scale of the logarithm is set by the mass of the scalar partner of the pion, i.e. the scale of the dynamical symmetry breaking within the chiral multiplet. In the nonlinear theory this scale will not be larger than the cutoff scale, $4\pi f$. Using the cutoff scale, *Peris* observes a 20% reduction for the in the axial charge of the quark which is about the right magnitude to explain the observed value of the axial charge of the baryon in the

constituent quark model. He also remarked that other ultraviolet completions could generate a modification of the quark axial charge even at leading order, i.e. g_A is really a free parameter in the effective field theory.

The value of the charge form factors of dynamically broken generators will depend on the ultraviolet completion of the Little Higgs model. The principal question concerns how the dynamical symmetry breaking is transmitted to the fermions. As a minimum, the symmetry breaking is reflected through the Yukawa couplings of the Goldstone bosons to the fermions. In this case the next-to-leading corrections may be estimated from Goldstone loop corrections to the charge form factors and the scale of the logarithmic divergences should not be larger than $4\pi f$. However, the light fermions may have a more complex relation to the fundamental fermions of the ultraviolet completion of the theory and the Little Higgs theory may have to include modifications of the charge form factors even at leading order, as in the case of the baryon where $G_A \neq 1$. We conclude that the residual logarithmic divergences found in Subsection 4.3.1 are a real physical effect, but they also indicate additional sensitivity to the UV completion of the Little Higgs models usually not included in the phenomenology of these models.

Assuming the minimal case discussed above, we estimate the contributions of the logarithmically divergent terms to the functions X and Y. Removing $1/\varepsilon$ terms from (4.3.80) and setting $\mu = \Lambda$ we find

$$\Delta X_{div} = \Delta Y_{div} = \frac{x_t}{64}\frac{1}{1-x_L}\frac{v^2}{f^2}\left[\ln\frac{\Lambda^2}{M_\Phi^2} - \frac{1}{5}\ln\frac{\Lambda^2}{M_{W_L}^2}\right]. \tag{4.3.90}$$

Setting

$$\Lambda = 4\pi f, \qquad m_H = 115\,\text{GeV}, \qquad v = 246\,\text{GeV} \tag{4.3.91}$$

and using the values of M_{W_L} and m_t in Table 4.3 we find for $f/v = 5$ and $x_L = 0.8$

$$\Delta X_{div} = \Delta Y_{div} = 0.049, \tag{4.3.92}$$

which should be compared with $X_{\text{SM}} \simeq 1.49$ and $Y_{\text{SM}} \simeq 0.95$. Thus for this choice of parameters the correction amounts to 3% and 5% for X and Y, respectively. Larger values are obtained for x_L closer to unity but such values are disfavored by the measured value of ΔM_s. Smaller values are found for larger f. In summary the effect of the logarithmic divergences turns out to be small. However, we would like to emphasize that this estimate only takes into account the contributions, where the fermions couple to the Goldstone bosons only through the mass terms, not the G_A-like terms, and the sensitivity to the ultraviolet completion of the LH model could in principle be larger than estimated here.

4.4 Numerical Analysis

For a numerical analysis we are mainly interested in the effects of the corrections coming from LH contributions. For that purpose we will consider the ratios

$$R_+ \equiv \frac{Br\left(K^+ \to \pi^+ \nu\bar{\nu}\right)_{\rm LH}}{Br\left(K^+ \to \pi^+ \nu\bar{\nu}\right)_{\rm SM}}, \tag{4.4.93}$$

$$R_L \equiv \frac{Br\left(K_L \to \pi^0 \nu\bar{\nu}\right)_{\rm LH}}{Br\left(K_L \to \pi^0 \nu\bar{\nu}\right)_{\rm SM}} = \frac{Br\left(B \to X_{s,d} \nu\bar{\nu}\right)_{\rm LH}}{Br\left(B \to X_{s,d} \nu\bar{\nu}\right)_{\rm SM}} = \left[\frac{X_{\rm LH}}{X_{\rm SM}}\right]^2, \tag{4.4.94}$$

$$R_{s,d} \equiv \frac{Br\left(B_{s,d} \to \mu^+\mu^-\right)_{\rm LH}}{Br\left(B_{s,d} \to \mu^+\mu^-\right)_{\rm SM}} = \left[\frac{Y_{\rm LH}}{Y_{\rm SM}}\right]^2, \tag{4.4.95}$$

where all the relevant input parameters are given in Table 4.3.

In order to define the ratios (4.4.94) and (4.4.95) we have to assume that the values of the CKM parameters in the LH model are the same as in the SM. This is a reasonable assumption since both models belong to the class of MFV models for which the so-called universal unitarity triangle exists [55, 56]. Moreover, in principle CKM parameters can be determined from tree level processes independently of new physics contributions. In the following we will choose $x_L \leq 0.8$ since we know from the recent CDF and D$\emptyset$ measurement of ΔM_s [57, 58] that values for x_L close to unity are already excluded. Moreover, as stated above we will take the CKM parameters to be the same for the SM and LH model and fixed to the central values collected in Table 4.3, where $\overline{m}_t = \overline{m}_t(m_t)$ in the $\overline{\rm MS}$ scheme. Then the ratios in (4.4.94) and (4.4.95) only depend on the one-loop functions X and Y and the dependence on the CKM parameters is only present in (4.4.93) due to the relevant charm contribution in $K^+ \to \pi^+ \nu\bar{\nu}$ in which the new physics contributions are negligible.

$\overline{m}_t = 163.8(32)\,\text{GeV}$	$\lvert V_{ub}\rvert = 0.00423(35)$
$M_W = 80.425(38)\,\text{GeV}$	$\lvert V_{cb}\rvert = 0.0416(7)$[59]
$\alpha = 1/127.9$	$\lambda = 0.225(1)$ [60]
$\sin^2\theta_W = 0.23120(15)$	$\gamma = 71^\circ \pm 16^\circ$ [61]

Table 4.3: Values of the experimental and theoretical quantities used as input parameters.

For the three new parameters f, x_L and s parameterizing the LH model we will choose the ranges

$$f/v = 5 \text{ or } 10, \quad 0.2 \leq x_L \leq 0.8, \quad 0.3 \leq s \leq 0.95. \tag{4.4.96}$$

This parameter space is larger than the one allowed by other processes [5, 8] which typically imply $f/v \geq 10$ or even higher. But we want to demonstrate that even for f/v as low as 5 the corrections from LH contributions to X and Y are small.

In Figure 4.2 we show the ratios (4.4.93)-(4.4.95) as functions of s for different values of x_L and $f/v = 5$. The corresponding plots for $f/v = 10$ are shown in Fig. 4.3.

We observe that R_+, R_L and $R_{d,s}$ increase with increasing s and x_L. For $f/v = 5$, $s = 0.95$ and $x_L = 0.8$ they reach 1.23, 1.33 and 1.51, respectively. However for $f/v = 10$ they are all below 1.15 and consequently it will be difficult to distinguish the LH predictions for the branching ratios in question from the SM ones.

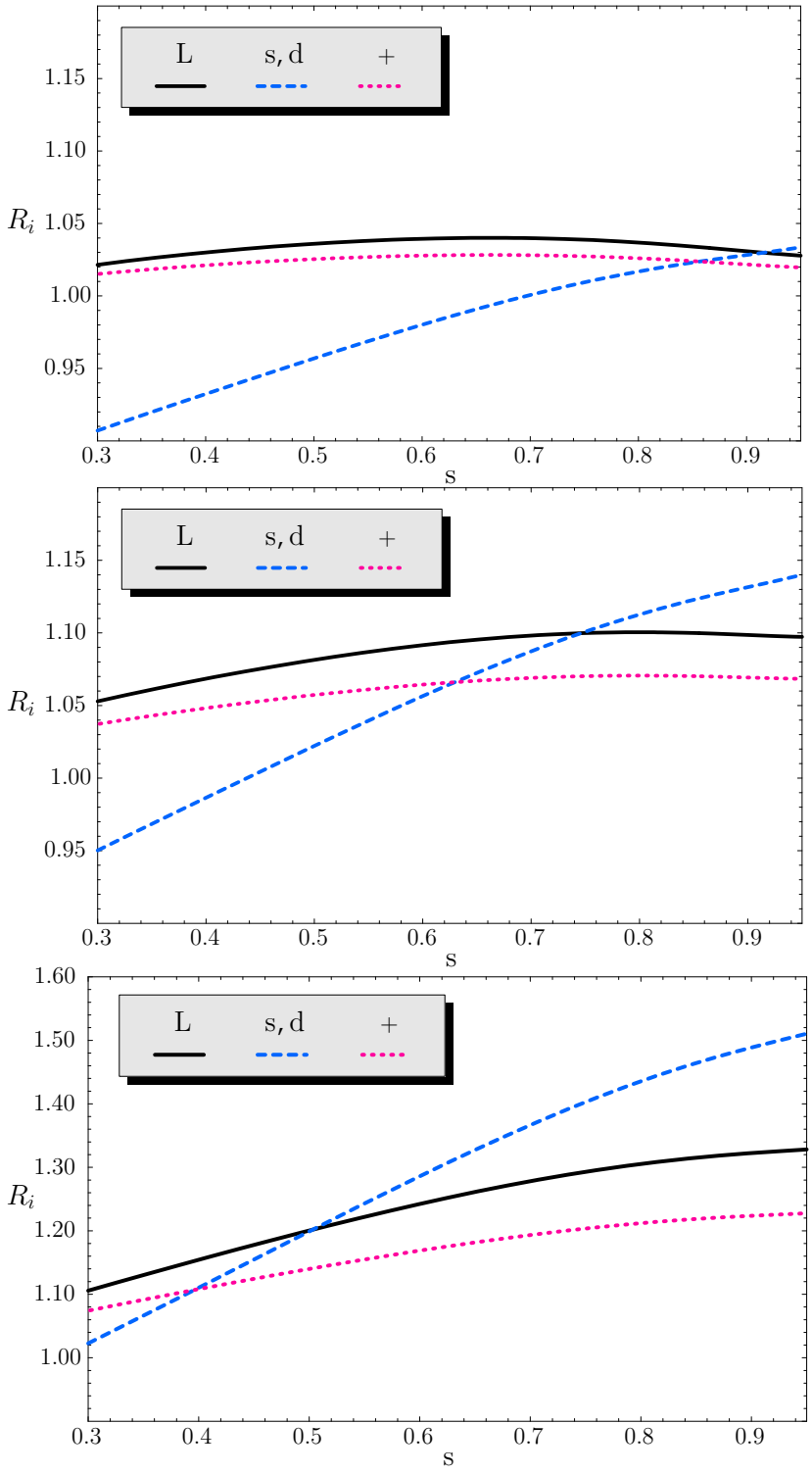

Figure 4.2: Normalized branching ratios R_L, $R_{s,d}$, R_+ for different $x_L = 0.2, 0.5, 0.8$ (from top to bottom) and $f/v = 5$.

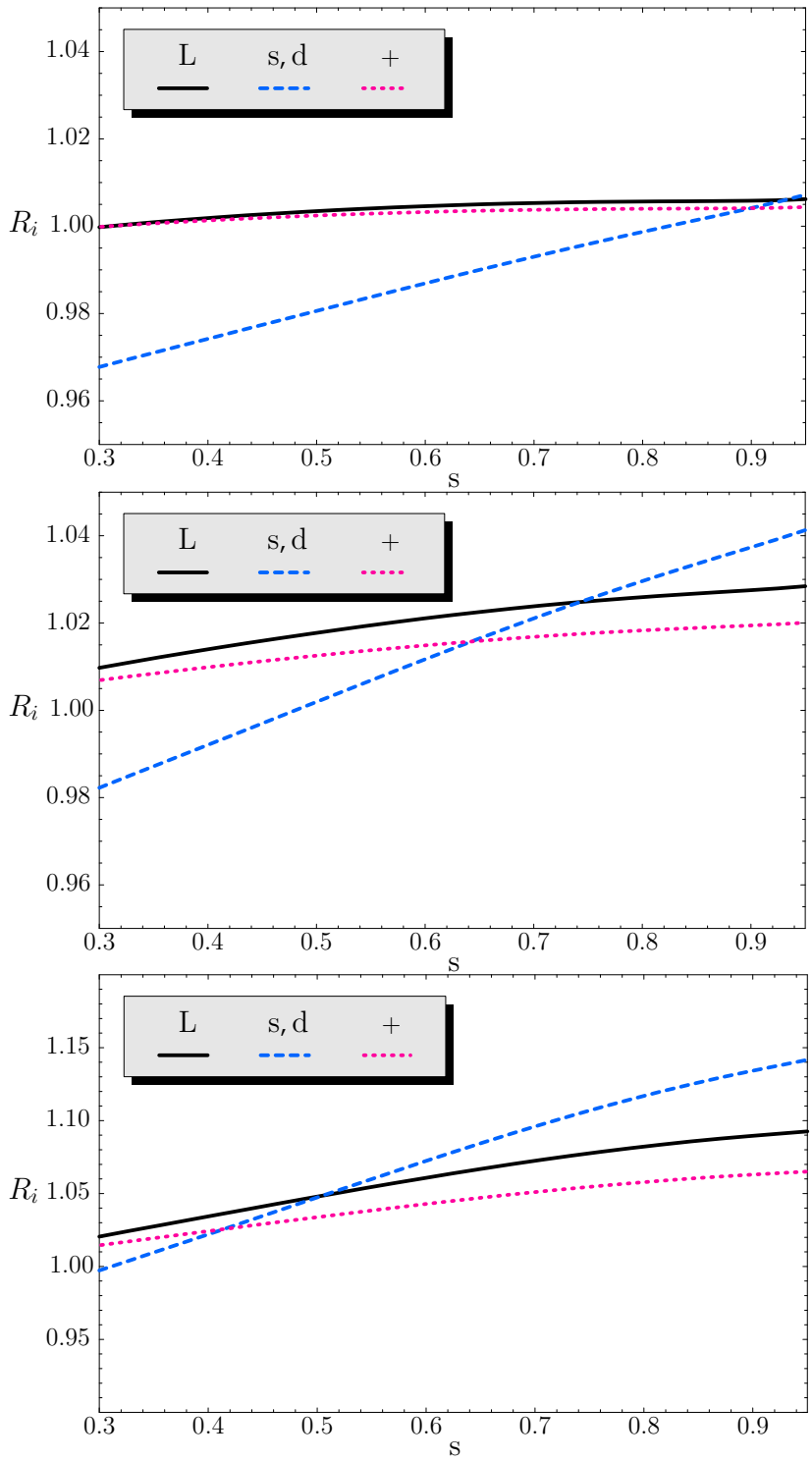

Figure 4.3: Normalized branching ratios R_L, $R_{s,d}$, R_+ for different $x_L = 0.2, 0.5, 0.8$ (from top to bottom) and $f/v = 10$.

Chapter 5

The Littlest Higgs Model with T-Parity

When introducing the superpotential of the MSSM in the most general form one has to consider several baryon- and lepton-number violating terms, which lead to a number of theoretical predictions that contradict experimental observations, like the decay of the proton. In order to explain this discrepancy between theory and experiment a new symmetry, called R-parity, is introduced. Under this symmetry all SM particles are defined to possess positive parity while their superpartners acquire a negative sign. A direct consequence of a preserved R-parity is the fact that the lightest supersymmetric particle (LSP) can not decay and therefore provides a viable dark matter candidate. To fit observations, such a particle is assumed to have a mass of 100 GeV to 1 TeV, to be neutral and to interact typically through weak and gravitational interactions.

As already discussed in the previous chapter the LH model was proposed to solve the little hierarchy problem and to protect the Higgs scalar from quadratically divergent mass at the one-loop level. However, in order to be consistent with the severe constraints coming from electroweak precision tests [8], the scale f in the LH model should be of the order of 3 TeV, which re-introduces an unacceptable fine tuning. This is due to the fact that in the LH model higher dimensional operators originating either from the expansion of the Σ field or from integrating out heavy gauge bosons affect these electroweak observables.

To evade these problems *Cheng* and *Low* suggested in [9] a new discrete symmetry, called T-parity. Like R-parity in SUSY, T-parity is a mechanism in Little Higgs models to get rid of troublesome couplings that are in conflict with experimental observations. To do so one assumes the SM particles to have positive parities, while troublesome extra fields acquire a minus sign under the parity transformation. In the next sections we want to illustrate how T-parity can be incorporated into the Littlest Higgs model.

5.1 Introducing T-parity

In order to implement T-parity into the LH model based on an $SU(5)/SO(5)$ non-linear sigma model, we recall that the unbroken and broken generators T^a and X^a satisfy $\Sigma_0 T_a \Sigma_0 = -T_a^T$ and $\Sigma_0 X_a \Sigma_0 = X_a^T$, respectively. These relations lead to the observation that the coset space $SU(5)/SO(5)$ is a symmetric space, in which the unbroken T^a and broken symmetry generators X^a obey

$$\Big[T^a, T^b\Big] \sim T^c, \quad \Big[T^a, X^b\Big] \sim X^c, \quad \Big[X^a, X^b\Big] \sim T^c. \tag{5.1.1}$$

From (5.1.1) we see that the Lie algebra with its schematic commutation relations is invariant under the transformation

$$T^a \to T^a, \quad X^a \to -X^a. \tag{5.1.2}$$

This transformation is an automorphism of the Lie algebra and can be used to define T-parity in a consistent way. Since the broken generators are assigned a minus sign under T-parity, we can determine T-parity to act on gauge fields and scalars as

$$\begin{aligned} W_L^\mu &\to W_L^\mu, \\ W_H^\mu &\to -W_H^\mu, \\ \Pi &\to -\Omega\Pi\Omega. \end{aligned} \tag{5.1.3}$$

In the last line of (5.1.3) we had to introduce a matrix $\Omega = \mathrm{diag}\,(1,1,-1,1,1)$, which commutes with all the generators and gives the Higgs a positive parity in order to serve as SM Higgs boson. Furthermore this choice of Ω also keeps the triplet odd, which forbids a dangerous vev v' for the triplet. Thus, by (5.1.3) and the use of Ω, T-parity is defined in a consistent way.

To impose T-parity on the gauge fields, the coupling constants of the two gauge groups $[SU(2) \times U(1)]_1$ and $[SU(2) \times U(1)]_2$ are set to be equal, i.e. $g_1 = g_2$ and $g_1' = g_2'$. A direct consequence of this setting is the fact that the gauge sector given in (4.1.17) is invariant under the following transformation of gauge fields

$$W_1^a \leftrightarrow W_2^a, \quad B_1 \leftrightarrow B_2. \tag{5.1.4}$$

Using these assignments one can convince oneself that (4.1.17) is invariant under T-parity by applying (5.1.3).

To implement T-parity in the fermion sector the left-handed SM fermions ψ_1, ψ_2 have to be embedded into incomplete representations Ψ_1, Ψ_2 of the full $SU(5)$ symmetry group. Moreover, a consistent introduction of T-parity requires a right-handed multiplet Ψ_R of the unbroken $SO(5)$. Thus, the field content of the multiplets can be expressed as

$$\Psi_1 = \begin{pmatrix} \psi_1 \\ 0 \\ 0 \end{pmatrix}, \quad \Psi_2 = \begin{pmatrix} 0 \\ 0 \\ \psi_2 \end{pmatrix}, \quad \Psi_R = \begin{pmatrix} \tilde{\psi}_R \\ \chi_R \\ \psi_R \end{pmatrix}, \tag{5.1.5}$$

with ψ_R being the right-handed mirror fermion doublet. The remaining singlet χ_R and doublet $\tilde{\psi}_R$ in (5.1.5) receive large masses by the introduction of further fermions [10, 62] and are assumed to decouple from the theory. The two doublets ψ_1 and ψ_2 transform linearly under the $[SU(2)]_1$ and $[SU(2)]_2$ gauge groups, respectively. Due to the transformation properties of the gauge generators given in (5.1.2) T-parity relates the fields Ψ_1 and Ψ_2 by introducing a minus sign. That is, under T-parity both multiplets transform as

$$\Psi_1 \leftrightarrow -\Sigma_0 \Psi_2. \tag{5.1.6}$$

Thus, following this transformation property of Ψ_1 and Ψ_2 the remaining right-handed fields Ψ_R need to transform under T-parity as

$$\Psi_R \rightarrow -\Psi_R. \tag{5.1.7}$$

Having determined how T-parity acts on the different fermion fields Ψ_1, Ψ_2 and Ψ_R we are able to identify the T-even and T-odd eigenstates. The linear combination

$$\psi_{SM} = \frac{1}{\sqrt{2}} \left(\psi_1 - \psi_2\right), \tag{5.1.8}$$

turns out to be the T-even eigenstate, while the T-odd combination is given by

$$\psi_H = \frac{1}{\sqrt{2}} \left(\psi_1 + \psi_2\right). \tag{5.1.9}$$

The ψ_{SM} in (5.1.8) are the SM left-handed doublets, which are even under T-parity, while the T-odd combinations are left-handed mirror fermion doublets, which will have significant phenomenological impact, as we will see later.

Finally, we need to modify the top-sector in order to incorporate T-parity into the model. Typically, this is done by adding two new singlet fields t'_1, t'_2 as well as their right-handed counterparts, t'_{1R} and t'_{2R}. These fields are supposed to transform under T-parity as

$$t'_1 \leftrightarrow -t'_2, \quad t'_{1R} \leftrightarrow -t'_{2R}. \tag{5.1.10}$$

Taking into account these transformation properties we can write down the kinetic terms for the left- and right-handed multiplets, respectively. Following [11] a kinetic term for Ψ_1 and Ψ_2 is given by

$$\mathcal{L}_{kin} \supset \bar{\Psi}_1 i\gamma^\mu D^1_\mu \Psi_1 + \bar{\Psi}_2 i\gamma^\mu D^2_\mu \Psi_2, \tag{5.1.11}$$

where the covariant derivatives are given by

$$\begin{aligned} D^1_\mu &= \partial_\mu - i\sqrt{2} g Q^a_1 W^a_{1\mu} - i\sqrt{2} g' Y_1^{(\psi_1)} B_{1\mu} - i\sqrt{2} g' Y_2^{(\psi_1)} B_{2\mu}, \\ D^2_\mu &= \partial_\mu + i\sqrt{2} g Q^{aT}_2 W^a_{2\mu} - i\sqrt{2} g' Y_1^{(\psi_2)} B_{1\mu} - i\sqrt{2} g' Y_2^{(\psi_2)} B_{2\mu}. \end{aligned} \tag{5.1.12}$$

Finally, the corresponding $U(1)$ charges $Y_i^{(\psi_j)}$ are fixed by the requirement of gauge invariance and T-parity and are given in Table 5.1.

In terms of mass eigenstates of the gauge bosons and fermions, as denoted in (4.1.22), (5.1.8) and (5.1.9), the Lagrangian (5.1.11) can schematically be re-written by

$$\mathcal{L}_{kin} \supset \bar{\psi}_{SM} i\gamma^\mu D_\mu^L \psi_{SM} + \bar{\psi}_H i\gamma^\mu D_\mu^H \psi_H + c\bar{\psi}_{SM} i\gamma^\mu V_{H\mu} \psi_H, \tag{5.1.13}$$

where $V_{H\mu}$ denotes the heavy gauge bosons. As one can see, (5.1.13) contains the usual kinetic terms for the SM doublet fermions with D_μ^L being the SM covariant derivative. However, they also include new interactions between mirror fermions, SM fermions and heavy gauge bosons.

Similarly, a kinetic term for the top partner fields is given by [11]

$$\mathcal{L}_{kin} \supset \bar{t}'_1 i\gamma^\mu D'^1_\mu t'_1 + \bar{t}'_2 i\gamma^\mu D'^2_\mu t'_2, \tag{5.1.14}$$

where the primed covariant derivatives contain only $U(1)$ gauge bosons and are given by

$$D'^i_\mu = \partial_\mu - i\sqrt{2}g' Y_1^{(t'_i)} B_{1\mu} - i\sqrt{2}g' Y_2^{(t'_i)} B_{2\mu}. \tag{5.1.15}$$

Finally, we note that the covariant derivatives for the right-handed SM fermions are introduced in analogy to (5.1.12) and (5.1.15) with the relevant quantum numbers given in Table 5.1. For the right-handed mirror fermions the kinetic terms have to be constructed via the CCWZ formalism [62, 63] and have been worked out in detail in [11].

We want to conclude this section by noting that there is a further possibility to incorporate T-parity in the model [62]. In contrast to the previous approach the SM fermions could also be put into a complete multiplet of the unbroken $SO(5)$ and a kinetic term via the CCWZ formalism [63] could be constructed. This allows to lift the masses of the mirror fermions and the spectrum would be identical to that of the LH model. Unfortunately, this is not possible, since the Yukawa-type interactions, responsible for the masses of the mirror fermions contain vertices with one SM fermion, one mirror fermion and a Goldstone boson. Such couplings yield finite contributions to the four fermion operator $c_f \left(\bar{\psi}_{SM}\bar{\sigma}_\mu \psi_{SM}\right)\left(\bar{\psi}_{SM}\bar{\sigma}^\mu \psi_{SM}\right)$ with the coefficient c_f being $c_f \sim 1/f^2$. However, experiments require this coefficient to be $c_f \leq 1/\left(5 - 15\,\text{TeV}\right)^2$ [64] and thus, the fine-tuning problem, which we wanted to solve, is re-introduced.

5.2 The Littlest Higgs Model with T-Parity

5.2.1 Gauge and Scalar Sector

In this and the next subsection we want to use the ideas of Section 5.1 to write down an explicit model, from which we can derive the Feynman rules relevant for a phenomenological analysis.

As in the LH the starting point of our considerations is the scalar kinetic term, whereas the two different coupling constants have been set equal, i.e. $g_1 = g_2 \equiv \sqrt{2}g$ and $g'_1 = g'_2 \equiv \sqrt{2}g'$.

Thus the gauge sector of the LHT contains much less parameters than the one of the LH model and the scalar kinetic term is now given by

$$\mathcal{L}_{kin} = \frac{f^2}{8}\mathrm{Tr}\left(D_\mu\Sigma\right)\left(D^\mu\Sigma\right)^\dagger, \tag{5.2.16}$$

where the covariant derivative is defined by

$$D_\mu\Sigma = \partial_\mu\Sigma - i\sqrt{2}\sum_{j=1}^{2}\left[gW_{j\mu}^a\left(Q_j^a\Sigma + \Sigma Q_j^{aT}\right) + g'B_{j\mu}\left(Y_j\Sigma + \Sigma Y_j\right)\right]. \tag{5.2.17}$$

Due to the symmetry breaking at the scale f, (5.2.17) leads to linear combinations of gauge bosons which remain massless

$$W_L^a = \frac{W_1^a + W_2^a}{\sqrt{2}}, \qquad B_L = \frac{B_1 + B_2}{\sqrt{2}}, \tag{5.2.18}$$

while the second orthogonal linear combinations

$$W_H^a = \frac{W_1^a - W_2^a}{\sqrt{2}}, \qquad B_H = \frac{B_1 - B_2}{\sqrt{2}} \tag{5.2.19}$$

get a mass of the order of the breaking scale f. The indices "L" and "H" in (5.2.18) and (5.2.19) denote the light bosons (T-even), which serve as SM gauge bosons, and new heavy gauge bosons (T-odd), respectively. In the process of EWSB, $SU(2)_L \times U(1)_Y$ is broken down to $U(1)_Q$ via the usual Higgs mechanism, generating the known mixing of the light gauge bosons. Additionally, in the neutral heavy gauge boson sector linear combinations of W_H^3 and B_H will produce the new mass eigenstates Z_H and A_H. After the spontaneous breakdown at the scale v the mass eigenstates read

$$\begin{aligned}
W_L^\pm &= \frac{W_L^1 \mp iW_L^2}{\sqrt{2}}, \qquad & W_H^\pm &= \frac{W_H^1 \mp iW_H^2}{\sqrt{2}}, \\
Z_L &= \cos\theta_W W_L^3 - \sin\theta_W B_L, \quad & Z_H &= W_H^3 + x_H\frac{v^2}{f^2}B_H, \\
A_L &= \sin\theta_W W_L^3 + \cos\theta_W B_L, \quad & A_H &= -x_H\frac{v^2}{f^2}W_H^3 + B_H,
\end{aligned} \tag{5.2.20}$$

with θ_W being the usual weak mixing angle and

$$x_H = \frac{5gg'}{4\left(5g^2 - g'^2\right)}. \tag{5.2.21}$$

The masses of the physical eigenstates (5.2.20) are given by

$$M_{W_H} = fg\left(1 - \frac{v^2}{8f^2}\right), \quad M_{Z_H} = M_{W_H}, \quad M_{A_H} = \frac{fg'}{\sqrt{5}}\left(1 - \frac{5v^2}{8f^2}\right), \tag{5.2.22}$$

and

$$M_{W_L} = \frac{gv}{2}\left(1 - \frac{v^2}{12f^2}\right), \quad M_{Z_L} = \frac{gv}{2\cos\theta_W}\left(1 - \frac{v^2}{12f^2}\right), \quad M_{A_L} = 0, \tag{5.2.23}$$

where the light gauge bosons only get contributions from the second symmetry breakdown at the scale v. Also, from (5.2.23) one can see that the custodial $SU(2)$ symmetry is preserved, since the mass relation $M_{W_L} = M_{Z_L}\cos\theta_W$ holds at tree level.

5.2.2 The Fermion Sector

Apart from the scalar and gauge sector we also have to incorporate T-parity in the fermion sector. To construct a T-invariant Yukawa interaction for the top quark one can start with (4.1.40) and T-symmetrize it. As shown in [11] such an interaction is given by

$$\begin{aligned}\mathcal{L}_{top} &= -\frac{1}{2\sqrt{2}}\lambda_1 f \epsilon_{ijk}\epsilon_{xy}\left[\left(\bar{Q}_1\right)_i \Sigma_{jx}\Sigma_{ky} - \left(\bar{Q}_2\Sigma_0\right)_i \tilde{\Sigma}_{jx}\tilde{\Sigma}_{ky}\right] u_R^3 \\ &\quad -\lambda_2 f\left(\bar{t}'_1 t'_{1R} + \bar{t}'_2 t'_{2R}\right) + h.c.,\end{aligned} \tag{5.2.24}$$

where $\tilde{\Sigma}$, the image of Σ under T-parity, is

$$\tilde{\Sigma} \equiv T\left[\Sigma\right] = \Sigma_0 \Omega \Sigma^\dagger \Omega \Sigma_0. \tag{5.2.25}$$

As in the LH model the third generation Yukawa sector has to be modified in order to prevent the Higgs mass from dangerous one loop quadratic divergences. For this reason the multiplets Q_1 and Q_2 have to be completed to representations of the $SU(3)_1$ and $SU(3)_2$ subgroups of the full $SU(5)$. With the fermions ψ_1 and ψ_2

$$\psi_i = -i\sigma_2 \begin{pmatrix} t_i \\ b_i \end{pmatrix} \tag{5.2.26}$$

the incomplete multiplets Q_1 and Q_2 in (5.2.24) are given by

$$Q_1 = \begin{pmatrix} \psi_1 \\ t'_1 \\ 0 \end{pmatrix}, \quad Q_2 = \begin{pmatrix} 0 \\ t'_2 \\ \psi_2 \end{pmatrix}. \tag{5.2.27}$$

Furthermore, with the right-handed singlet quark field u_R^3 being neutral under T-parity,

$$u_R^3 \to u_R^3, \tag{5.2.28}$$

and using the transformation properties Q_1, Q_2 and t'_{1R}, t'_{2R}, respectively,

$$Q_1 \leftrightarrow -\Sigma_0 Q_2, \quad t'_{1R} \leftrightarrow -t'_{2R}, \tag{5.2.29}$$

one can see that (5.2.24) is invariant under T-parity.

To express the Lagrangian (5.2.24) in terms of mass eigenstates we introduce the following T-even eigenstates of the top partners

$$t'_\pm = \frac{t'_1 \mp t'_2}{\sqrt{2}}, \quad t'_{\pm R} = \frac{t'_{1R} \mp t'_{2R}}{\sqrt{2}}, \tag{5.2.30}$$

which mix with the first component of the SM quark doublet and finally lead to the T-even mass eigenstates

$$\begin{aligned} t_L &= c_L u_L^3 - s_L t'_+, \quad (T_+)_L = s_L u_L^3 + c_L t'_+, \\ t_R &= c_R u_R^3 - s_R t'_{+R}, \quad (T_+)_R = s_R u_R^3 + c_R t'_{+R}. \end{aligned} \tag{5.2.31}$$

In (5.2.31) u_L^3 is the first component of the left-handed SM quark doublet while the sines and cosines of the mixing angles are found to be

$$\begin{aligned} s_L &= x_L \frac{v}{f}\left[1+\frac{v^2}{f^2}d_2\right], \\ c_L &= 1-\frac{x_L^2}{2}\frac{v^2}{f^2}, \\ s_R &= \sqrt{x_L}\left[1-\frac{v^2}{f^2}(1-x_L)\left(\frac{1}{2}-x_L\right)\right], \\ c_R &= \sqrt{1-x_L}\left[1+\frac{v^2}{f^2}x_L\left(\frac{1}{2}-x_L\right)\right], \end{aligned} \tag{5.2.32}$$

with x_L and d_2 given in (4.1.49) and (4.2.68).

In contrast to the T-even eigenstates the T-odd combination does not mix with the mirror fermions and can simply be identified with

$$(T_-)_L \equiv t'_-, \quad (T_-)_R \equiv t'_{-R}. \tag{5.2.33}$$

As one can see from (5.2.31), the physical top quark is a linear combination of the third generation SM up-type quark and the new LHT field t'. This mixing can be described by the mixing angles in (5.2.32) and will obviously affect SM Feynman rules for the top quark at order v^2/f^2. Using the field definitions in (5.2.31) we can re-express (5.2.24) in terms of the physical mass eigenstates, where the corresponding masses are given by

$$\begin{aligned} m_t &= \frac{\lambda_1\lambda_2 v}{\sqrt{\lambda_1^2+\lambda_2^2}}\left[1+\frac{v^2}{f^2}\left(-\frac{1}{3}+\frac{1}{2}x_L(1-x_L)\right)\right], \\ m_{T_+} &= \frac{f}{v}\frac{m_t}{\sqrt{x_L(1-x_L)}}\left[1+\frac{v^2}{f^2}\left(\frac{1}{3}-x_L(1-x_L)\right)\right], \\ m_{T_-} &= \frac{f}{v}\frac{m_t}{\sqrt{x_L}}\left[1-\frac{v^2}{f^2}\left(\frac{1}{3}-\frac{1}{2}x_L(1-x_L)\right)\right]. \end{aligned} \tag{5.2.34}$$

For the other quark flavors, however, it will not be necessary to modify the Yukawa Lagrangian as in the top sector since their Yukawa coupling is at least one order of magnitude smaller than the Yukawa coupling of the top quark and thus their contributions to the quadratic divergences turn out to be negligible. Therefore we do not need to introduce additional singlets for the remaining up-type quarks and the Yukawa coupling is accordingly given by

$$\mathcal{L}_{up} = -\frac{1}{2\sqrt{2}}\lambda_u f \epsilon_{ijk}\epsilon_{xy}\left[\left(\bar{Q}_1\right)_i \Sigma_{jx}\Sigma_{ky} - \left(\bar{Q}_2\Sigma_0\right)_i \tilde{\Sigma}_{jx}\tilde{\Sigma}_{ky}\right] u_R + h.c.. \tag{5.2.35}$$

In contrast to (5.2.27) the incomplete multiplets Q_1, Q_2 now consist only of the $SU(2)$ doublets ψ_1 and ψ_2. Concerning the down-type Yukawa Lagrangian, in principle, one has to proceed as in the case of the up-type sector via T-symmetrization. However, here an additional factor

$X \equiv (\Sigma_{33})^{-1/4}$ has to be included in order to conserve hypercharge. A gauge invariant down-type Yukawa term is therefore given by

$$\mathcal{L}_{down} = \frac{i}{2\sqrt{2}}\lambda_d f \epsilon_{ij}\epsilon_{xyz}\left[\left(\bar{\Psi}_2\right)_x \Sigma_{iy}\Sigma_{jz}X - \left(\bar{\Psi}_1\Sigma_0\right)_x \tilde{\Sigma}_{iy}\tilde{\Sigma}_{jz}\tilde{X}\right] d_R + h.c., \tag{5.2.36}$$

where this time the sum over $i,j = 1,2$ and $x,y,z = 3,4,5$ and the incomplete multiplets Ψ_1, Ψ_2 contain the $SU(2)$ doublet fields q_1, q_2 without an additional factor σ^2,

$$\Psi_1 = \begin{pmatrix} q_1 \\ 0 \\ 0 \end{pmatrix}, \quad \Psi_2 = \begin{pmatrix} 0 \\ 0 \\ q_2 \end{pmatrix}. \tag{5.2.37}$$

From (5.2.35) and (5.2.36) we obtain, after diagonalization, the physical masses of the up- and down-type quarks which are given by

$$m_u^i = \lambda_u^i v\left(1 - \frac{v^2}{3f^2}\right), \quad i = 1,2 \tag{5.2.38}$$

$$m_d^j = \lambda_d^j v\left(1 - \frac{v^2}{12f^2}\right), \quad j = 1,2,3. \tag{5.2.39}$$

So far we have only discussed the mass generation for SM-like fermions. However, since the mirror fermions have not been observed experimentally we have to give them a mass of order $\mathcal{O}(f)$. This can be achieved by giving them a mass via the following Yukawa interaction

$$\mathcal{L}_{mirror} = -\kappa_{ij} f\left(\bar{\Psi}_2^i \xi + \bar{\Psi}_1^i \Sigma_0 \Omega \xi^\dagger \Omega\right)\Psi_R^j + h.c., \tag{5.2.40}$$

where the summation over $i,j = 1,2,3$ is implicit. The set of mirror fermions Ψ_R is embedded in a complete multiplet of $SO(5)$, whose transformation is non-linear under $SU(5)$. Thus, in (5.2.40), $\xi = e^{i\Pi/f}$ is needed to give the Ψ_R multiplet interactions with other fields, which obey linear transformation rules, and to make $\mathcal{L}_{mirror}$ $SU(5)$ invariant. The masses acquired by both the mirror quarks and leptons are given by [16]

$$m_{Hi}^u = \sqrt{2}\kappa_i f\left(1 - \frac{v^2}{8f^2}\right) \equiv m_{Hi}\left(1 - \frac{v^2}{8f^2}\right), \tag{5.2.41}$$

$$m_{Hi}^d = \sqrt{2}\kappa_i f = m_{Hi}, \tag{5.2.42}$$

where the κ_i denote the eigenvalues of the mass matrix κ.

Imposing gauge invariance on the Yukawa sector of the LHT model the $U(1)$ charges of the fermions can be defined up to one free parameter. However, this parameter can be fixed by requiring the Lagrangian to be invariant under T-parity, which finally yields the $U(1)$ quantum numbers shown in Table 5.1.

q_1	$(1/30, 2/15)$	q_2	$(2/15, 1/30)$
t'_1	$(8/15, 2/15)$	t'_2	$(2/15, 8/15)$
t'_{1R}	$(8/15, 2/15)$	t'_{2R}	$(2/15, 8/15)$
u_R	$(1/3, 1/3)$	d_R	$(-1/6, -1/6)$
ℓ_1	$(-1/5, -3/10)$	ℓ_2	$(-3/10, -1/5)$
e_R	$(-1/2, -1/2)$		

Table 5.1: $U(1)_1 \times U(1)_2$ *quantum numbers of the fermion fields.*

Derivation of Feynman Rules

Having presented how T-parity can be embedded into the LH model we discussed the kinetic and interactions terms as well as the particle content of the LHT model. However, in order to make predictions for physical observables, we have to derive all the relevant Feynman rules. Although other papers [10, 11, 16] concerned with calculations in the LHT model already state some Feynman rules a complete list was first published in [17]. In Appendix A.2 we present the Feynman rules for the interaction of fermions, gauge and Goldstone bosons since they have not been derived by other authors so far. For our calculation they are essential, since we want to confirm the X, Y and Z functions, obtained from a unitary gauge calculation, in 't Hooft-Feynman gauge.

5.2.3 Flavor Mixing in the Mirror Sector

As discussed in detail in [16], one of the most important ingredients of the mirror sector is the existence of four CKM-like unitary matrices, two for mirror quarks and two for mirror leptons:

$$V_{Hu}, \quad V_{Hd}, \quad V_{H\nu}, \quad V_{H\ell}. \tag{5.2.43}$$

In order to see how they arise, we briefly recall the Dirac-type mass term, which was presented in (5.2.40). In analogy to the CKM mechanism in subsection 2.1.4, the 3×3 matrix κ can be biunitarily diagonalized by the two unitary matrices V_H and U_H

$$\kappa = V_H \kappa_D U_H^\dagger. \tag{5.2.44}$$

To understand how charged currents are affected by this rotation we schematically recall the gauge interaction part of the kinetic terms in the T-parity eigenbasis that is given by

$$g\bar{Q}_- \not{A}_- Q_+ + g\bar{Q}_+ \not{A}_- Q_-, \tag{5.2.45}$$

where A_- and Q_- are the heavy T-odd gauge bosons and fermions and Q_+ are the T-even eigenstates. Rotating the T-even and T-odd flavor eigenstates into mass eigenstates identified with the index H and L, we then obtain for the quark sector

$$g\bar{Q}_H V_H^\dagger \not{A}_H \begin{pmatrix} V_u u_L \\ V_d d_L \end{pmatrix} + g \begin{pmatrix} \bar{u}_L V_u^\dagger \\ \bar{d}_L V_d^\dagger \end{pmatrix} \not{A}_H V_H Q_H, \tag{5.2.46}$$

and similarly for the lepton sector

$$g\bar{L}_H V_H^{(\ell)\dagger} \not{A}_H \begin{pmatrix} V_\nu \nu_L \\ V_\ell \ell_L \end{pmatrix} + g \begin{pmatrix} \bar{\nu}_L V_\nu^\dagger \\ \bar{\ell}_L V_\ell^\dagger \end{pmatrix} \not{A}_H V_H^{(\ell)} L_H. \tag{5.2.47}$$

In (5.2.46) and (5.2.47) Q_H and L_H denote doublets of heavy quarks and leptons, respectively. Similarly to the CKM mechanism the rotation matrices relevant for flavor physics are given by

$$V_H^\dagger V_u \equiv V_{Hu}, \quad V_H^\dagger V_d \equiv V_{Hd}, \tag{5.2.48}$$

and

$$V_H^{(\ell)\dagger} V_\nu \equiv V_{H\nu}, \quad V_H^{(\ell)\dagger} V_\ell \equiv V_{H\ell}. \tag{5.2.49}$$

Moreover, it can easily be seen that the matrices in (5.2.48) and (5.2.49) are related to the CKM and PMNS matrices by

$$V_{Hu}^\dagger V_{Hd} = V_{CKM} \quad \text{and} \quad V_{H\nu}^\dagger V_{H\ell} = V_{PMNS}^\dagger. \tag{5.2.50}$$

The mixing matrices in (5.2.48) and (5.2.49) parameterize the flavor violating interactions between SM fermions and mirror fermions mediated by the heavy gauge bosons $W_H^\pm$, Z_H and A_H.

In contrast to the CKM or PMNS matrix, the matrices V_{Hd} and $V_{H\ell}$ are parameterized by three angles and three phases [65]. This is due to the fact that in the LHT model there are new interactions, mediated by the heavy gauge bosons $W_H^\pm$, Z_H and A_H. The mixing matrix V_{Hd} is involved in the interactions of ordinary SM down quarks and either an up mirror quark ($W_H^\pm$ mediated), or a down mirror quark (Z_H or A_H mediated). As discussed in [16], these interactions can generally be described by a 3×3 unitary matrix containing 3 mixing angles and 6 complex phases. In order to determine the number of physically parameters in this matrix some of these phases can be eliminated by rotating the interaction states. However, in contrast to the CKM matrix only 3 phases can be rotated away, since the phases of the SM fields have already been fixed in order to remove the unphysical parameters in the CKM matrix. Thus, it turns out that V_{Hd} can be parameterized in terms of 3 mixing angles and 3 phases. After having discussed the basic structure of V_{Hd} it is straightforward to determine V_{Hu} with the help of (5.2.50).

Here we will present the parameterization of V_{Hd}, whose analogon in the lepton sector is the matrix $V_{H\ell}$. Following [65], we parameterize V_{Hd} in terms of three mixing angles θ_{ij}^d and three complex phases δ_{ij}^d as a product of three rotations, and introducing a complex phase in each of them, thus obtaining

$$V_{Hd} = \begin{pmatrix} 1 & 0 & 0 \\ 0 & c_{23}^d & s_{23}^d e^{-i\delta_{23}^d} \\ 0 & -s_{23}^d e^{i\delta_{23}^d} & c_{23}^d \end{pmatrix} \begin{pmatrix} c_{13}^d & 0 & s_{13}^d e^{-i\delta_{13}^d} \\ 0 & 1 & 0 \\ -s_{13}^d e^{i\delta_{13}^d} & 0 & c_{13}^d \end{pmatrix} \begin{pmatrix} c_{12}^d & s_{12}^d e^{-i\delta_{12}^d} & 0 \\ -s_{12}^d e^{i\delta_{12}^d} & c_{12}^d & 0 \\ 0 & 0 & 1 \end{pmatrix}. \tag{5.2.51}$$

Performing the product one obtains the expression

$$V_{Hd} = \begin{pmatrix} c_{12}^d c_{13}^d & s_{12}^d c_{13}^d e^{-i\delta_{12}^d} & s_{13}^d e^{-i\delta_{13}^d} \\ -s_{12}^d c_{23}^d e^{i\delta_{12}^d} - c_{12}^d s_{23}^d s_{13}^d e^{i(\delta_{13}^d-\delta_{23}^d)} & c_{12}^d c_{23}^d - s_{12}^d s_{23}^d s_{13}^d e^{i(\delta_{13}^d-\delta_{12}^d-\delta_{23}^d)} & s_{23}^d c_{13}^d e^{-i\delta_{23}^d} \\ s_{12}^d s_{23}^d e^{i(\delta_{12}^d+\delta_{23}^d)} - c_{12}^d c_{23}^d s_{13}^d e^{i\delta_{13}^d} & -c_{12}^d s_{23}^d e^{i\delta_{23}^d} - s_{12}^d c_{23}^d s_{13}^d e^{i(\delta_{13}^d-\delta_{12}^d)} & c_{23}^d c_{13}^d \end{pmatrix} . \tag{5.2.52}$$

As in the case of the CKM matrix, the angles θ_{ij}^d can all be made to lie in the first quadrant with $0 \leq \delta_{12}^d, \delta_{23}^\delta, \delta_{13}^d < 2\pi$. The matrix V_{Hu} is then determined through $V_{Hu} = V_{Hd} V_{\rm CKM}^\dagger$.

In the course of our analysis of FCNC rare decays and LFV decays it will be useful to introduce the following quantities ($i = 1, 2, 3$):

$$\xi_i^{(K)} = V_{Hd}^{*is} V_{Hd}^{id}\,, \qquad \xi_i^{(d)} = V_{Hd}^{*ib} V_{Hd}^{id}\,, \qquad \xi_i^{(s)} = V_{Hd}^{*ib} V_{Hd}^{is}\,, \tag{5.2.53}$$

that we will need for the analysis of rare K and $B_{d,s}$ decays

$$\chi_i^{(\mu e)} = V_{H\ell}^{*ie} V_{H\ell}^{i\mu}\,, \qquad \chi_i^{(\tau e)} = V_{H\ell}^{*ie} V_{H\ell}^{i\tau}\,, \qquad \chi_i^{(\tau\mu)} = V_{H\ell}^{*i\mu} V_{H\ell}^{i\tau}\,, \tag{5.2.54}$$

that govern $\mu \to e$, $\tau \to e$ and $\tau \to \mu$ transitions, respectively.

5.2.4 The Parameters of the LHT Model

The new parameters of the LHT model, relevant for the present study, are

$$f\,, \quad m_{H1}^q\,, \quad m_{H2}^q\,, \quad m_{H3}^q\,, \quad \theta_{12}^q\,, \quad \theta_{13}^q\,, \quad \theta_{23}^q\,, \quad \delta_{12}^q \quad \delta_{13}^q \quad \delta_{23}^q\,, \tag{5.2.55}$$

which can be probed by FCNC processes in K and B meson systems, as discussed in detail in [15, 17] and the ones in the mirror lepton sector

$$m_{H1}^\ell\,, \quad m_{H2}^\ell\,, \quad m_{H3}^\ell\,, \quad \theta_{12}^\ell\,, \quad \theta_{13}^\ell\,, \quad \theta_{23}^\ell\,, \quad \delta_{12}^\ell \quad \delta_{13}^\ell \quad \delta_{23}^\ell\,, \tag{5.2.56}$$

which can be probed with the help of LFV decays, as discussed in detail in [66].

The determination of the parameters in (5.2.55) and (5.2.56) with the help of K and B meson systems and LFV processes is clearly a formidable task. However, if the new particles present in the LHT model are discovered once LHC starts its operation, the parameter f will be determined from M_{W_H}, M_{Z_H} or M_{A_H}. Similarly the mirror quark and lepton masses m_{H1}^q and m_{Hi}^ℓ will be measured.

The only remaining free parameters among the ones listed in (5.2.55) and (5.2.56) will then be $\theta_{ij}^{q,\ell}$ and $\delta_{ij}^{q,\ell}$, which can be determined once many FCNC and LFV processes have been measured.

Chapter 6

Phenomenology of Rare Decays in the LHT Model

Rare decays play a crucial role for the discovery potential of B experiments such as the LHCb or a Super B Factory. As they involve loop-suppressed flavor-changing neutral currents, they are highly-sensitive probes for new degrees of freedom beyond the Standard Model.

In this chapter we want to present the calculation of several important rare decays in the LHT that are likely to be of crucial interest when K and B experiments are operating. This chapter is organized as follows. In the first section we want to introduce some theoretical ingredients which are relevant for describing the phenomenology of rare decays. In the subsequent section several rare decays are calculated within the LHT so that we can finally present a numerical analysis of these decays in the LHT.

6.1 Rare K and B Decays beyond MFV

6.1.1 Preliminaries

Before presenting the details of the calculations of rare K and B decays in the LHT model in question, it will be useful to have a general look at rare decays within models with new flavor and CP-violating interactions but with the same local operators of the SM or more generally of constrained MFV (CMFV) models, as defined in [56, 67].

It should be emphasized that while the formulae given below bear many similarities to the ones given in [68], they differ from the latter ones in the following important manner. In [68] a simple beyond-MFV scenario of new physics has been considered in which new physics affected only the Z^0-penguin function C that became a complex quantity, but remained universal for K, B_d and B_s decays. In this manner several CMFV relations involving only CP-conserving quantities remained valid and the main new effects were seen in CP-violating quantities like $Br(K_L \to \pi^0\nu\bar{\nu})$ and the CP-asymmetries in $B \to X_s\ell^+\ell^-$. In particular, the full system

of rare K, B_d and B_s decays considered in this section could be described by three complex functions

$$X = |X|\, e^{i\,\theta_X}\,, \qquad Y = |Y|\, e^{i\,\theta_Y}\,, \qquad Z = |Z|\, e^{i\,\theta_Z}\,, \tag{6.1.1}$$

with correlations between these functions resulting from the universality of the Z^0-penguin function $C = |C| \exp(i\theta_C)$. As a result the CMFV correlations between observables in K, B_d and B_s were only affected in the cases in which θ_i played a role. In the LHT model the structure of new flavor violating interactions is much richer. Let us spell it out in explicit terms.

6.1.2 X_i, Y_i, Z_i functions

In the CMFV models the new physics contributions enter for all practical purposes only through the functions X, Y and Z that multiply the CKM factors $\lambda_t^{(i)}$

$$\lambda_t^{(K)} = V_{ts}^*\, V_{td}\,, \qquad \lambda_t^{(d)} = V_{tb}^*\, V_{td}\,, \qquad \lambda_t^{(s)} = V_{tb}^*\, V_{ts}\,, \tag{6.1.2}$$

for K, B_d and B_s systems respectively. As in the LH model the CKM elements we will use are those determined from tree level decays.

It will be useful to keep this structure in the LHT model and absorb all new physics contributions in the functions X_i, Y_i, Z_i with $i = K, d, s$ defined as follows:

$$X_i = X_{\rm SM} + \bar{X}_{\rm even} + \frac{1}{\lambda_t^{(i)}}\bar{X}_i^{\rm odd} \equiv |X_i|\, e^{i\,\theta_X^i}\,, \tag{6.1.3}$$

$$Y_i = Y_{\rm SM} + \bar{Y}_{\rm even} + \frac{1}{\lambda_t^{(i)}}\bar{Y}_i^{\rm odd} \equiv |Y_i|\, e^{i\,\theta_Y^i}\,, \tag{6.1.4}$$

$$Z_i = Z_{\rm SM} + \bar{Z}_{\rm even} + \frac{1}{\lambda_t^{(i)}}\bar{Z}_i^{\rm odd} \equiv |Z_i|\, e^{i\,\theta_Z^i}\,. \tag{6.1.5}$$

Here $X_{\rm SM}$, $Y_{\rm SM}$ and $Z_{\rm SM}$ are the SM contributions for which explicit expressions can be found in Appendix A.4. $\bar{X}_{\rm even}$, $\bar{Y}_{\rm even}$ and $\bar{Z}_{\rm even}$ are the contributions from the T-even sector, that is the contributions of T_+ and of t at order v^2/f^2 necessary to make the GIM mechanism [29] work. The latter contributions, similar to $X_{\rm SM}$, $Y_{\rm SM}$ and $Z_{\rm SM}$, are real and independent of $i = K, d, s$. They can be extracted from [7] and will be given in Section 6.2. Finally, the remaining functions $\bar{X}_i^{\rm odd}$, $\bar{Y}_i^{\rm odd}$ and $\bar{Z}_i^{\rm odd}$, that represent the T-odd sector of the LHT model can be obtained from penguin and box diagrams with internal mirror fermions. The details of this calculation can be found in Section 6.2. In what follows we will present the most interesting branching ratios in terms of X_i and Y_i.

6.2 Calculating Rare and CP-violating Decays

In order to calculate the functions X_i, Y_i and Z_i in (6.1.3), (6.1.4) and (6.1.5) we have to determine the contributions $\bar{X}_{\rm even}$, $\bar{Y}_{\rm even}$ and $\bar{Z}_{\rm even}$ coming from the T-even sector and $\bar{X}_i^{\rm odd}$,

$\bar{Y}_i^{\text{odd}}$, $\bar{Z}_i^{\text{odd}}$ resulting from the T-odd sector. Among these functions, the contribution $\bar{X}_{\text{even}}$ and $\bar{Y}_{\text{even}}$ in (6.1.3) and (6.1.4), respectively, can be easily extracted from [7] by using the functions X and Y calculated in Chapter 4. However, in the LHT model T-parity enforces the gauge couplings of the two $SU(2)_i \otimes U(1)_i$, $i = 1, 2$ factors to be equal, which implies for the mixing angles

$$s = c = s' = c' = \frac{1}{\sqrt{2}}. \tag{6.2.6}$$

Due to T-parity one can also see from the diagrams in Appendix A.1 that all contributions from the classes 1, 2, 4 and 6 vanish. Additionally, there are also no corrections from the breakdown of custodial symmetry and the left-over divergence, discussed in detail in Subsection 4.3.2.

The remaining contributions therefore arise from the classes 3 and 5 and can be summarized as

$$\bar{X}_{\text{even}} = x_L^2 \frac{v^2}{f^2} \left[U_3(x_t, x_T) + \frac{x_L}{1 - x_L} \frac{x_t}{8} \right], \tag{6.2.7}$$

$$\bar{Y}_{\text{even}} = x_L^2 \frac{v^2}{f^2} \left[V_3(x_t, x_T) + \frac{x_L}{1 - x_L} \frac{x_t}{8} \right], \tag{6.2.8}$$

with $U_3(x_t, x_T)$ and $V_3(x_t, x_T)$ given in Appendix A.3.

The contributions $\bar{X}_i^{\text{odd}}$ and $\bar{Y}_i^{\text{odd}}$ resulting from fermions in the mirror sector cannot be extracted from previous results and have to be calculated from the diagrams shown in Figures 6.1 and 6.2. Analogously, in the case of $\bar{Y}_i^{\text{odd}}$, diagrams with external charged leptons have to be considered. For the calculation of $\bar{X}_i^{\text{odd}}$ and $\bar{Y}_i^{\text{odd}}$ we first use the unitary gauge to find the results (6.2.9) and (6.2.10). Subsequently, we confirm it by using the 't Hooft-Feynman gauge, where in this renormalizable gauge also diagrams with Goldstone bosons have to be included.

6.2.1 Calculation in Unitary and 't Hooft-Feynman Gauge

In the decays considered here only the penguin diagrams involving Z_L contribute, since there are no couplings of Z_H and A_H to $\nu\bar{\nu}$ and $\mu^+\mu^-$ due to T-parity. Moreover, the diagrams with triple gauge boson vertices vanish in the case of internal A_H and Z_H contributions.

Compared to the SM the diagrams in Figure 6.1 are not suppressed by v^2/f^2 and yield a contribution $\mathcal{O}(1)$. These $\mathcal{O}(1)$ contributions have to vanish as otherwise it would not be possible to decouple the mirror fermions in the limit $f \to \infty$. Indeed, this cancellation of $\mathcal{O}(1)$ contributions is assured by the vectorial coupling of Z_L to the mirror fermions.

A consequence of this vectorial coupling is the fact that the charged ($W_H^\pm$) and neutral (Z_H, A_H) gauge boson contributions of $\mathcal{O}(1)$ to the Z_L-penguin vanish independently in the unitary gauge, since the difference in the couplings $\bar{d}_H^i Z_L^\mu d_H^i$ and $\bar{u}_H^i Z_L^\mu u_H^i$ compensates the missing diagrams with triple gauge boson vertices in the neutral gauge boson case. Determining the remaining v^2/f^2 corrections to the neutral gauge boson interactions we find that

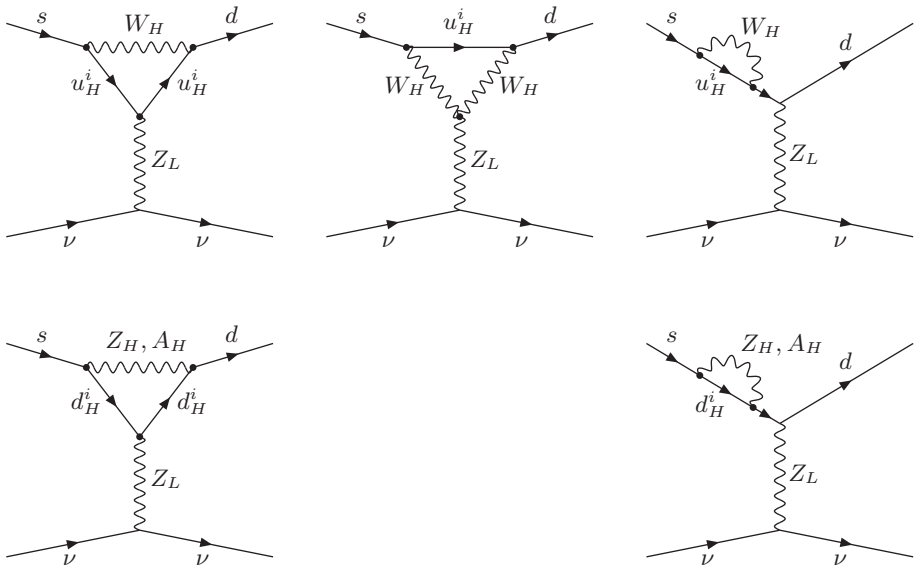

Figure 6.1: *Z_L-penguin diagrams contributing in the T-odd sector.*

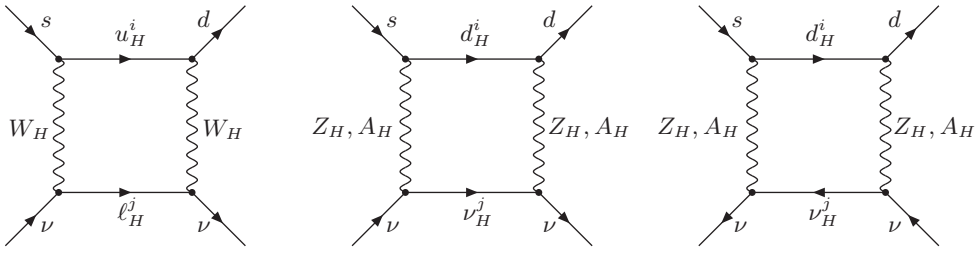

Figure 6.2: *Box diagrams in the unitary gauge.*

this only yields an overall factor which multiplies the vanishing Z_H and A_H contributions. Therefore the contributions from mirror fermions to the Z_L penguin vanish in the unitary gauge.

To determine the contributions coming from the box diagrams in Figure 6.2 we assume the mirror leptons to be degenerate in mass. Having checked numerically that this is a good approximation this assumption will simplify our results.

For the box diagrams in Figure 6.2 we find, similarly to $\Delta F = 2$ transitions considered in [15, 16], that the relevant part of the gauge boson propagator is the $g^{\mu\nu}$ part, where the contributions from the second part proportional to $k^\mu k^\nu / M_{W_H}^2$ cancel each other between the last two box diagrams in Figure 6.2. Therefore we conclude that the neutral gauge boson box contributions to $\bar{X}_i^{\rm odd}$ and $\bar{Y}_i^{\rm odd}$ are gauge independent, which means that the neutral gauge boson contributions to Z_L-penguins must vanish in an arbitrary gauge. As discussed below we confirm this through an explicit calculation in the Feynman gauge. The result for the box

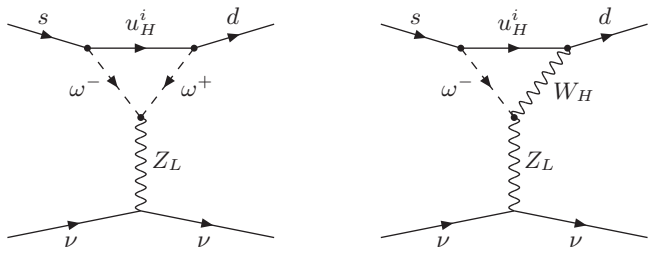

Figure 6.3: $\mathcal{O}\left(v^2/f^2\right)$ *contributions to* Z_L*-penguin in the 't Hooft-Feynman gauge.*

contributions involving $W_H^\pm$ however is divergent in the unitary gauge. This is contrary to the box contributions in a renormalizable gauge, where box diagrams are finite by power counting. Consequently the box diagram contributions involving $W_H^\pm$ must be gauge dependent.

In order to confirm our result (6.2.9) and (6.2.10) in the 't Hooft-Feynman gauge we also have to take into account diagrams with Goldstone bosons, which are absent in unitary gauge. For the Z_L-penguin diagrams the $\mathcal{O}(1)$ contributions vanish as expected and we have to consider $\mathcal{O}\left(v^2/f^2\right)$ corrections. As in the unitary gauge, there are no contributions from diagrams involving only gauge bosons. However, diagrams with Goldstone bosons contribute at $\mathcal{O}\left(v^2/f^2\right)$. It shows that the $\mathcal{O}\left(v^2/f^2\right)$ corrections to vertices involving SM quarks, mirror quarks and Goldstone boson vertices cancel in the calculation. This implies that the neutral gauge boson contributions to the Z_L-penguin, not having triple gauge boson vertices and corresponding vertices with Goldstone bosons, vanish also in the 't Hooft-Feynman gauge as expected. Thus in the 't Hooft-Feynman gauge only two diagrams at $\mathcal{O}\left(v^2/f^2\right)$ in Figure 6.3 contribute to the Z_L-penguin vertex. Calculating these diagrams and including finite contributions of the penguin and box diagram leaves us with the final results for $\bar{X}_i^{\text{odd}}$ and $\bar{Y}_i^{\text{odd}}$, confirming those in the unitary gauge.

6.2.2 Final Results for the T-odd sector

Due to our calculation of $\bar{X}_i^{\text{odd}}$ and $\bar{Y}_i^{\text{odd}}$ in the unitary gauge and in the 't Hooft-Feynman gauge we conclude, similarly to the LH model without T-parity [7], that the left-over divergence obtained in the unitary gauge is not an artifact of a non-renormalizable gauge but a physical gauge independent result. Thus the final results for $\bar{X}_i^{\text{odd}}$ and $\bar{Y}_i^{\text{odd}}$ in the LHT model can be summarized as

$$\bar{X}_i^{\text{odd}} = \left[\xi_2^{(i)}\left(J^{\nu\bar{\nu}}(z_2,y) - J^{\nu\bar{\nu}}(z_1,y)\right) + \xi_3^{(i)}\left(J^{\nu\bar{\nu}}(z_3,y) - J^{\nu\bar{\nu}}(z_1,y)\right)\right], \quad (6.2.9)$$

$$\bar{Y}_i^{\text{odd}} = \left[\xi_2^{(i)}\left(J^{\mu\bar{\mu}}(z_2,y) - J^{\mu\bar{\mu}}(z_1,y)\right) + \xi_3^{(i)}\left(J^{\mu\bar{\mu}}(z_3,y) - J^{\mu\bar{\mu}}(z_1,y)\right)\right], \quad (6.2.10)$$

where

$$J^{\nu\bar{\nu}}(z_i,y) = \frac{1}{64}\frac{v^2}{f^2}\Big[z_i S_{\rm odd} + F^{\nu\bar{\nu}}(z_i,y;W_H) + 4\Big(G(z_i,y;Z_H) + G_1(z_i',y';A_H) + G_2(z_i,y;\eta)\Big)\Big], \quad (6.2.11)$$

$$J^{\mu\bar{\mu}}(z_i,y) = \frac{1}{64}\frac{v^2}{f^2}\Big[z_i S_{\rm odd} + F^{\mu\bar{\mu}}(z_i,y;W_H) - 4\Big(G(z_i,y;Z_H) + G_1(z_i',y';A_H) - G_2(z_i,y;\eta)\Big)\Big], \quad (6.2.12)$$

$$S_{\rm odd} = \frac{1}{\varepsilon} + \log\frac{\mu^2}{M_{W_H}^2}\,. \quad (6.2.13)$$

The functions $F^{\nu\bar{\nu}}$, $F^{\mu\bar{\mu}}$, G, G_1 and G_2 are given in Appendix A.4 and the various variables are defined as follows

$$z_i = \frac{m_{Hi}^2}{M_{W_H}^2} = \frac{m_{Hi}^2}{M_{Z_H}^2}\,, \qquad z_i' = a z_i \quad \text{with} \quad a = \frac{5}{\tan^2\theta_W}\,, \quad (6.2.14)$$

$$y = \frac{m_{H\ell}^2}{M_{W_H}^2} = \frac{m_{H\ell}^2}{M_{Z_H}^2}\,, \qquad y' = ya\,, \quad \eta = \frac{1}{a}\,. \quad (6.2.15)$$

In the unitary gauge the results in (6.2.9)-(6.2.12) follow from box diagrams only, since the Z_L-penguin diagrams do not contribute in this gauge, as discussed in Section 6.2.1. In the 't Hooft-Feynman gauge the contribution of the Z_L-penguin diagram is found to be

$$\Delta J^{\nu\bar{\nu}} = \Delta J^{\mu\bar{\mu}} \equiv \frac{1}{64}\frac{v^2}{f^2}\left(z_i S_{\rm odd} - 8 z_i R_2(z_i) + \frac{3}{2} z_i + 2 z_i F_2(z_i)\right)\,, \quad (6.2.16)$$

where the functions R_2 and F_2 are given in Appendix A.4.

In order to estimate the size of $S_{\rm odd}$ we will, as in Subsection 4.3.2, remove $1/\varepsilon$ terms from (6.2.13) and set $\mu = \Lambda$ to obtain

$$J_{\rm div}^{\nu\bar{\nu}} = J_{\rm div}^{\mu\bar{\mu}} = z_i \frac{1}{64}\frac{v^2}{f^2}\log\frac{\Lambda^2}{M_{W_H}^2}\,, \quad (6.2.17)$$

as a minimal estimate of the UV sensitivity of the model. Setting

$$\Lambda = 4\pi f\,, \qquad v = 246\,\text{GeV}\,, \quad (6.2.18)$$

we find that for $f = 1000\,\text{GeV}$, implying $M_{W_H} = 652\,\text{GeV}$,

$$J_{\rm div}^{\nu\bar{\nu}} = J_{\rm div}^{\mu\bar{\mu}} = z_i \cdot 0.006\,. \quad (6.2.19)$$

Performing a more thorough analysis as done in [17], we observe that the divergences constitute a sizable fraction of the total result. The coefficient of z_i in the divergent terms $J_{\rm div}^{\nu\bar{\nu}}$ and $J_{\rm div}^{\mu\bar{\mu}}$ is of the same order of magnitude as the analogous linear coefficient in the

convergent contributions, but roughly four times larger. At first sight this could imply the loss of predictive power of the theory as our estimate of the divergent contribution is clearly an approximation. On the other hand the divergence found has a *universal* character and we can simply write

$$J^{\nu\bar{\nu}}_{\rm div} = J^{\mu\bar{\mu}}_{\rm div} = \delta_{\rm div}\, z_i \tag{6.2.20}$$

and treat $\delta_{\rm div}$ as a free parameter. Assuming that $\delta_{\rm div}$ encloses all effects coming from the UV completion, which is true if light fermions do not have a more complex relation to the fundamental fermions of the UV completion that could spoil its flavor independence, one can in principle fit $\delta_{\rm div}$ to the data and trade it for one observable. At present this is not feasible, but could become realistic when more data for FCNC processes will be available.

On the other hand, implementing T-parity removes all divergences from the T-even sector. This is easy to understand. The only new T-even particle is T_+ which can be thought of as an arbitrary singlet field mixing with the SM top quark, independently of the NLSM. Of the "pion" matrix Π, only the SM Higgs doublet is present in the T-even sector, and all modifications in its couplings appear due to the mixing of T_+ with t. Thus the T-even sector of the LHT model is effectively decoupled from the breaking $SU(5) \to SO(5)$ of the non-linear sigma model, which has been the basic reason for the appearance of the singularity described above and in Chapter 4.

6.3 Important Rare Decays

6.3.1 $K^+ \to \pi^+\nu\bar{\nu}$ and $K_L \to \pi^0\nu\bar{\nu}$

The first decays we want to discuss are the rare decays $K^+ \to \pi^+\nu\bar{\nu}$ and $K_L \to \pi^0\nu\bar{\nu}$. They play an important role in the field of flavor changing neutral currents due to their theoretical cleanness and their large sensitivity to short-distance QCD effects that can be calculated very systematically.

For the determination of the branching ratios we apply the formulae presented in [68] to the case of the LHT model. They are given by

$$Br(K^+ \to \pi^+\nu\bar{\nu}) = \kappa_+ \left[\tilde{r}^2 A^4 R_t^2 |X_K|^2 + 2\tilde{r}\bar{P}_c(x) A^2 R_t |X_K| \cos\beta_X^K + \bar{P}_c(x)^2\right], \tag{6.3.21}$$

$$Br(K_L \to \pi^0\nu\bar{\nu}) = \kappa_L \tilde{r}^2 A^4 R_t^2 |X_K|^2 \sin^2\beta_X^K, \tag{6.3.22}$$

with the relevant quantities taken from [69],

$$\tilde{r} = \left|\frac{V_{ts}}{V_{cb}}\right| \simeq 0.98, \quad \kappa_+ = (5.08 \pm 0.17)\cdot 10^{-11}, \quad \kappa_L = (2.22 \pm 0.07)\cdot 10^{-10}. \tag{6.3.23}$$

The function $P_c(x)$ in (6.3.21) comprises both the NNLO corrections [69] and the long distance contributions [70], and its value has been determined

$$\bar{P}_c(x) = \left(1 - \frac{\lambda^2}{2}\right) P_c(x), \quad P_c(x) = 0.42 \pm 0.05. \tag{6.3.24}$$

Finally, the remaining angle β_X^K is defined as the difference

$$\beta_X^K = \beta - \beta_s - \theta_X^K \,, \tag{6.3.25}$$

whereas the values for A, R_b, β and β_s are collected in Table 6.2.

Of particular interest is the relation

$$\sin 2(\beta + \varphi_{B_d}) = \sin 2\beta_X^K \,, \tag{6.3.26}$$

that for $\varphi_{B_d} = 0$, $\theta_X^K = 0$ reduces to the MFV relation of [71, 72]. A violation of this relation would signal the presence of new complex phases and generally non-MFV interactions. In this context the ratio

$$\frac{Br(K_L \to \pi^0 \nu\bar{\nu})}{Br(K_L \to \pi^0 \nu\bar{\nu})_{\rm SM}} = \left|\frac{X_K}{X_{\rm SM}}\right|^2 \left[\frac{\sin\beta_X^K}{\sin(\beta-\beta_s)}\right]^2 \tag{6.3.27}$$

is very useful, as it is very sensitive to θ_X^K and is theoretically very clean.

The most recent SM predictions for the branching ratios read [69]

$$Br(K^+ \to \pi^+ \nu\bar{\nu}) = (8.0 \pm 1.1)\cdot 10^{-11} \,, \qquad Br(K_L \to \pi^0 \nu\bar{\nu}) = (2.9 \pm 0.4)\cdot 10^{-11} \,, \tag{6.3.28}$$

to be compared with the present experimental measurements [73, 74]

$$Br(K^+ \to \pi^+ \nu\bar{\nu}) = (1.47^{+1.30}_{-0.89})\cdot 10^{-10} \,, \quad Br(K_L \to \pi^0 \nu\bar{\nu}) < 2.1\cdot 10^{-7}\,(90\%\text{C.L.}) \,. \tag{6.3.29}$$

Recent reviews of the $K \to \pi\nu\bar{\nu}$ decays can be found in [75, 76].

6.3.2 $B_{s,d} \to \mu^+\mu^-$

Here, we will mainly be interested in the following ratios

$$\frac{Br(B_s \to \mu^+\mu^-)}{Br(B_s \to \mu^+\mu^-)_{\rm SM}} = \left|\frac{Y_s}{Y_{\rm SM}}\right|^2 , \tag{6.3.30}$$

$$\frac{Br(B_d \to \mu^+\mu^-)}{Br(B_d \to \mu^+\mu^-)_{\rm SM}} = \left|\frac{Y_d}{Y_{\rm SM}}\right|^2 , \tag{6.3.31}$$

$$\frac{Br(B_d \to \mu^+\mu^-)}{Br(B_s \to \mu^+\mu^-)} = \frac{\tau(B_d)}{\tau(B_s)}\frac{m_{B_d}}{m_{B_s}}\frac{F_{B_d}^2}{F_{B_s}^2}\left|\frac{V_{td}}{V_{ts}}\right|^2\left|\frac{Y_d}{Y_s}\right|^2 , \tag{6.3.32}$$

where the departure of the last factor from unity signals non-MFV interactions. In obtaining these formulae we assume that the CKM parameters have been determined in tree level decays independently of new physics so that they cancel in the ratios in question.

In the LHT model [15],

$$\frac{\Delta M_d}{\Delta M_s} = \frac{m_{B_d}}{m_{B_s}}\frac{\hat{B}_{B_d}F_{B_d}^2}{\hat{B}_{B_s}F_{B_s}^2}\left|\frac{V_{td}}{V_{ts}}\right|^2\frac{C_{B_d}}{C_{B_s}} \,, \tag{6.3.33}$$

where

$$C_{B_q} = \frac{\Delta M_q}{(\Delta M_q)_{\rm SM}} \qquad (q = d, s)\,. \tag{6.3.34}$$

Consequently, using (6.3.32) and (6.3.33), the golden relation between $Br(B_{d,s} \to \mu^+\mu^-)$ and $\Delta M_d/\Delta M_s$ valid in CMFV models [77] gets modified as follows:

$$\frac{Br(B_s \to \mu^+\mu^-)}{Br(B_d \to \mu^+\mu^-)} = \frac{\hat{B}_{B_d}}{\hat{B}_{B_s}} \frac{\tau(B_s)}{\tau(B_d)} \frac{\Delta M_s}{\Delta M_d}\, r\,, \quad r = \left|\frac{Y_s}{Y_d}\right|^2 \frac{C_{B_d}}{C_{B_s}}\,, \tag{6.3.35}$$

with r being in general different from unity.

The most recent SM predictions read [67]

$$Br(B_s \to \mu^+\mu^-) = (3.35 \pm 0.32)\cdot 10^{-9}\,, \qquad Br(B_d \to \mu^+\mu^-) = (1.03 \pm 0.09)\cdot 10^{-10}\,, \tag{6.3.36}$$

to be compared with the experimental upper bounds from CDF [78]

$$Br(B_s \to \mu^+\mu^-) < 1 \cdot 10^{-7}\,, \qquad Br(B_d \to \mu^+\mu^-) < 3 \cdot 10^{-8}\,. \tag{6.3.37}$$

6.3.3 $K_L \to \pi^0\ell^+\ell^-$

The rare decays $K_L \to \pi^0 e^+ e^-$ and $K_L \to \pi^0\mu^+\mu^-$ are dominated by CP-violating contributions. In the SM the main contribution comes from the indirect (mixing-induced) CP-violation and its interference with the direct CP-violating contribution [79, 80, 81, 82]. The direct CP-violating contribution to the branching ratio is in the ballpark of $4 \cdot 10^{-12}$, while the CP-conserving contribution is at most $3 \cdot 10^{-12}$. Among the rare K meson decays, the decays in question belong to the theoretically cleanest, but certainly cannot compete with the $K \to \pi\nu\bar{\nu}$ decays. Moreover, the dominant indirect CP-violating contributions are practically determined by the measured decays $K_S \to \pi^0\ell^+\ell^-$ and the parameter ε_K. Consequently they are not as sensitive as the $K_L \to \pi^0\nu\bar{\nu}$ decay to new physics contributions, present only in the subleading direct CP violation. However, as pointed out in [68], in the presence of large new CP-violating phases the direct CP-violating contribution can become the dominant contribution and the branching ratios for $K_L \to \pi^0\ell^+\ell^-$ can be enhanced by a factor of 2–3, with a stronger effect in the case of $K_L \to \pi^0\mu^+\mu^-$ [81, 82].

Adapting the formulae in [80, 81, 82, 83] with the help of [68] to the LHT model we find

$$Br(K_L \to \pi^0\ell^+\ell^-) = \left(C^\ell_{\rm dir} \pm C^\ell_{\rm int}\,|a_s| + C^\ell_{\rm mix}\,|a_s|^2 + C^\ell_{\rm CPC}\right)\cdot 10^{-12}\,, \tag{6.3.38}$$

where

$$C^e_{\rm dir} = (4.62 \pm 0.24)(\omega_{7V}^2 + \omega_{7A}^2)\,, \qquad C^\mu_{\rm dir} = (1.09 \pm 0.05)(\omega_{7V}^2 + 2.32\omega_{7A}^2)\,, \tag{6.3.39}$$

$$C^e_{\rm int} = (11.3 \pm 0.3)\omega_{7V}\,, \qquad C^\mu_{\rm int} = (2.63 \pm 0.06)\omega_{7V}\,, \tag{6.3.40}$$

$$C^e_{\rm mix} = 14.5 \pm 0.05\,, \qquad C^\mu_{\rm mix} = 3.36 \pm 0.20\,, \tag{6.3.41}$$

$$C^e_{\rm CPC} \simeq 0\,, \qquad C^\mu_{\rm CPC} = 5.2 \pm 1.6\,, \tag{6.3.42}$$

$$|a_s| = 1.2 \pm 0.2, \tag{6.3.43}$$

with

$$\omega_{7V} = \frac{1}{2\pi}\left[P_0 + \frac{|Y_K|}{\sin^2\theta_W}\frac{\sin\beta_Y^K}{\sin(\beta-\beta_s)} - 4|Z_K|\frac{\sin\beta_Z^K}{\sin(\beta-\beta_s)}\right]\left[\frac{\mathrm{Im}\,\lambda_t}{1.4\cdot 10^{-4}}\right], \quad (6.3.44)$$

$$\omega_{7A} = -\frac{1}{2\pi}\frac{|Y_K|}{\sin^2\theta_W}\frac{\sin\beta_Y^K}{\sin(\beta-\beta_s)}\left[\frac{\mathrm{Im}\,\lambda_t}{1.4\cdot 10^{-4}}\right], \quad (6.3.45)$$

where $P_0 = 2.88 \pm 0.06$ [84] includes NLO QCD corrections and

$$\beta_Y^K = \beta - \beta_s - \theta_Y^K, \qquad \beta_Z^K = \beta - \beta_s - \theta_Z^K, \quad (6.3.46)$$

with Z_K defined in (6.1.5).

The effect of the new physics contributions is mainly felt in ω_{7A}, as the corresponding contributions in ω_{7V} cancel each other to a large extent.

The present experimental bounds

$$Br(K_L\to\pi^0e^+e^-) < 28\cdot 10^{-11} \quad [85], \qquad Br(K_L\to\pi^0\mu^+\mu^-) < 38\cdot 10^{-11} \quad [86] \quad (6.3.47)$$

are still by one order of magnitude larger than the SM predictions [83]

$$Br(K_L\to\pi^0e^+e^-)_{\rm SM} = 3.54^{+0.98}_{-0.85}\left(1.56^{+0.62}_{-0.49}\right)\cdot 10^{-11}, \quad (6.3.48)$$

$$Br(K_L\to\pi^0\mu^+\mu^-)_{\rm SM} = 1.41^{+0.28}_{-0.26}\left(0.95^{+0.22}_{-0.21}\right)\cdot 10^{-11}, \quad (6.3.49)$$

with the values in parentheses corresponding to the "−" sign in (6.3.38).

In order to evaluate (6.3.38) we have to determine the missing function Z_K, which contains both $\bar{Z}_{\rm even}$ and $\bar{Z}_K^{\rm odd}$. For the calculation of $C^{\rm even}$ we simply use the function $C_{\rm even}$ from Chapter 4 and impose T-parity, which leads to

$$\begin{aligned} C^{\rm even}_{\rm unitary} &= \frac{x_L^2}{8}\frac{v^2}{f^2}S_{\rm even}\left(\frac{x_t-x_T}{2} - d_2x_T\frac{v^2}{f^2}\right) \\ &\quad -\frac{x_L^2}{16}\frac{v^2}{f^2}\left(\frac{-6-5x_t+5x_t^2-3x_T+3x_tx_T}{2(x_t-1)}\right. \\ &\quad \left. +\frac{8x_t-10x_t^2+5x_t^3}{(x_t-1)^2}\log x_t - (4x_t+x_T)\log x_T\right) \\ &\quad +\frac{x_L^2}{8}\frac{v^4}{f^4}x_T\left(-\frac{3}{2}d_2 + x_L^2 + d_2\log x_T\right), \end{aligned} \quad (6.3.50)$$

with

$$S_{\rm even} = \frac{1}{\varepsilon} + \log\frac{\mu^2}{M_{W_L}^2}, \quad (6.3.51)$$

and d_2 defined in (4.2.68).

Using the function $D_{\rm SM}$ in the unitary gauge,

$$\begin{aligned} D^{\rm SM}_{\rm unitary}(x_t) &= \frac{x_t}{4}S_{\rm even} + \frac{-153x_t+383x_t^2-245x_t^3+27x_t^4}{72(x_t-1)^3} \\ &\quad -\frac{16-64x_t+36x_t^2+93x_t^3-84x_t^4+9x_t^5}{36(x_t-1)^4}\log x_t, \end{aligned} \quad (6.3.52)$$

which has been calculated in [17], we can derive D_{even} in the LHT model similar to $B \to X_s\gamma$ in [7] as

$$D^{\text{even}}_{\text{unitary}} = \frac{v^2}{f^2}x_L^2\left[\left(1+2d_2\frac{v^2}{f^2}\right)D^{\text{SM}}_{\text{unitary}}(x_T) - D^{\text{SM}}_{\text{unitary}}(x_t)\right]. \tag{6.3.53}$$

Subsequently, after having dropped $\mathcal{O}(v^4/f^4)$ terms,

$$\begin{aligned} D^{\text{even}}_{\text{unitary}} &= \frac{v^2}{f^2}x_L^2\left[\frac{x_T}{4}\left(1+2d_2\frac{v^2}{f^2}\right)S_{\text{even}} - D^{\text{SM}}_{\text{unitary}}(x_t)\right] \\ &\quad + \frac{v^2}{f^2}x_L^2\left[-\frac{41-24\log x_T}{18} + \frac{x_T}{8}\left(1+2d_2\frac{v^2}{f^2}\right)(3-2\log x_T)\right], \end{aligned} \tag{6.3.54}$$

so that we can finally write down the gauge independent function $\bar{Z}_{\text{even}}$ as

$$\bar{Z}_{\text{even}} = C^{\text{even}}_{\text{unitary}} + \frac{1}{4}D^{\text{even}}_{\text{unitary}}. \tag{6.3.55}$$

Since all the divergences in (6.3.55) cancel, $\bar{Z}_{\text{even}}$ turns out to be finite, being consistent with the statement in the last paragraph of Subsection 6.2.2.

Analogously in the T-odd sector we can derive the contribution Z_{odd},

$$Z_{\text{odd}}(z_i) = C_{\text{odd}}(z_i) + \frac{1}{4}D_{\text{odd}}(z_i), \tag{6.3.56}$$

by using (6.2.16), from which we find in the 't Hooft-Feynman gauge

$$C_{\text{odd}}(z_i) = \Delta J^{\mu\bar{\mu}} = \frac{1}{64}\frac{v^2}{f^2}\left[z_i S_{\text{odd}} - 8z_i R_2(z_i) + \frac{3}{2}z_i + 2z_i F_2(z_i)\right]. \tag{6.3.57}$$

The divergent part S_{odd} in (6.3.57) is defined in (6.5.92), whereas the functions R_2 and F_2 are listed in Appendix A.4.

Finally, using our calculation of $B \to X_s\gamma$ in [15] we determine $D_{\text{odd}}(z_i)$ to be

$$D_{\text{odd}}(z_i) = \frac{1}{4}\frac{v^2}{f^2}\left[D_0(z_i) - \frac{1}{6}E_0(z_i) - \frac{1}{30}E_0(z_i')\right] \tag{6.3.58}$$

with D_0 and E_0 given in Appendix A.4. With the help of C_{odd} and D_{odd} we can now write down the final result $\bar{Z}^{\text{odd}}_K$, which reads

$$\bar{Z}^{\text{odd}}_K = \left[\xi_2^{(K)}\big(Z_{\text{odd}}(z_2) - Z_{\text{odd}}(z_1)\big) + \xi_3^{(K)}\big(Z_{\text{odd}}(z_3) - Z_{\text{odd}}(z_1)\big)\right]. \tag{6.3.59}$$

To estimate the remaining divergence in Z_{odd} coming from $C_{\text{odd}}(z_i)$, we proceed as outlined in Subsection 6.2.2.

6.4 Numerical Impact of the LHT on Rare Decays

6.4.1 Preliminaries and Benchmark Scenarios

To consider the numerical impact on the branching ratios of the last subsections we assume three scenarios both for the structure of the V_{Hd} matrix and the mass spectrum of mirror

fermions. Due to the new sources of flavor and CP violation in the mirror sector of the LHT we will see a modification of the CMFV correlations between K^0, B_d^0 and B_s^0 systems [55, 56, 67]. In the first two scenarios we set the phases δ_{12}^d and δ_{23}^d to zero, while in the third scenario we perform a general scan over all mirror fermion masses and V_{Hd} parameters with δ_{12}^d and δ_{23}^d different from zero. We find that such a simplification does not affect the general results of the analysis. Consequently such a numerical analysis helps us to gain a global view of the possible signatures of mirror fermions in the processes considered and of T_+ present in the T-even contributions.

$\lvert V_{ub}\rvert = 3.68(14)\cdot 10^{-3}$ [87]	$G_F = 1.16637(1)\cdot 10^{-5}\,\text{GeV}^{-2}$
$\lvert V_{cb}\rvert = 0.0416(9)$ [59]	$M_W = 80.425(38)\,\text{GeV}$
$\lambda = \lvert V_{us}\rvert = 0.225(1)$ [60]	$\alpha = 1/127.9$
$\lvert V_{ts}\rvert = 0.0409(9)$ [61]	$\sin^2\theta_W = 0.23120(15)$
$A = 0.822(16)$	$m_{K^0} = 497.65(2)\,\text{MeV}$
$R_b = 0.447(31)$	$m_{B_d} = 5.2794(5)\,\text{GeV}$
$\beta = 26.3(21)^\circ$	$m_{B_s} = 5.370(2)\,\text{GeV}$
$\beta_s = -1.28(7)^\circ$	$F_K = 160(1)\,\text{MeV}$ [88]
$\overline{m}_\text{c} = 1.30(5)\,\text{GeV}$	$F_{B_d} = 189(27)\,\text{MeV}$
$\overline{m}_\text{t} = 163.8(32)\,\text{GeV}$	$F_{B_s} = 230(30)\,\text{MeV}$ [89]

Table 6.1: *Values of the experimental and theoretical quantities used as input parameters.*

Benchmark Scenarios

Scenario 1 (green):
This scenario yields large departures from the SM and MFV in B_s decays and can solve some problems mentioned in [15]. For example, it is possible to explain the discrepancy between the value of $\sin 2\beta$ coming from tree-level decays and the one coming from the CP-asymmetry $A_{CP}(B_d \to \psi K_S)$. Moreover, it also gives reasons to understand the mass difference $(\Delta M_s)_{LHT} < (\Delta M_s)_{SM}$, as favored by the CDF and DØ measurement [57, 58]. In this scenario the parameters are assumed to be

$$m_{H1} \approx m_{H2} = 500\,\text{GeV}\,, \qquad m_{H3} = 1000\,\text{GeV}\,, \tag{6.4.60}$$

$$\frac{1}{\sqrt{2}} \leq s_{12}^d \leq 0.99\,, \qquad 5\cdot 10^{-5} \leq s_{23}^d \leq 2\cdot 10^{-4}\,, \qquad 4\cdot 10^{-2} \leq s_{13}^d \leq 0.6\,. \tag{6.4.61}$$

δ_{12}^d and δ_{23}^d are set to zero, while the phase δ_{13}^d is arbitrary and the hierarchical structure of the CKM matrix, $s_{13} \ll s_{23} \ll s_{12}$, is changed to

$$s_{23}^d \ll s_{13}^d \leq s_{12}^d\,, \qquad (V_{Hd}) \tag{6.4.62}$$

leading to the following V_{Hd}

$$V_{Hd} = \begin{pmatrix} c_{12}^d & s_{12}^d & s_{13}^d e^{-i\delta_{13}^d} \\ -s_{12}^d & c_{12}^d & s_{23}^d \\ -c_{12}^d s_{13}^d e^{i\delta_{13}^d} & -s_{12}^d s_{13}^d e^{i\delta_{13}^d} & 1 \end{pmatrix}. \tag{6.4.63}$$

With the degeneracy $m_{H1} \approx m_{H2}$ the T-odd contributions in ε_K proportional to $\mathrm{Im}(\xi_2^K)$ and $\mathrm{Re}(\xi_2^K)$ vanish, and only the T-odd term proportional to $\mathrm{Im}(\xi_3^K)\mathrm{Re}(\xi_3^K)$ contributes. Since $\mathrm{Im}(\xi_3^K) = s_{13}^d c_{23}^d s_{23}^d \sin\delta_{13}^d$, the hierarchy chosen in this scenario for V_{Hd}, with $s_{23}^d \ll 1$, has the advantage of suppressing mirror fermion effects in ε_K, allowing at the same time large CP-violating effects in the $B_s^0 - \bar{B}_s^0$ system [15]. Furthermore, ΔM_s can be smaller than its SM value in this scenario, and interesting effects in the $B_d^0 - \bar{B}_d^0$ system are also found.

Scenario 2 (brown):
In studying this scenario we aim to enhance mirror fermion contributions to rare K decays, keeping negligible effects in the experimentally well measured quantities ΔM_K and ε_K. For this purpose we choose the mirror fermion masses as in Scenario 1 (see (6.4.60)) since the near degeneracy between m_{H1} and m_{H2} helps to suppress mirror fermion effects in ΔM_K.

Concerning ε_K, we recall that with the degeneracy $m_{H1} \approx m_{H2}$ the T-odd contributions proportional to $\mathrm{Im}(\xi_2^K)$ and $\mathrm{Re}(\xi_2^K)$ vanish, and only the T-odd term proportional to $\mathrm{Im}(\xi_3^K)\mathrm{Re}(\xi_3^K)$ contributes. In Scenario 1 the hierarchical structure of V_{Hd} was chosen as to satisfy $\mathrm{Im}(\xi_3^K) \simeq 0$. Here, instead, we suppress mirror fermion effects in ε_K due to the second and third generations by requiring $\mathrm{Re}(\xi_3^K) = 0$. Setting also in this scenario the phases δ_{12}^d and δ_{23}^d to zero, the explicit expression of the real part reads

$$\mathrm{Re}(\xi_3^K) = -c_{12}^d s_{12}^d \left({s_{23}^d}^2 - {c_{23}^d}^2 {s_{13}^d}^2 \right) + (\cos\delta_{13}^d)\, c_{23}^d s_{23}^d s_{13}^d \left({c_{12}^d}^2 - {s_{12}^d}^2 \right), \tag{6.4.64}$$

which vanishes for θ_{12}^d, θ_{23}^d and θ_{13}^d (chosen in the first quadrant) satisfying

$$c_{12}^d = s_{12}^d = \frac{1}{\sqrt{2}}, \tag{6.4.65}$$

$$s_{23}^d = \frac{s_{13}^d}{\sqrt{1 + {s_{13}^d}^2}}. \tag{6.4.66}$$

We note that while the value of θ_{12}^d is fixed to 45° by (6.4.65), θ_{23}^d and θ_{13}^d have no specified value nor order of magnitude, but (6.4.66) implies that only one of them is a free parameter. The matrix V_{Hd} can then be expressed in terms of the two free parameters θ_{13}^d and δ_{13}^d as

$$V_{Hd} = \begin{pmatrix} \frac{c_{13}^d}{\sqrt{2}} & \frac{c_{13}^d}{\sqrt{2}} & s_{13}^d e^{-i\delta_{13}^d} \\ -\frac{1}{\sqrt{2}\sqrt{1+{s_{13}^d}^2}}\left(1 + \left(s_{13}^d\right)^2 e^{i\delta_{13}^d}\right) & \frac{1}{\sqrt{2}\sqrt{1+{s_{13}^d}^2}}\left(1 - \left(s_{13}^d\right)^2 e^{i\delta_{13}^d}\right) & \frac{s_{13}^d c_{13}^d}{\sqrt{1+{s_{13}^d}^2}} \\ \frac{s_{13}^d}{\sqrt{2}\sqrt{1+{s_{13}^d}^2}}\left(1 - e^{i\delta_{13}^d}\right) & -\frac{s_{13}^d}{\sqrt{2}\sqrt{1+{s_{13}^d}^2}}\left(1 + e^{i\delta_{13}^d}\right) & \frac{c_{13}^d}{\sqrt{1+{s_{13}^d}^2}} \end{pmatrix}. \tag{6.4.67}$$

Its structure becomes much simpler if the angle θ_{13}^d is sufficiently small, i. e., $s_{13}^d \leq 0.1$, and reads

$$V_{Hd} \approx \begin{pmatrix} \frac{1}{\sqrt{2}} & \frac{1}{\sqrt{2}} & s_{13}^d e^{-i\delta_{13}^d} \\ -\frac{1}{\sqrt{2}} & \frac{1}{\sqrt{2}} & s_{13}^d \\ \frac{s_{13}^d}{\sqrt{2}}(1-e^{i\delta_{13}^d}) & -\frac{s_{13}^d}{\sqrt{2}}(1+e^{i\delta_{13}^d}) & 1 \end{pmatrix}. \tag{6.4.68}$$

As we will see the very different structure of V_{Hd} as compared to $V_{\rm CKM}$ implies enhancements in rare K decays, without introducing problematic effects in ΔM_K and ε_K. Moreover, as V_{Hd} in (6.4.68) has a structure different also from the one of Scenario 1 in (6.4.63), the new physics effects in the $B_d^0 - \bar{B}_d^0$ and mainly in the $B_s^0 - \bar{B}_s^0$ system turn out to be small, although visible.

Scenario 3 (blue):

Scenarios 1 and 2 turn out to be the most interesting ones with large new physics effects in the B_s and K systems, respectively. Such visible enhancements follow from the structure of V_{Hd}, primarily required to satisfy the ε_K and ΔM_K constraints, through $\mathrm{Im}(\xi_3^K) \approx 0$ in Scenario 1 and through $\mathrm{Re}(\xi_3^K) = 0$ in Scenario 2. A further consequence of the V_{Hd} structure is that in Scenario 1 spectacular effects can be obtained in the B_s system but not in the K system and vice versa in Scenario 2. An even more interesting picture would be the simultaneous manifestation of large enhancements in both B and K observables. In order not to miss such a possibility, in addition to the scenarios described above, we have performed a general scan over mirror fermion masses and V_{Hd} parameters. To have a global view of the most general LHT effects, we have allowed here the phases δ_{12}^d and δ_{23}^d to differ from zero. Qualitatively their effect is not significant, although they can help in achieving very large effects in certain observables. We find that there exist some sets of masses and V_{Hd} parameters where the new physics effects turn out to be spectacular in both B and K systems. We note that they do not really constitute a scenario, they rather appear in the plots shown in the next section as isolated (blue) points. In contrast to previous scenarios, in fact, the blue points corresponding to large new physics effects are quite sensitive to the particular configuration of mirror fermion masses and V_{Hd} parameters.

6.4.2 Numerical Analysis

Breakdown of the Universality

Since in the LHT the universality of the functions X_i, Y_i and Z_i is broken by the presence of the mirror fermions we expect many quantities to deviate from MFV relations. One of the first correlations where this breakdown of universality becomes obvious is the space of $(|X_s|, |X_K|)$. In Fig. 6.4 we show the ranges of possible points for X_s and X_K in the different scenarios defined above. The solid line represents the MFV scenario, in which the functions X_i do not depend on the index i, i.e. $X_s = X_K$. Any departure from this line indicates

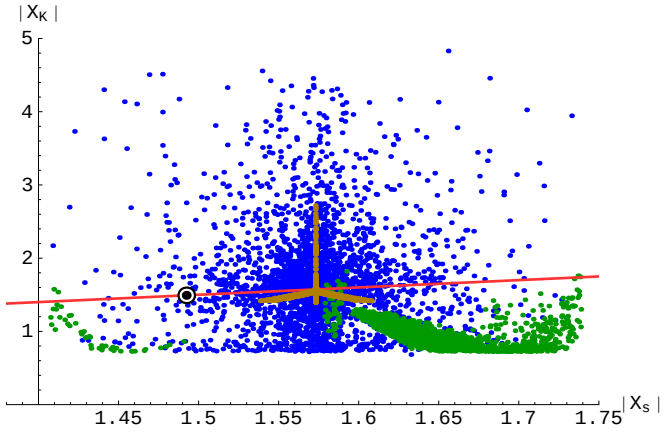

Figure 6.4: *Breakdown of the universality between $|X_K|$ versus $|X_s|$, where the black dot corresponds to the SM value.*

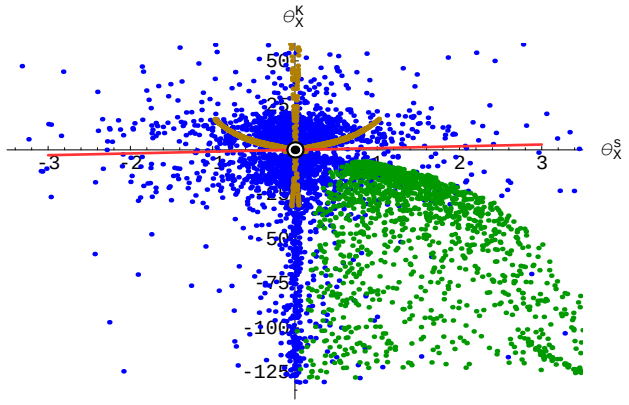

Figure 6.5: *Breakdown of the universality between θ_X^K versus θ_X^s, where the black dot corresponds to the SM value.*

a deviation from MFV relations and thus provides a hint for physics beyond the SM. From Fig. 6.4 we can see that $|X_s|$ and $|X_K|$ vary within the range

$$1.40 \leq |X_s| \leq 1.75, \quad 0.7 \leq |X_K| \leq 4.7, \tag{6.4.69}$$

which implies that CP-conserving effects in the K system can be much larger than in the B_s system. This is due to the fact that contributions from the T-odd sector in (6.1.3) are enhanced by a factor $1/\lambda_t^{(i)}$. In the case of the K system this leads to an enhancement of $1/\lambda_t^{(K)} \simeq 1/\left(4 \cdot 10^{-4}\right)$ whereas in the $B_{d,s}$ system $1/\lambda_t^{(d)} \simeq 1/\left(1 \cdot 10^{-2}\right)$ and $1/\lambda_t^{(s)} \simeq 1/\left(4 \cdot 10^{-2}\right)$. Therefore effects in the K system tend to be larger compared to the $B_{d,s}$ system.

Apart from the departure of MFV in CP-conserving processes we can also observe deviations from MFV relations in the CP-violating quantities θ_X^s and θ_X^K. In Fig. 6.5 we can see

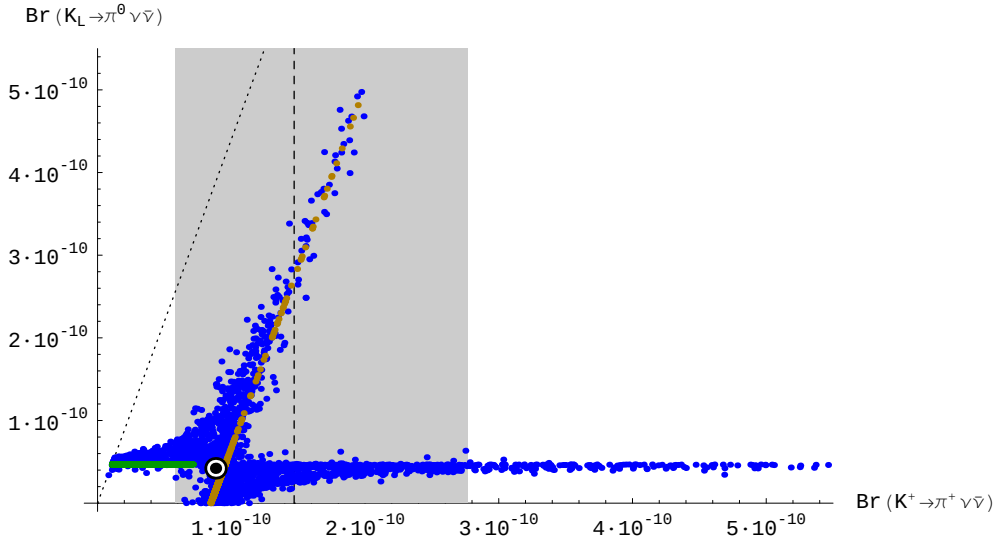

Figure 6.6: $Br\left(K_L \to \pi^0\nu\bar{\nu}\right)$ *as a function of* $Br\left(K^+ \to \pi^+\nu\bar{\nu}\right)$. *The shaded area represents the experimental* 1σ*-range for* $Br\left(K^+ \to \pi^+\nu\bar{\nu}\right)$. *The GN-bound is displayed by the dotted line, while the solid line separates the two areas where* $Br\left(K_L \to \pi^0\nu\bar{\nu}\right)$ *is larger or smaller than* $Br\left(K^+ \to \pi^+\nu\bar{\nu}\right)$.

that the ranges in the space $\left(\theta_X^s, \theta_X^K\right)$ turn out to be

$$-3.5^\circ \leq \theta_X^s \leq 3.5^\circ, \quad -130^\circ \leq \theta_X^K \leq 55^\circ, \tag{6.4.70}$$

which means that CP-violating effects in $b \to s$ transitions are very small in contrast to those in K_L decays.

The Rare Decays $K^+ \to \pi^+\nu\bar{\nu}$ and $K_L \to \pi^0\nu\bar{\nu}$

In Fig. 6.6 we present the correlation between $Br\left(K^+ \to \pi^+\nu\bar{\nu}\right)$ and $Br\left(K_L \to \pi^0\nu\bar{\nu}\right)$ for the three scenarios described above. The grey shaded area in Fig. 6.6 depicts the allowed 1σ-range for $Br\left(K^+ \to \pi^+\nu\bar{\nu}\right)$ [73], while the dotted line corresponds to the model independent bound by *Grossman* and *Nir* [90]. It can be seen in the plot that the Scenario 3 yields two branches of possible points. The first one, parallel to the Grossman-Nir bound, can enhance $Br\left(K_L \to \pi^0\nu\bar{\nu}\right)$ up to $\mathcal{O}\left(5 \cdot 10^{-10}\right)$ but still lies within the 1σ range of $Br\left(K^+ \to \pi^+\nu\bar{\nu}\right)$. The second branch corresponds to values of $Br\left(K^+ \to \pi^+\nu\bar{\nu}\right)$ up to $\mathcal{O}\left(5 \cdot 10^{-10}\right)$ while the points for $Br\left(K_L \to \pi^0\nu\bar{\nu}\right)$ are close to the SM prediction. In the case of the Scenario 2 the picture described in the previous scenario simplifies considerably, since the first branch reduces to a single line and the second branch disappears completely. Finally in the Scenario 1 the branching ratio of $Br\left(K^+ \to \pi^+\nu\bar{\nu}\right)$ is always smaller than the SM value and can even get close to the Grossman-Nir bound, whereas $Br\left(K_L \to \pi^0\nu\bar{\nu}\right)$ sticks close to its SM value.

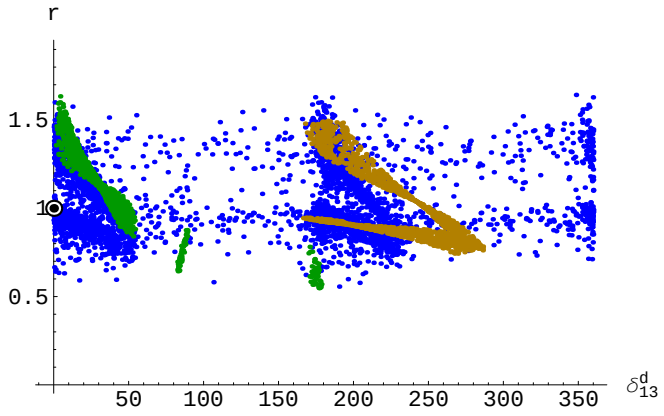

Figure 6.7: *The ratio r as a function of δ_{13}^d with the black dot denoting the SM value.*

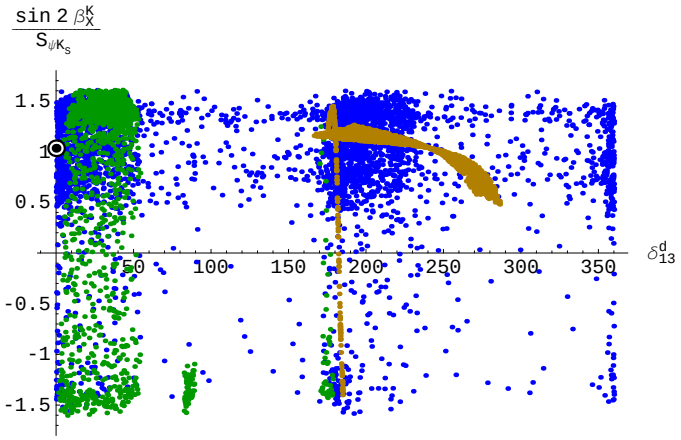

Figure 6.8: $\sin 2\beta_X^K / S_{\psi K_S}$ *as a function of δ_{13}^d with the black dot denoting the SM value.*

Deviations from MFV relations

In Fig. 6.7 we illustrate the variation of the ratio r defined in (6.3.35) in dependence of the new phase δ_{13}^d of the mixing matrix V_{Hd}. One can see that in Scenario 1, 2, 3 each large deviations from the SM value, which is denoted by the black dot, are possible. Any departure from unity, which can be measured by the parameter r, signals a violation of the golden relation between $B_{d,s} \to \mu^+\mu^-$ and $\Delta M_{d,s}$, which hints for new physics beyond the SM. In all scenarios considered here we find a range

$$0.6 \leq r \leq 1.7\,, \tag{6.4.71}$$

where the lower and upper bounds for r can be reached most easily in the Scenario 1.

Moreover, in Fig. 6.8 we present the correlation between the ratio $\sin 2\beta_X^K / \sin(2\beta + 2\varphi_{B_d})$ and the new phase δ_{13}^d, where in a MFV scenario this relation is given by $\sin 2\beta_X^K \equiv \sin(2\beta + 2\varphi_{B_d}) = S_{\psi K_S}$. As before any deviation of this ratio from unity would indicate contributions

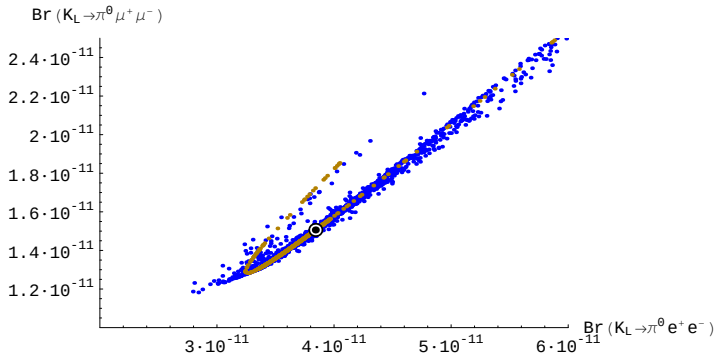

Figure 6.9: $Br\left(K_L \to \pi^0\mu^+\mu^-\right)$ *as a function of* $Br\left(K_L \to \pi^0 e^+e^-\right)$

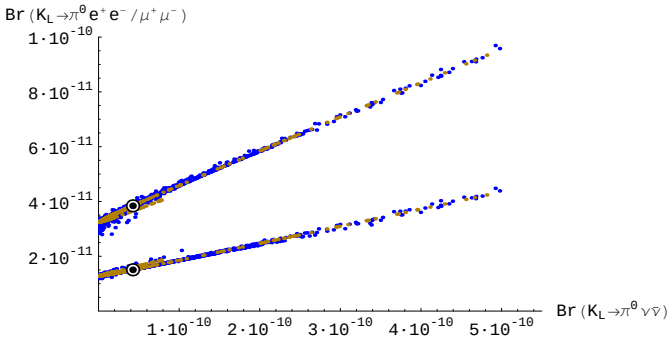

Figure 6.10: $Br\left(K_L \to \pi^0 e^+e^-\right)$ (upper curve) and $Br\left(K_L \to \pi^0\mu^+\mu^-\right)$ (lower curve) as functions of $Br\left(K_L \to \pi^0\nu\bar{\nu}\right)$. The corresponding SM predictions are represented by dark points.

that are coming from new physics. Since we know from the $S_{\psi K_s}$ asymmetry in [61, 67] that φ_{B_d} is constrained to be at most a few degrees, the existence of a phase β_X^K can produce these large deviations from unity as seen in Fig. 6.8.

The Decays $K_L \to \pi^0\ell^+\ell^-$

In Fig. 6.9 the correlation between $Br\left(K_L \to \pi^0 e^+e^-\right)$ and $Br\left(K_L \to \pi^0\mu^+\mu^-\right)$ is considered. We observe that this correlation is only moderately sensitive to the three different scenarios and that the branching ratios can be a factor two larger compared to the SM values, which are denoted by the black dots.

Furthermore we show $Br\left(K_L \to \pi^0 e^+e^-\right)$ and $Br\left(K_L \to \pi^0\mu^+\mu^-\right)$ as a function of the branching ratio $Br\left(K_L \to \pi^0\nu\bar{\nu}\right)$. It can be seen in Fig. 6.10 that a large enhancement of

$Br\left(K_L \to \pi^0 \nu\bar{\nu}\right)$ automatically implies an enhancement of $K_L \to \pi^0 \ell^+ \ell^-$. Furthermore, with the determination of $K_L \to \pi^0 \ell^+ \ell^-$ we would be able to predict $Br\left(K_L \to \pi^0 \nu\bar{\nu}\right)$ rather precisely.

6.5 Signatures of the LHT in Lepton Flavor Violating Decays

6.5.1 $\ell_i \to \ell_j \gamma$

Some of the most popular LFV processes used to constrain new physics contributions are the processes $\ell_i \to \ell_j \gamma$, which are bounded by the following current experimental upper limits [91, 92][1]

$$Br(\mu \to e\gamma) < 1.2 \cdot 10^{-11}\,, \tag{6.5.72}$$

$$Br(\tau \to \mu\gamma) < 1.6 \cdot 10^{-8}\,, \qquad Br(\tau \to e\gamma) < 9.4 \cdot 10^{-8}\,. \tag{6.5.73}$$

Among these the most interesting decay is the LFV process $\mu \to e\gamma$, since for this process the MEGA collaboration [91] will improve the upper bound down to $\mathcal{O}\left(10^{-13} - 10^{-14}\right)$ in the coming years.

In order to obtain the branching ratio $Br(\mu \to e\gamma)$ in the LHT model we take into account several elements of the $Br(B \to X_s\gamma)$ calculation in this model [15]. The generalization to $\tau \to \mu\gamma$ and $\tau \to e\gamma$ will then be automatic. For details of this calculation the reader is referred to [66].

The relevant diagrams for $\mu \to e\gamma$ in the LHT model are shown in Fig. 6.11, where we only consider contributions coming from mirror fermions as particles from the T-even sector give negligible contributions. Moreover diagrams involving the heavy scalar triplet Φ can be neglected since at this order in v/f they do not contribute (see [15, 17] for details).

Having calculated these diagrams we can write the resulting branching ratio as the sum of three different terms representing the $W_H^\pm$, Z_H and A_H contributions

$$Br(\mu \to e\gamma)_{\rm LHT} = \frac{3\alpha}{2\pi} \left|\Delta_{W_H} + \Delta_{Z_H} + \Delta_{A_H}\right|^2 . \tag{6.5.74}$$

Using the abbreviations

$$y_i = \frac{{m_{Hi}^\ell}^2}{M_{W_H}^2}\,, \qquad y_i' = a\, y_i \quad \text{with} \quad a = \frac{5}{\tan^2\theta_W} \simeq 16.6\,, \tag{6.5.75}$$

we explicitly find for Δ_{W_H}

$$\Delta_{W_H} = \frac{1}{4}\frac{v^2}{f^2} \sum_i \chi_i^{(\mu e)} H(y_i)\,, \tag{6.5.76}$$

where H is given in Appendix A.5 and $\chi_i^{(\mu e)}$ is defined in (5.2.54).

[1] The bounds in [92] have been obtained by combining Belle [93] and BaBar [94] results.

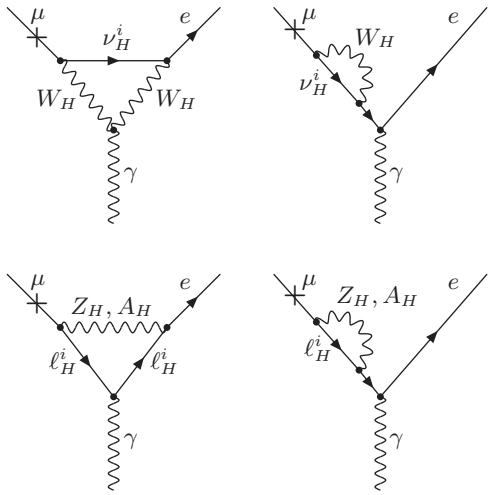

Figure 6.11: *Diagrams contributing to $\mu \to e\gamma$ in the LHT model.*

The neutral gauge boson contributions can directly be deduced from (4.10) of [15]. Including a factor 3 that takes into account the difference between the electric charges of quarks and leptons, we obtain from the last two terms in (4.10) of [15]

$$\Delta_{Z_H} = \frac{1}{4}\frac{v^2}{f^2}\sum_i \chi_i^{(\mu e)}\left[-\frac{1}{2}E_0'(y_i)\right], \tag{6.5.77}$$

$$\Delta_{A_H} = \frac{1}{4}\frac{v^2}{f^2}\sum_i \chi_i^{(\mu e)}\left[-\frac{1}{10}E_0'(y_i')\right]. \tag{6.5.78}$$

Finally, adding up these three contributions in (6.5.76)–(6.5.78), we arrive at the following result

$$Br(\mu \to e\gamma)_{\rm LHT} = \frac{3\alpha}{2\pi}\left|\bar{D}'^{\mu e}_{\rm odd}\right|^2, \tag{6.5.79}$$

with

$$\bar{D}'^{\mu e}_{\rm odd} = \frac{1}{4}\frac{v^2}{f^2}\left[\sum_i \chi_i^{(\mu e)}\left(D_0'(y_i) - \frac{7}{6}E_0'(y_i) - \frac{1}{10}E_0'(y_i')\right)\right], \tag{6.5.80}$$

and y_i defined in (6.5.75) and D_0', E_0' given in Appendix A.5.

The corresponding branching ratios for $\tau \to e\gamma$ and $\tau \to \mu\gamma$ can easily be found in analogy to $\mu \to e\gamma$ and read

$$Br(\tau \to e\gamma) = \frac{3\alpha}{2\pi}Br(\tau^- \to \nu_\tau e^- \bar{\nu}_e)\left|\bar{D}'^{\tau e}_{\rm odd}\right|^2, \tag{6.5.81}$$

$$Br(\tau \to \mu\gamma) = \frac{3\alpha}{2\pi}Br(\tau^- \to \nu_\tau \mu^- \bar{\nu}_\mu)\left|\bar{D}'^{\tau\mu}_{\rm odd}\right|^2, \tag{6.5.82}$$

where $\bar{D}'^{\tau e}_{\rm odd}$ and $\bar{D}'^{\tau\mu}_{\rm odd}$ can be obtained from (6.5.80) by replacing (μe) with (τe) and $(\tau\mu)$, respectively. Furthermore [88]

$$Br(\tau^- \to \nu_\tau e^- \bar{\nu}_e) = (17.84 \pm 0.05)\%, \qquad Br(\tau^- \to \nu_\tau \mu^- \bar{\nu}_\mu) = (17.36 \pm 0.05)\%. \tag{6.5.83}$$

6.5.2 Semileptonic τ Decays

In the last years the Belle [95] and BaBar [96] collaborations presented improved upper bounds for the decays $\tau \to \ell P$ ($P = \pi, \eta, \eta'$), which have been combined [92] to

$$Br(\tau \to \mu\pi) < 5.8 \cdot 10^{-8}\,, \qquad Br(\tau \to \mu\eta) < 5.1 \cdot 10^{-8}\,, \qquad Br(\tau \to \mu\eta') < 5.3 \cdot 10^{-8}\,, \tag{6.5.84}$$

$$Br(\tau \to e\pi) < 4.4 \cdot 10^{-8}\,, \qquad Br(\tau \to e\eta) < 4.5 \cdot 10^{-8}\,, \qquad Br(\tau \to e\eta') < 9.0 \cdot 10^{-8}\,, \tag{6.5.85}$$

thus increasing the interest in investigating these branching ratios in the LHT model.

In this subsection we will study these semileptonic decays with the help of the recent analysis of rare K and B decays in the LHT model [17]. In the case of $\tau \to \mu\pi$ the diagrams are completely analogous to the ones contributing to $K \to \pi\nu\bar{\nu}$. However, as π^0 has the following flavor structure

$$\pi^0 = \frac{\bar{u}u - \bar{d}d}{\sqrt{2}}\,, \tag{6.5.86}$$

we have to consider two sets of diagrams, with both $\bar{u}u$ and $\bar{d}d$ in the final state. From the analysis of rare K and B decays [17] we can directly obtain the corresponding effective Hamiltonians for $\tau \to \mu\pi$, which involve the short-distance functions $\bar{X}^{\tau\mu}_{\rm odd}$ and $-\bar{Y}^{\tau\mu}_{\rm odd}$ for $\bar{u}u$ and $\bar{d}d$, respectively. Taking into account the opposite sign that is conventionally chosen to define the two short distance functions, the effective Hamiltonian that includes both sets of diagrams is then given as follows

$$\mathcal{H}_{\rm eff} = \frac{G_F}{\sqrt{2}}\frac{\alpha}{2\pi\sin^2\theta_W}\left(\bar{X}^{\tau\mu}_{\rm odd}(\bar{u}u)_{V-A} - \bar{Y}^{\tau\mu}_{\rm odd}(\bar{d}d)_{V-A}\right)(\bar{\mu}\tau)_{V-A}\,. \tag{6.5.87}$$

The structure of $\bar{X}^{\tau\mu}_{\rm odd}$ and $\bar{Y}^{\tau\mu}_{\rm odd}$ in (6.5.87) is the same as those of the functions calculated in the context of rare K and B decays [17]. Adapting them to the lepton sector we find:

$$\bar{X}^{\tau\mu}_{\rm odd} = \left[\chi_2^{(\tau\mu)}\left(J^{u\bar{u}}(y_2,z) - J^{u\bar{u}}(y_1,z)\right) + \chi_3^{(\tau\mu)}\left(J^{u\bar{u}}(y_3,z) - J^{u\bar{u}}(y_1,z)\right)\right], \tag{6.5.88}$$

$$\bar{Y}^{\tau\mu}_{\rm odd} = \left[\chi_2^{(\tau\mu)}\left(J^{d\bar{d}}(y_2,z) - J^{d\bar{d}}(y_1,z)\right) + \chi_3^{(\tau\mu)}\left(J^{d\bar{d}}(y_3,z) - J^{d\bar{d}}(y_1,z)\right)\right], \tag{6.5.89}$$

where

$$J^{u\bar{u}}(y_i,z) = \frac{1}{64}\frac{v^2}{f^2}\Bigg[y_i S_{\rm odd} + F^{u\bar{u}}(y_i,z;W_H) + 4\Big(G(y_i,z;Z_H) + G_1(y_i',z';A_H) + G_2(y_i,z;\eta)\Big)\Bigg], \tag{6.5.90}$$

$$J^{d\bar{d}}(y_i,z) = \frac{1}{64}\frac{v^2}{f^2}\Bigg[y_i S_{\rm odd} + F^{d\bar{d}}(y_i,z;W_H) - 4\Big(G(y_i,z;Z_H) + G_1(y_i',z';A_H) - G_2(y_i,z;\eta)\Big)\Bigg], \tag{6.5.91}$$

$$S_{\rm odd} = \frac{1}{\varepsilon} + \log\frac{\mu^2}{M_{W_H}^2} \longrightarrow \log\frac{(4\pi f)^2}{M_{W_H}^2}\,, \tag{6.5.92}$$

with the functions $F^{u\bar{u}}$, $F^{d\bar{d}}$, G, G_1 and G_2 given in Appendix A.5, the leptonic variables y_i and y_i' defined in (6.5.75) and the analogous variables for degenerate mirror quarks given by

$$z = \frac{{m_H^q}^2}{M_{W_H}^2}\,, \qquad z' = a\,z\,, \quad \eta = \frac{1}{a}\,. \tag{6.5.93}$$

Evaluating the matrix elements by

$$\langle 0|(\bar{u}u)_{V-A}|\pi^0\rangle = -\langle 0|(\bar{d}d)_{V-A}|\pi^0\rangle = \frac{F_\pi p_\pi^\mu}{\sqrt{2}}\,, \tag{6.5.94}$$

where $F_\pi \simeq 131\,\text{MeV}$ is the pion decay constant, we arrive at the final branching ratio

$$Br(\tau \to \mu\pi) = \frac{G_F^2\alpha^2 F_\pi^2 m_\tau^3 \tau_\tau}{128\pi^3 \sin^4\theta_W}\,|\bar{X}_{\text{odd}}^{\tau\mu} + \bar{Y}_{\text{odd}}^{\tau\mu}|^2\,, \tag{6.5.95}$$

with τ_τ and m_τ being the lifetime and mass of the decaying τ, and neglecting suppressed pion and muon mass contributions of the order $\mathcal{O}(m_\pi^2/m_\tau^2)$ and $\mathcal{O}(m_\mu^2/m_\tau^2)$. Analogously we can obtain the branching ratio for the $\tau \to e\pi$ decay very easily from (6.5.95) by simply replacing $(\tau\mu)$ with (τe). The generalization of (6.5.95) to the decays $\tau \to \mu\eta$ and $\tau \to \mu\eta'$ is then straightforward too, although slightly complicated by mixing in the $\eta - \eta'$ system. For details the reader is referred to [66].

6.5.3 $\mu^- \to e^-e^+e^-$, $\tau^- \to \mu^-\mu^+\mu^-$ and $\tau^- \to e^-e^+e^-$

Next, we will consider the decay $\mu^- \to e^-e^+e^-$, for which the experimental upper bound reads [97]

$$Br(\mu^- \to e^-e^+e^-) < 1.0 \cdot 10^{-12}\,. \tag{6.5.96}$$

Using the analogies to the $b \to s\mu^+\mu^-$ transition, analyzed in the LHT model in [17] this decay is governed by contributions from γ- and Z^0-penguins and by box diagrams. However, two identical particles are now present in the final state which prevent us from using directly the known final expressions for $b \to s\mu^+\mu^-$, although some intermediate results from the latter decay turned out to be useful here. Also the general result for $\mu^- \to e^-e^+e^-$ obtained in [98], which has been corrected in [20, 22], turned out to be very helpful.

Performing the calculation in the unitary gauge, where we find the contribution from the Z^0-penguin to vanish [17], we find for the relevant amplitudes from photon penguins and box diagrams[2]:

$$\begin{aligned}
\mathcal{A}_{\gamma'} &= \frac{G_F}{\sqrt{2}}\frac{e^2}{8\pi^2}\frac{1}{q^2}\bar{D}'^{\mu e}_{\text{odd}}\Big[\bar{e}(p_1)(m_\mu i\sigma_{\alpha\beta}q^\beta(1+\gamma_5))\mu(p)\Big]\otimes[\bar{e}(p_2)\gamma^\alpha e(p_3)] \\
&\qquad -(p_1 \leftrightarrow p_2)\,, \qquad (6.5.97)\\
\mathcal{A}_{\gamma} &= -\left[4\frac{G_F}{\sqrt{2}}\frac{e^2}{8\pi^2}\bar{Z}^{\mu e}_{\text{odd}}\,[\bar{e}(p_1)\gamma_\alpha(1-\gamma_5)\mu(p)]\otimes[\bar{e}(p_2)\gamma^\alpha e(p_3)] - (p_1 \leftrightarrow p_2)\right]\,, \qquad (6.5.98)\\
\mathcal{A}_{\text{box}} &= 2\frac{G_F}{\sqrt{2}}\frac{\alpha}{2\pi\sin^2\theta_W}\bar{Y}^{\mu e}_{e,\text{odd}}\,[\bar{e}(p_1)\gamma_\alpha(1-\gamma_5)\mu(p)]\otimes[\bar{e}(p_2)\gamma^\alpha(1-\gamma_5)e(p_3)]\,. \qquad (6.5.99)
\end{aligned}$$

[2] Following [98], our sign conventions are chosen such that $\mathcal{H}_{\text{eff}}$ is determined from $-\mathcal{A}$.

The function $\bar{D}'^{\mu e}_{\rm odd}$ is given in (6.5.80), while the functions $\bar{Y}^{\mu e}_{e,\rm odd}$ and $\bar{Z}^{\mu e}_{\rm odd}$ can easily be obtained from those calculated in [17]. The analogy with the $b \to s\mu^+\mu^-$ decay, together with the observation that the $\mu^- \to e^-e^+e^-$ decay in question involves only leptons in both the initial and final states, allow us to write[3]

$$\begin{aligned}\bar{Y}^{\mu e}_{e,\rm odd} &= \chi_2^{(\mu e)} \sum_{i=1}^{3} |V^{ie}_{H\ell}|^2 \left[J^{d\bar{d}}(y_2,y_i) - J^{d\bar{d}}(y_1,y_i)\right] \\ &\quad + \chi_3^{(\mu e)} \sum_{i=1}^{3} |V^{ie}_{H\ell}|^2 \left[J^{d\bar{d}}(y_3,y_i) - J^{d\bar{d}}(y_1,y_i)\right], \end{aligned} \tag{6.5.100}$$

with $J^{d\bar{d}}$ given in (6.5.91). Following a similar reasoning we can write for the $\bar{Z}^{\mu e}_{\rm odd}$ function

$$\bar{Z}^{\mu e}_{\rm odd} = \left[\chi_2^{(\mu e)}\big(Z_{\rm odd}(y_2) - Z_{\rm odd}(y_1)\big) + \chi_3^{(\mu e)}\big(Z_{\rm odd}(y_3) - Z_{\rm odd}(y_1)\big)\right], \tag{6.5.101}$$

where

$$Z_{\rm odd}(y_i) = C_{\rm odd}(y_i) + \frac{1}{4} D_{\rm odd}(y_i)\,. \tag{6.5.102}$$

The explicit expressions for the $C_{\rm odd}$ and $D_{\rm odd}$ functions are given in Appendix A.5[4]. Here, we just note that as a consequence of the charge difference between the leptons involved in $\mu^- \to e^-e^+e^-$ and the quarks involved in $b \to s\mu^+\mu^-$, $D_{\rm odd}$ in (6.5.102) differs from the analogous function found in [17].

Comparing these expressions to the general expressions for the amplitudes given in [22, 98], we easily obtain $\Gamma(\mu^- \to e^-e^+e^-)$. Normalizing to $\Gamma(\mu^- \to e^-\bar{\nu}_e\nu_\mu)$, we find the branching ratio for the decay $\mu^- \to e^-e^+e^-$ to be

$$\begin{aligned} Br(\mu^- \to e^-e^+e^-) &= \frac{\Gamma(\mu^- \to e^-e^+e^-)}{\Gamma(\mu^- \to e^-\bar{\nu}_e\nu_\mu)} \\ &= \frac{\alpha^2}{\pi^2}\Bigg[3\left|\bar{Z}^{\mu e}_{\rm odd}\right|^2 + 3\,{\rm Re}\left(\bar{Z}^{\mu e}_{\rm odd}(\bar{D}'^{\mu e}_{\rm odd})^*\right) + \left|\bar{D}'^{\mu e}_{\rm odd}\right|^2\left(\log\frac{m_\mu}{m_e} - \frac{11}{8}\right) \\ &\quad + \frac{1}{2\sin^4\theta_W}\left|\bar{Y}^{\mu e}_{e,\rm odd}\right|^2 - \frac{2}{\sin^2\theta_W}{\rm Re}\left(\bar{Z}^{\mu e}_{\rm odd}(\bar{Y}^{\mu e}_{e,\rm odd})^*\right) \\ &\quad - \frac{1}{\sin^2\theta_W}{\rm Re}\left(\bar{D}'^{\mu e}_{\rm odd}(\bar{Y}^{\mu e}_{e,\rm odd})^*\right)\Bigg]. \end{aligned} \tag{6.5.103}$$

For $\tau^- \to \mu^-\mu^+\mu^-$ we make the following replacements in (6.5.97)–(6.5.103):

$$V^{ie}_{H\ell} \to V^{i\mu}_{H\ell}\,, \qquad (\mu e) \to (\tau\mu)\,, \qquad m_\mu \to m_\tau\,, \qquad m_e \to m_\mu\,, \tag{6.5.104}$$

[3]The subscript e of $\bar{Y}^{\mu e}_{e,\rm odd}$ denotes which of the SM charged leptons appears on the flavor conserving side of the relevant box diagrams.

[4]Note that the functions $C_{\rm odd}$ and $D_{\rm odd}$ are gauge dependent and have been calculated in the 't Hooft-Feynman gauge. However, the function $\bar{Z}^{\mu e}_{\rm odd}$ is gauge independent, so that it can be used also in the unitary gauge calculation above.

so that, in particular, $\bar{Y}^{\tau\mu}_{\mu,\text{odd}}$ is now present. Furthermore, in (6.5.103) the normalization $\Gamma(\mu^- \to e^-\nu_\mu\bar{\nu}_e)$ is replaced by $\Gamma(\tau^- \to \mu^-\nu_\tau\bar{\nu}_\mu)$, so that the final result for $Br(\tau^- \to \mu^-\mu^+\mu^-)$ contains an additional factor $Br(\tau^- \to \mu^-\nu_\tau\bar{\nu}_\mu)$. In the case of $\tau^- \to e^-e^+e^-$ the replacements in (6.5.100)–(6.5.103) amount only to

$$(\mu e) \to (\tau e)\,, \qquad m_\mu \to m_\tau\,, \tag{6.5.105}$$

having now $\bar{Y}^{\tau e}_{e,\text{odd}}$, and in (6.5.103) $\Gamma(\mu^- \to e^-\nu_\mu\bar{\nu}_e)$ is replaced by $\Gamma(\tau^- \to e^-\nu_\tau\bar{\nu}_e)$ and an additional factor $Br(\tau^- \to e^-\nu_\tau\bar{\nu}_e)$ appears. In doing this we neglect $m_{e,\mu}$ with respect to m_τ in all three expressions.

6.5.4 $\mu - e$ Conversion in Nuclei

Similarly to the decays $\mu \to e\gamma$ and $\mu^- \to e^-e^+e^-$, stringent experimental upper bounds on $\mu - e$ conversion in nuclei exist. In particular, the experimental upper bound on $\mu - e$ conversion in $^{48}_{22}$Ti reads [99]

$$R(\mu\text{Ti} \to e\text{Ti}) < 4.3 \cdot 10^{-12}\,, \tag{6.5.106}$$

and the dedicated J-PARC experiment PRISM/PRIME should reach a sensitivity of $\mathcal{O}(10^{-18})$ [100].

A very detailed calculation of the $\mu-e$ conversion rate in various nuclei has been performed in [101], using the methods developed by *Czarnecki et al.* [102]. It has been emphasized in [101] that the atomic number dependence of the conversion rate can be used to distinguish between different theoretical models of LFV. Useful general formulae can also be found in [98].

We have calculated the $\mu-e$ conversion rate in nuclei in the LHT model using the general model-independent formulae of both [98] and [101]. We have checked numerically that, for relatively light nuclei such as Ti, both results agree within 10%. Therefore, we will give the result for $\mu - e$ conversion in nuclei derived from the general expression given in [98], as it has a more transparent structure than the one of [101].

Following a similar reasoning as in the previous section, we find from (58) of [98]

$$\begin{aligned}\Gamma(\mu\text{X} \to e\text{X}) = {} & \frac{G_F^2}{8\pi^4}\alpha^5\frac{Z_{\text{eff}}^4}{Z}|F(q)|^2 m_\mu^5 \\ & \cdot\left|Z\left(4\bar{Z}^{\mu e}_{\text{odd}} + \bar{D}'^{\mu e}_{\text{odd}}\right) - (2Z+N)\frac{\bar{X}^{\mu e}_{\text{odd}}}{\sin^2\theta_W} + (Z+2N)\frac{\bar{Y}^{\mu e}_{\text{odd}}}{\sin^2\theta_W}\right|^2\,,\end{aligned} \tag{6.5.107}$$

where $\bar{X}^{\mu e}_{\text{odd}}$ and $\bar{Y}^{\mu e}_{\text{odd}}$ are obtained from (6.5.88) and (6.5.89) by making the replacement $(\tau\mu) \to (\mu e)$, and $\bar{D}'^{\mu e}_{\text{odd}}$ and $\bar{Z}^{\mu e}_{\text{odd}}$ are given in (6.5.80) and (6.5.101), respectively. Z and N denote the proton and neutron number of the nucleus. Z_{eff} has been determined in [103] and $F(q^2)$ is the nucleon form factor. For $\text{X} = {}^{48}_{22}$Ti, $Z_{\text{eff}} = 17.6$ and $F(q^2 \simeq -m_\mu^2) \simeq 0.54$ [104].

The $\mu - e$ conversion rate $R(\mu\mathrm{X} \to e\mathrm{X})$ is then given by

$$R(\mu\mathrm{X} \to e\mathrm{X}) = \frac{\Gamma(\mu\mathrm{X} \to e\mathrm{X})}{\Gamma^{\mathrm{X}}_{\mathrm{capture}}}\,, \tag{6.5.108}$$

with $\Gamma^{\mathrm{X}}_{\mathrm{capture}}$ being the μ capture rate of the element X. The experimental value is given by $\Gamma^{\mathrm{Ti}}_{\mathrm{capture}} = (2.590 \pm 0.012) \cdot 10^6\,\mathrm{s}^{-1}$ [105].

In our numerical analysis of Section 6.6 we will restrict ourselves to $\mu-e$ conversion in $^{48}_{22}$Ti, for which the most stringent experimental upper bound exists and where the approximations entering (6.5.107) work very well. For details, we refer the reader to [98, 101, 104].

6.5.5 $\tau^- \to \mu^- e^+ e^-$ and $\tau^- \to e^- \mu^+ \mu^-$

These decays have two types of contributions. First of all they proceed as in $\tau^- \to \mu^-\mu^+\mu^-$ and $\tau^- \to e^-e^+e^-$ through $\Delta L = 1$ penguin and box diagrams. However, they also receive contributions from $\Delta L = 2$ box diagrams. Since this time there are no identical particles in the final state, the effective Hamiltonians for these contributions can directly be obtained from the decay $B \to X_s\ell^+\ell^-$. The generalization to $\tau^- \to e^-\mu^+\mu^-$ will then be automatic.

As the QCD corrections are not involved now, only three operators originating in magnetic photon penguins, Z^0-penguins, standard photon penguins and the relevant box diagrams have to be considered. Keeping the notation from $B \to X_s\mu^+\mu^-$ but translating the quark flavors into lepton flavors these operators are

$$\mathcal{Q}_7 = \frac{e}{8\pi^2} m_\tau \bar{\mu}\sigma^{\alpha\beta}(1+\gamma_5)\tau F_{\alpha\beta}\,, \tag{6.5.109}$$

that enters, of course with different external states, also the $\mu \to e\gamma$ decay, and

$$\mathcal{Q}_9 = (\bar{\mu}\tau)_{V-A}(\bar{e}e)_V\,, \qquad \mathcal{Q}_{10} = (\bar{\mu}\tau)_{V-A}(\bar{e}e)_A\,. \tag{6.5.110}$$

The effective Hamiltonian is then given by

$$\mathcal{H}_{\mathrm{eff}}(\tau^- \to \mu^- e^+ e^-) = -\frac{G_F}{\sqrt{2}}\left[C_7^{\tau\mu}\mathcal{Q}_7 + C_9^{\tau\mu}\mathcal{Q}_9 + C_{10}^{\tau\mu}\mathcal{Q}_{10}\right]\,. \tag{6.5.111}$$

The Wilson coefficient for the operator $\mathcal{Q}_7$ can easily be found from Subsection 6.5.1 and Section 7 of [17]. We find

$$C_7^{\tau\mu} = -\frac{1}{2}\bar{D}'^{\,\tau\mu}_{\mathrm{odd}}\,, \tag{6.5.112}$$

with $\bar{D}'^{\,\tau\mu}_{\mathrm{odd}}$ obtained from (6.5.80) by replacing (μe) with $(\tau\mu)$.

The Wilson coefficients of the operators $\mathcal{Q}_9$ and $\mathcal{Q}_{10}$ receive not only contributions from $\Delta L = 1$ γ-penguin, Z^0-penguin and box diagrams, but also from $\Delta L = 2$ box diagrams. For $C_9^{\tau\mu}$ and $C_{10}^{\tau\mu}$ we can then write

$$C_9^{\tau\mu} = \frac{\alpha}{2\pi}\tilde{C}_9^{\tau\mu}\,, \qquad C_{10}^{\tau\mu} = \frac{\alpha}{2\pi}\tilde{C}_{10}^{\tau\mu}\,, \tag{6.5.113}$$

$$\tilde{C}_9^{\tau\mu} = \frac{\bar{Y}_{e,\mathrm{odd}}^{\tau\mu}}{\sin^2\theta_W} - 4\bar{Z}_{\mathrm{odd}}^{\mu e} - \Delta_{\tau\mu}\,, \qquad \tilde{C}_{10}^{\tau\mu} = -\frac{\bar{Y}_{e,\mathrm{odd}}^{\tau\mu}}{\sin^2\theta_W} + \Delta_{\tau\mu}\,, \tag{6.5.114}$$

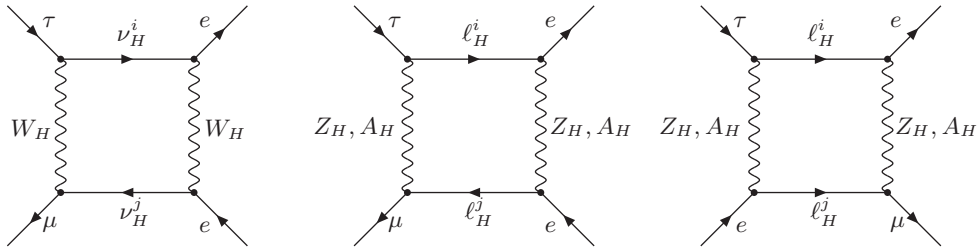

Figure 6.12: *Diagrams of $\Delta L = 2$ type contributing to $\tau^- \to \mu^- e^+ e^-$ in the LHT model.*

with the functions $\bar{Y}^{\tau\mu}_{e,\text{odd}}$ and $\bar{Z}^{\tau\mu}_{\text{odd}}$ obtained from (6.5.100) and (6.5.101) by replacing (μe) by $(\tau\mu)$. $\Delta_{\tau\mu}$ represents the additional $\Delta L = 2$ contribution which is not present in the case of $b \to s\ell^+\ell^-$ and will be explained below. As there are no light fermions in the T-odd sector, the mass independent term present in C_9 in the case of $b \to s\ell^+\ell^-$ in (X.5) of [106] is absent here. Effectively this corresponds to setting $\eta = 1$ in the latter equation and of course removing QCD corrections.

For the $\Delta L = 2$ diagrams shown in Fig. 6.12 contributing to this decay the corresponding effective Hamiltonian can be obtained from $\Delta B = 2$ processes, that is from (3.11) of [106], through the replacements of local operators, removing the symmetry factor 2 and performing the following change in the mixing factors:

$$\chi_i^{(\tau e)} \chi_j^{(\mu e)} \longrightarrow \chi_i^{(\tau e)} \chi_j^{(\mu e)^*} . \tag{6.5.115}$$

We find

$$\begin{aligned} \Delta_{\tau\mu} &= \frac{2\pi}{\alpha} \frac{G_F}{32\pi^2} \sqrt{2} M_{W_L}^2 \frac{v^2}{f^2} \sum_{i,j} \chi_i^{(\tau e)} \chi_j^{(\mu e)^*} F_H(y_i, y_j) \\ &= \frac{1}{16 \sin^2\theta_W} \frac{v^2}{f^2} \sum_{i,j} \chi_i^{(\tau e)} \chi_j^{(\mu e)^*} F_H(y_i, y_j) , \end{aligned} \tag{6.5.116}$$

with $F_H(z_i, y_j)$ defined by

$$F_H(z_i, y_j) = F(z_i, y_j; W_H) + G(z_i, y_j; Z_H) + A_1(z_i, y_j; Z_H) + A_2(z_i, y_j; Z_H) . \tag{6.5.117}$$

Effectively the presence of the diagrams in Fig. 6.12 introduces corrections to the Wilson coefficients $\tilde{C}_9$ and $\tilde{C}_{10}$ in (6.5.114). As the relevant operator has the structure $(V-A) \otimes (V-A)$, the shifts in $\tilde{C}_9$ and $\tilde{C}_{10}$ are equal up to an overall sign.

Finally, introducing

$$\hat{s} = \frac{(p_{e^+} + p_{e^-})^2}{m_\tau^2} , \qquad R^{\tau\mu}(\hat{s}) = \frac{\frac{d}{d\hat{s}}\Gamma(\tau^- \to \mu^- e^+ e^-)}{\Gamma(\tau^- \to \mu^- \bar{\nu}_\mu \nu_\tau)} \tag{6.5.118}$$

and neglecting m_e with respect to m_τ we find for the differential decay rate $R^{\tau\mu}(\hat{s})$

$$R^{\tau\mu}(\hat{s}) = \frac{\alpha^2}{4\pi^2}(1-\hat{s})^2\Bigg[(1+2\hat{s})\left(|\tilde{C}_9^{\tau\mu}|^2+|\tilde{C}_{10}^{\tau\mu}|^2\right) +4\left(1+\frac{2}{\hat{s}}\right)|C_7^{\tau\mu}|^2+12\,\mathrm{Re}\left(C_7^{\tau\mu}(\tilde{C}_9^{\tau\mu})^*\right)\Bigg]. \quad (6.5.119)$$

The branching ratio is then given as follows:

$$Br(\tau^-\to\mu^-e^+e^-) = Br(\tau^-\to\mu^-\bar{\nu}_\mu\nu_\tau)\int_{4m_e^2/m_\tau^2}^1 R^{\tau\mu}(\hat{s})\,d\hat{s}\,. \quad (6.5.120)$$

The branching ratio for $\tau^-\to e^-\mu^+\mu^-$ can easily be obtained from the above expressions by interchanging $\mu\leftrightarrow e$, where $\chi_i^{(e\mu)}=\chi_i^{(\mu e)^*}$.

For quasi-degenerate mirror leptons the $\Delta L=1$ part clearly dominates as the GIM-like suppression acts only on one mirror lepton propagator, whereas it acts twice in the $\Delta L=2$ case. Moreover, in the latter case the effective Hamiltonian is quartic in the $V_{H\ell}$ couplings, whereas it is to a very good approximation quadratic in the case of $\Delta L=1$. As these factors are all smaller than 1, quite generally $\Delta L=2$ contributions will then be additionally suppressed by the mixing matrix elements. Consequently, the $\Delta L=1$ part is expected to dominate and the shift $\Delta_{\tau\mu}$ can be neglected. On the other hand, for very special structures of the $V_{H\ell}$ matrix, the double GIM suppression of $\Delta L=2$ with respect to $\Delta L=1$ contributions could be compensated by the $V_{H\ell}$ factors. Therefore it is safer to use the more general expressions given above.

6.5.6 $(g-2)_\mu$

The anomalous magnetic moment of the muon $a_\mu=(g-2)_\mu/2$ provides an excellent test for physics beyond the SM and has been measured very precisely at the E821 experiment [107] in Brookhaven. The latest result of the $(g-2)$ Collaboration of E821 reads

$$a_\mu^{\rm exp} = (11659208.0\pm6.3)\cdot10^{-10}\,, \quad (6.5.121)$$

whereas the SM prediction is given by [108]

$$a_\mu^{\rm SM} = a_\mu^{\rm QED}+a_\mu^{\rm ew}+a_\mu^{\rm had} = (11659180.4\pm5.1)\cdot10^{-10}\,. \quad (6.5.122)$$

While the QED and electroweak contributions to $a_\mu^{\rm SM}$ are known very precisely [109, 110], the theoretical uncertainty is dominated by the hadronic vacuum polarization and light-by-light contributions. These contributions have been evaluated in [108, 111, 112, 113].

The anomalous magnetic moment a_μ can be extracted from the photon-muon vertex function $\Gamma^\mu(p',p)$

$$\bar{u}(p')\Gamma^\mu(p',p)u(p) = \bar{u}(p')\left[\gamma^\mu F_V(q^2)+(p+p')^\mu F_M(q^2)\right]u(p)\,, \quad (6.5.123)$$

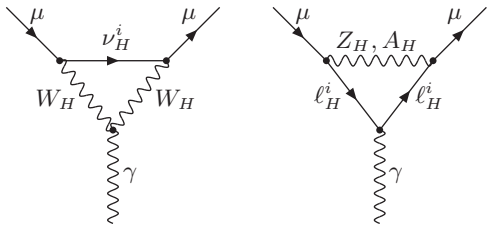

Figure 6.13: *Diagrams contributing to* $(g-2)_\mu$ *in the LHT model.*

where the anomalous magnetic moment of the muon a_μ can be read off as

$$a_\mu = -2mF_M(0)\,. \tag{6.5.124}$$

The diagrams which yield new contributions to a_μ in the LHT model are shown in Fig. 6.13. They either have a heavy neutral gauge boson (Z_H or A_H) and two heavy charged leptons ℓ_H^i ($i=1,2,3$) or two heavy charged gauge bosons ($W_H^\pm$) and one heavy neutrino ν_H^i ($i=1,2,3$) running in the loop.

Calculating the diagrams in Fig. 6.13 and using the Feynman rules given in [17], the contributions of the new particles for each generation $i=1,2,3$ are found to be:

$$\begin{aligned}
[a_\mu]^i_{X=A_H,Z_H} &= \frac{1}{2\pi^2}\frac{m_\mu^2}{M_X^2}\left|C_X^i\right|^2 r_i\left\{\left(\frac{5}{6}-\frac{5}{2}r_i+r_i^2+\left(r_i^3-3r_i^2+2r_i\right)\ln\frac{r_i-1}{r_i}\right)\right.\\
&\qquad\left.+\frac{{m_{Hi}^\ell}^2}{2M_X^2}\left(\frac{5}{6}+\frac{3}{2}r_i+r_i^2+\left(r_i^2+r_i^3\right)\ln\frac{r_i-1}{r_i}\right)\right\}, \qquad (6.5.125)\\
[a_\mu]^i_{X=W_H} &= -\frac{1}{4\pi^2}\frac{m_\mu^2}{M_X^2}\left|C_X^i\right|^2 r_i\left\{-2\left(\frac{5}{6}-\frac{3}{2}b_i+b_i^2+\left(b_i^2-b_i^3\right)\ln\frac{b_i+1}{b_i}\right)\right.\\
&\qquad\left.-\frac{{m_{Hi}^\ell}^2}{M_X^2}\left(\frac{5}{6}+\frac{5}{2}b_i+b_i^2-\left(2b_i+3b_i^2+b_i^3\right)\ln\frac{b_i+1}{b_i}\right)\right\}, \qquad (6.5.126)
\end{aligned}$$

where

$$r_i=\left(1-\frac{{m_{Hi}^\ell}^2}{M_X^2}\right)^{-1}, \qquad b=\frac{{m_{Hi}^\ell}^2}{M_X^2}\,r_i \tag{6.5.127}$$

and

$$C^i_{A_H}=\frac{g'}{20}\,V^{i\mu}_{H\ell}\,, \qquad C^i_{Z_H}=\frac{g}{4}\,V^{i\mu}_{H\ell}\,, \qquad C^i_{W_H}=\frac{g}{2\sqrt{2}}\,V^{i\mu}_{H\ell}\,. \tag{6.5.128}$$

The parameter m^ℓ_{Hi} in (6.5.125) and (6.5.126) denotes the mass of the mirror leptons while M_X is the mass of the heavy gauge bosons. We expanded our results in the small parameter m_μ/M_X. Our results in (6.5.125) and (6.5.126) for the muon anomalous magnetic moment are confirmed by the formulae in [114] for general couplings.

Replacing the parameters r_i and b_i by the more convenient parameter y_i, defined in

(6.5.75), leads us to the following expressions

$$[a_\mu]_{Z_H} = \frac{\sqrt{2}G_F}{32\pi^2}\frac{v^2}{f^2}m_\mu^2\sum_{i=1}^{3}\left|V_{H\ell}^{i\mu}\right|^2 L_1(y_i)\,, \tag{6.5.129}$$

$$[a_\mu]_{A_H} = \frac{\sqrt{2}G_F}{160\pi^2}\frac{v^2}{f^2}m_\mu^2\sum_{i=1}^{3}\left|V_{H\ell}^{i\mu}\right|^2 L_1(y_i')\,, \tag{6.5.130}$$

$$[a_\mu]_{W_H} = \frac{-\sqrt{2}G_F}{32\pi^2}\frac{v^2}{f^2}m_\mu^2\sum_{i=1}^{3}\left|V_{H\ell}^{i\mu}\right|^2 L_2(y_i)\,, \tag{6.5.131}$$

where the functions L_1 and L_2 are given in Appendix A.5.

Our final result for a_μ in the LHT model therefore is

$$a_\mu = [a_\mu]_{\rm SM} + \frac{\sqrt{2}G_F}{32\pi^2}\frac{v^2}{f^2}m_\mu^2\sum_{i=1}^{3}\left|V_{H\ell}^{i\mu}\right|^2\left[L_1(y_i) - L_2(y_i) + \frac{1}{5}L_1(y_i')\right]. \tag{6.5.132}$$

While we disagree with [18], we confirm the result of [19] except that according to us the factors $(V_{H\nu})^*_{2i}(V_{H\nu})_{2i}$ and $(V_{H\ell})^*_{2i}(V_{H\ell})_{2i}$ in equations (3.22)–(3.24) of that paper should be replaced by $|V_{H\ell}^{i\mu}|^2$.

6.6 Numerical Impact of the LHT on Lepton Flavor Violating Decays

6.6.1 Preliminaries and Benchmark Scenarios

In contrast to rare meson decays, the number of flavor violating decays in the lepton sector, for which useful constraints exist, is rather limited. Basically only the constraints on $Br(\mu \to e\gamma)$, $Br(\mu^- \to e^-e^+e^-)$, $R(\mu\mathrm{Ti} \to e\mathrm{Ti})$ and $Br(K_L \to \mu e)$ can be mentioned here. The situation may change significantly in the coming years and the next decade through the experiments briefly discussed in the introduction.

In this section we want to analyze numerically various branching ratios that we have calculated in Sections 6.5.1–6.5.6. In Subsection 6.6.3 we will extend our numerical analysis by studying various ratios of branching ratios and comparing them with those found in the MSSM. Our purpose is not to present a very detailed numerical analysis of all decays, but rather to concentrate on the most interesting ones from the present perspective and indicate rough upper bounds on all calculated branching ratios within the LHT model. To this end we will first set $f = 1\,\mathrm{TeV}$ and consider three benchmark scenarios for the remaining LHT parameters, as discussed below.

In Table 6.2 we collect the values of the input parameters that enter our numerical analysis. In order to simplify the analysis, we will set all input parameters to their central values. As all parameters are known with quite high precision, including the error ranges in the analysis

would amount only to percent effects in the observables considered, which is clearly beyond the scope of our analysis.

$m_e = 0.5110\,\text{MeV}$	$M_W = 80.425(38)\,\text{GeV}$
$m_\mu = 105.66\,\text{MeV}$	$\alpha = 1/137$
$m_\tau = 1.7770(3)\,\text{GeV}$	$G_F = 1.16637(1)\cdot 10^{-5}\,\text{GeV}^{-2}$
$\tau_\tau = 290.6(10)\cdot 10^{-3}\,\text{ps}$ [88]	$\sin^2\theta_W = 0.23122(15)$ [88]

Table 6.2: *Values of the experimental and theoretical quantities used as input parameters.*

Benchmark Scenarios

We will consider the following three scenarios:

Scenario A (red):

In this scenario we will choose

$$V_{H\ell} = V_{\text{PMNS}}^\dagger\,, \tag{6.6.133}$$

so that $V_{H\nu} \equiv \mathbb{1}$, and mirror leptons have no impact on flavor violating observables in the neutrino sector, such as neutrino oscillations. In particular we set the PMNS parameters to [115]

$$\sin\theta_{12} = \sqrt{0.300}\,, \qquad \sin\theta_{13} = \sqrt{0.030}\,, \qquad \sin\theta_{23} = \frac{1}{\sqrt{2}}\,, \qquad \delta_{13} = 65^\circ\,, \tag{6.6.134}$$

which is consistent with the experimental constraints on the PMNS matrix [88]. As no constraints on the PMNS phases exist, we have taken δ_{13} to be equal to the CKM phase and set the two Majorana phases to zero.

Furthermore, we take the mirror lepton masses to lie in the range

$$300\,\text{GeV} \leq m_{Hi}^\ell \leq 1.5\,\text{TeV}\,, \qquad (i = 1,2,3)\,. \tag{6.6.135}$$

Scenario B (green):

Here, we take

$$V_{H\ell} = V_{\text{CKM}}\,, \tag{6.6.136}$$

so that [87]

$$\theta_{12}^\ell = 13^\circ\,, \qquad \theta_{13}^\ell = 0.25^\circ\,, \qquad \theta_{23}^\ell = 2.4^\circ\,, \tag{6.6.137}$$

$$\delta_{12}^\ell = 0\,, \qquad \delta_{13}^\ell = 65^\circ\,, \qquad \delta_{13}^\ell = 0\,, \tag{6.6.138}$$

and the mirror lepton masses in the range (6.6.135).

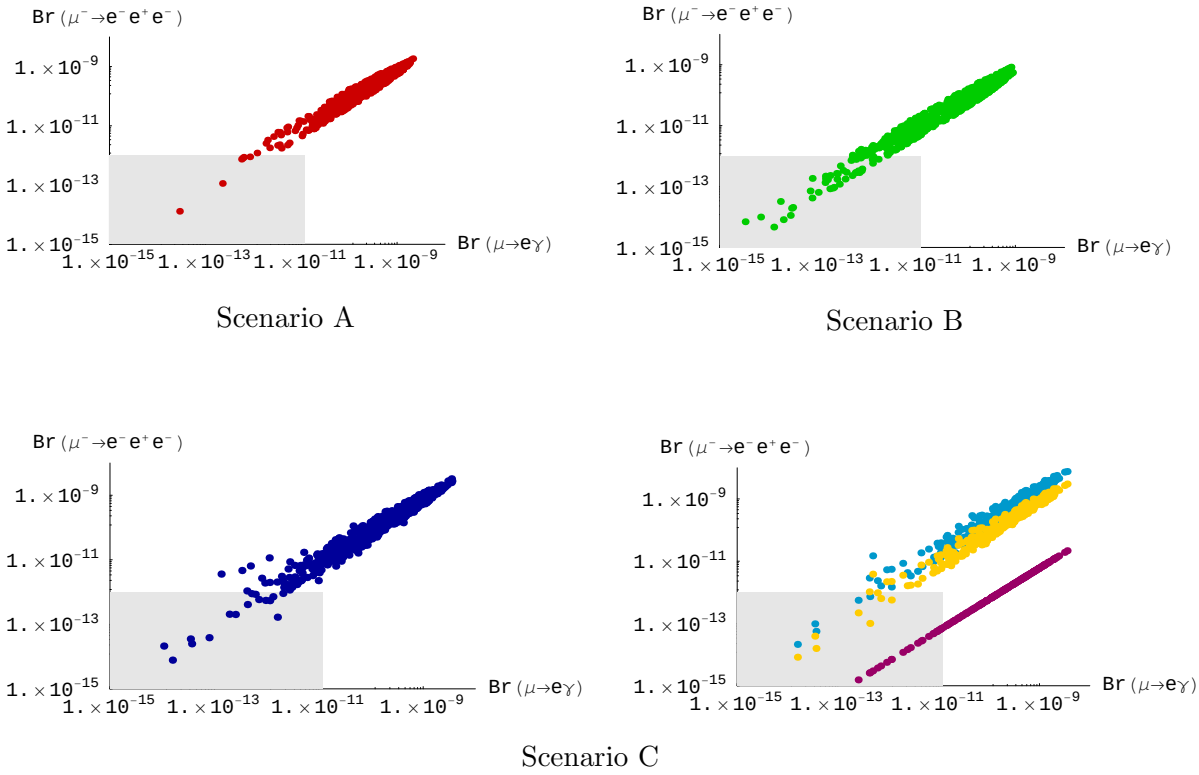

Figure 6.14: *Correlation between $\mu \to e\gamma$ and $\mu^- \to e^-e^+e^-$ in the scenarios of Section 6.6.1. In the right plot of Scenario C we show the contributions to $\mu^- \to e^-e^+e^-$ from $\bar{D}'^{\mu e}_{odd}$ (purple, lowermost), $\bar{Z}^{\mu e}_{odd}$ (orange, middle) and $\bar{Y}^{\mu e}_{e,odd}$ (light-blue, uppermost) separately. The shaded area represents the experimental constraints.*

Scenario C (blue):

Here we perform a general scan over the whole parameter space, with the only restriction being the range (6.6.135) for mirror lepton masses.

At a certain stage we will investigate the dependence on mass splittings in the mirror lepton spectrum.

$\mu \to e\gamma$, $\mu^- \to e^-e^+e^-$ and $\mu - e$ Conversion

In Fig. 6.14 we show the correlation between $\mu \to e\gamma$ and $\mu^- \to e^-e^+e^-$ in the scenarios in question together with the experimental bounds on these decays. We observe:

- In Scenario A the great majority of points is outside the allowed range, implying that the $V_{H\ell}$ matrix must be much more hierarchical than $V_{\rm PMNS}$ in order to satisfy the present upper bounds on $\mu \to e\gamma$ and $\mu^- \to e^-e^+e^-$.

- Also in Scenario B most of the points violate the current experimental bounds, although $V_{\rm CKM}$ is much more hierarchical than $V_{\rm PMNS}$. The reason is that the CKM hierarchy $s_{13} \ll s_{23} \ll s_{12}$ implies very small effects in transitions between the third and the first generation, like $\tau \to e\gamma$, while allowing relatively large effects in the $\mu \to e$ transitions. Thus in order to satisfy the experimental constraints on $\mu \to e\gamma$ and $\mu^- \to e^-e^+e^-$ a very different hierarchy of the $V_{H\ell}$ matrix is required, unless the mirror lepton masses are quasi-degenerate.

- In Scenario C there are more possibilities, but also here a strong correlation between $\mu \to e\gamma$ and $\mu^- \to e^-e^+e^-$ is observed. This is easy to understand, as both decays probe dominantly the combinations of $V_{H\ell}$ elements $\chi_i^{(\mu e)}$.

- For Scenario C, we also show the contributions to $\mu^- \to e^-e^+e^-$ from $\bar{D}'^{\mu e}_{\rm odd}$, $\bar{Z}^{\mu e}_{\rm odd}$ and $\bar{Y}^{\mu e}_{e,\rm odd}$ separately. We observe that the dominant contributions come from the functions $\bar{Z}^{\mu e}_{\rm odd}$ and above all $\bar{Y}^{\mu e}_{e,\rm odd}$, while the contribution of the operator $\mathcal{Q}_7$, given by $\bar{D}'^{\mu e}_{\rm odd}$, is by roughly two orders of magnitude smaller and thus fully negligible. This should be contrasted with the case of the MSSM where the dipole operator is dominant. We will return to the consequences of this finding in the next subsection.

- We emphasize that the strong correlation between $\mu \to e\gamma$ and $\mu^- \to e^-e^+e^-$ in the LHT model is not a common feature of all extensions of the SM, in which the structure of $\mu^- \to e^-e^+e^-$ is generally much more complicated than in the LHT model. It is clear from Fig. 6.14 that an improved upper bound on $\mu \to e\gamma$ by MEG in 2007 and in particular its discovery will provide important information on $\mu^- \to e^-e^+e^-$ within the model in question.

Next, in Fig. 6.15 we show the correlation between the $\mu - e$ conversion rate in $^{48}_{22}$Ti and $Br(\mu \to e\gamma)$, after imposing the existing constraints on $\mu \to e\gamma$ and $\mu^- \to e^-e^+e^-$. We observe that this correlation is much weaker than the one between $\mu \to e\gamma$ and $\mu^- \to e^-e^+e^-$. Furthermore, we find that the $\mu - e$ conversion rate in Ti is likely to be found close to the current experimental upper bound, and that in some regions of the parameter space the latter bound is even the most constraining one.

$\tau \to \mu\gamma$ and $\tau \to e\gamma$

In Fig. 6.16 we show the correlation between $Br(\tau \to \mu\gamma)$ and $Br(\tau \to e\gamma)$ in Scenario C, imposing the experimental bounds on $\mu \to e\gamma$ and $\mu^- \to e^-e^+e^-$. We observe that they both can be individually as high as $\sim 8 \cdot 10^{-10}$, but the highest values of $Br(\tau \to \mu\gamma)$ correspond generally to much lower values of $Br(\tau \to e\gamma)$ and vice versa. Still simultaneous values of both branching ratios as high as $2 \cdot 10^{-10}$ are possible.

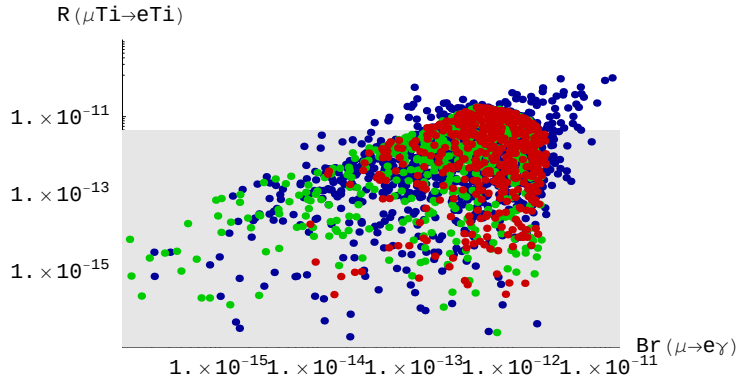

Figure 6.15: *$\mu - e$ conversion rate in $^{48}_{22}Ti$ as a function of $Br(\mu \to e\gamma)$, after imposing the existing constraints on $\mu \to e\gamma$ and $\mu^- \to e^-e^+e^-$. The shaded area represents the current experimental upper bound on $R(\mu Ti \to e Ti)$.*

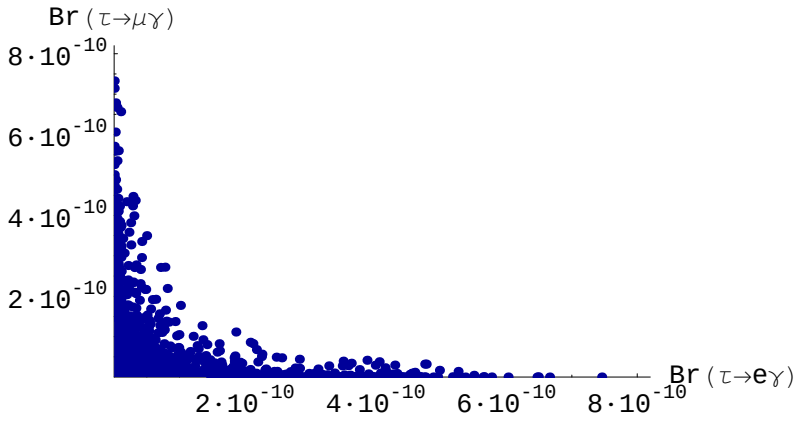

Figure 6.16: *Correlation between $Br(\tau \to e\gamma)$ and $Br(\tau \to \mu\gamma)$.*

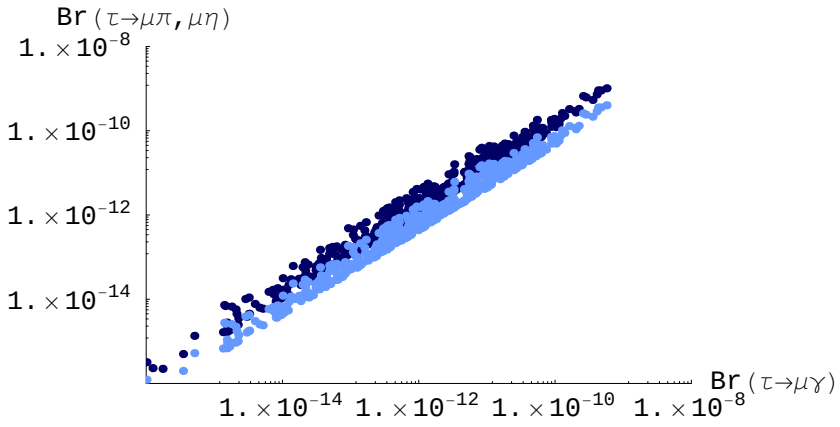

Figure 6.17: *$Br(\tau \to \mu\pi)$ (dark-blue) and $Br(\tau \to \mu\eta)$ (light-blue) as functions of $Br(\tau \to \mu\gamma)$.*

$\tau \to \mu\pi, \mu\eta, \mu\eta'$ and $\tau \to \mu\gamma$

In Fig. 6.17 we show $Br(\tau \to \mu\pi)$ and $Br(\tau \to \mu\eta)$ as functions of $Br(\tau \to \mu\gamma)$, imposing the constraints from $\mu \to e\gamma$ and $\mu^- \to e^-e^+e^-$. We find that $Br(\tau \to \mu\pi)$ can reach values as high as $2 \cdot 10^{-9}$ and $Br(\tau \to \mu\eta)$ can be as large as $7 \cdot 10^{-10}$, which is still by more than one order of magnitude below the recent bounds from Belle and BaBar. We do not show $Br(\tau \to \mu\eta')$ as it is very similar to $Br(\tau \to \mu\eta)$.

Completely analogous correlations can be found also for the corresponding decays $\tau \to e\pi, e\eta, e\eta'$ and $\tau \to e\gamma$. Indeed, this symmetry between $\tau \to \mu$ and $\tau \to e$ systems turns out to be a general feature of the LHT model, that can be found in all decays considered in the present section. We will return to this issue in Subsection 6.6.3.

An immediate consequence of these correlations is that, as in the case of $\tau \to \mu\gamma$ and $\tau \to e\gamma$, the highest values for $\tau \to \mu\pi$ are possible if $\tau \to e\pi$ is relatively small, and vice versa. Still the corresponding branching ratios can be simultaneously enhanced to $3 \cdot 10^{-10}$. Analogous statements apply to $\tau \to \mu(e)\eta$ and $\tau \to \mu(e)\eta'$.

6.6.2 Upper Bounds for LFV Processes

To estimate the impact of the LHT on all LFV processes we present in Table 6.3 an overview of upper bounds of all branching ratios considered so far, together with the corresponding experimental limits. In deriving these bounds we imposed the constraints coming from $\mu \to e\gamma$ and $R(\mu Ti \to eTi)$. The number in brackets are obtained by imposing the additional constraint $R(\mu Ti \to eTi)$, which has only a minor impact on the observables discussed. We can also see from Table 6.3 that the limits strongly depend on the choice of the scale f which has been set to $f = 500\,\text{GeV}$ and $f = 1000\,\text{GeV}$ with the range (6.6.135) for the mirror lepton

decay	$f = 1000\,\text{GeV}$	$f = 500\,\text{GeV}$	exp. upper bound
$\mu \to e\gamma$	$1.2 \cdot 10^{-11}$ $(1 \cdot 10^{-11})$	$1.2 \cdot 10^{-11}$ $(1 \cdot 10^{-11})$	$1.2 \cdot 10^{-11}$ [91]
$\mu^- \to e^-e^+e^-$	$1.0 \cdot 10^{-12}$ $(1 \cdot 10^{-12})$	$1.0 \cdot 10^{-12}$ $(1 \cdot 10^{-12})$	$1.0 \cdot 10^{-12}$ [97]
$\mu\text{Ti} \to e\text{Ti}$	$2 \cdot 10^{-10}$ $(5 \cdot 10^{-12})$	$4 \cdot 10^{-11}$ $(5 \cdot 10^{-12})$	$4.3 \cdot 10^{-12}$ [99]
$\tau \to e\gamma$	$8 \cdot 10^{-10}$ $(7 \cdot 10^{-10})$	$1 \cdot 10^{-8}$ $(1 \cdot 10^{-8})$	$9.4 \cdot 10^{-8}$ [92]
$\tau \to \mu\gamma$	$8 \cdot 10^{-10}$ $(8 \cdot 10^{-10})$	$2 \cdot 10^{-8}$ $(1 \cdot 10^{-8})$	$1.6 \cdot 10^{-8}$ [92]
$\tau^- \to e^-e^+e^-$	$7 \cdot 10^{-10}$ $(6 \cdot 10^{-10})$	$2 \cdot 10^{-8}$ $(2 \cdot 10^{-8})$	$2.0 \cdot 10^{-7}$ [116]
$\tau^- \to \mu^-\mu^+\mu^-$	$7 \cdot 10^{-10}$ $(6 \cdot 10^{-10})$	$3 \cdot 10^{-8}$ $(3 \cdot 10^{-8})$	$1.9 \cdot 10^{-7}$ [116]
$\tau^- \to e^-\mu^+\mu^-$	$5 \cdot 10^{-10}$ $(5 \cdot 10^{-10})$	$2 \cdot 10^{-8}$ $(2 \cdot 10^{-8})$	$2.0 \cdot 10^{-7}$ [117]
$\tau^- \to \mu^-e^+e^-$	$5 \cdot 10^{-10}$ $(5 \cdot 10^{-10})$	$2 \cdot 10^{-8}$ $(2 \cdot 10^{-8})$	$1.9 \cdot 10^{-7}$ [117]
$\tau \to \mu\pi$	$2 \cdot 10^{-9}$ $(2 \cdot 10^{-9})$	$5.8 \cdot 10^{-8}$ $(5.8 \cdot 10^{-8})$	$5.8 \cdot 10^{-8}$ [92]
$\tau \to e\pi$	$2 \cdot 10^{-9}$ $(2 \cdot 10^{-9})$	$4.4 \cdot 10^{-8}$ $(4.4 \cdot 10^{-8})$	$4.4 \cdot 10^{-8}$ [92]
$\tau \to \mu\eta$	$6 \cdot 10^{-10}$ $(6 \cdot 10^{-10})$	$2 \cdot 10^{-8}$ $(2 \cdot 10^{-8})$	$5.1 \cdot 10^{-8}$ [92]
$\tau \to e\eta$	$6 \cdot 10^{-10}$ $(6 \cdot 10^{-10})$	$2 \cdot 10^{-8}$ $(2 \cdot 10^{-8})$	$4.5 \cdot 10^{-8}$ [92]
$\tau \to \mu\eta'$	$7 \cdot 10^{-10}$ $(7 \cdot 10^{-10})$	$3 \cdot 10^{-8}$ $(3 \cdot 10^{-8})$	$5.3 \cdot 10^{-8}$ [92]
$\tau \to e\eta'$	$7 \cdot 10^{-10}$ $(7 \cdot 10^{-10})$	$3 \cdot 10^{-8}$ $(3 \cdot 10^{-8})$	$9.0 \cdot 10^{-8}$ [92]

Table 6.3: *Upper bounds on LFV decay branching ratios in the LHT model, for two different values of the scale f, after imposing the constraints on $\mu \to e\gamma$ and $\mu^- \to e^-e^+e^-$. The numbers given in brackets are obtained after imposing the additional constraint $R(\mu Ti \to eTi) < 5 \cdot 10^{-12}$. For $f = 500\,\text{GeV}$, also the bounds on $\tau \to \mu\pi, e\pi$ have been included. The current experimental upper bounds are also given.*

masses in both cases. In particular the upper bounds on τ decays increase by two orders of magnitude when the scale f is lowered to 500 GeV. Moreover, the recent upper bounds for $\tau \to \mu\pi, e\pi$ could be violated by roughly a factor 5. Therefore, in deriving the LHT bounds for $f = 500\,\text{GeV}$, we also have taken into account the latter bounds.

6.6.3 Comparing the LHT to Supersymmetry

We have seen in the previous subsection that many charged LFV processes could reach within the LHT model a level accessible to experiments performed in this decade. However, in view of many parameters involved, it is useful to look for correlations between various branching ratios that are less parameter dependent than individual branching ratios. In [20] a number of correlations characteristic for LFV decays in the MSSM in the absence of significant Higgs contributions have been worked out by *Ellis et al.* and have been analyzed in [21, 22, 24]. In particular, these correlations have been modified by *Paradisi* [23, 24, 25] in the presence of significant Higgs contributions.

These different patterns of LFV in the LHT and the MSSM can best be seen by studying

ratio	LHT	MSSM (dipole)	MSSM (Higgs)
$\frac{Br(\mu^-\to e^-e^+e^-)}{Br(\mu\to e\gamma)}$	$0.4\ldots2.5$	$\sim 6\cdot10^{-3}$	$\sim 6\cdot10^{-3}$
$\frac{Br(\tau^-\to e^-e^+e^-)}{Br(\tau\to e\gamma)}$	$0.4\ldots2.3$	$\sim 1\cdot10^{-2}$	$\sim 1\cdot10^{-2}$
$\frac{Br(\tau^-\to \mu^-\mu^+\mu^-)}{Br(\tau\to \mu\gamma)}$	$0.4\ldots2.3$	$\sim 2\cdot10^{-3}$	$0.06\ldots0.1$
$\frac{Br(\tau^-\to e^-\mu^+\mu^-)}{Br(\tau\to e\gamma)}$	$0.3\ldots1.6$	$\sim 2\cdot10^{-3}$	$0.02\ldots0.04$
$\frac{Br(\tau^-\to \mu^-e^+e^-)}{Br(\tau\to \mu\gamma)}$	$0.3\ldots1.6$	$\sim 1\cdot10^{-2}$	$\sim 1\cdot10^{-2}$
$\frac{Br(\tau^-\to e^-e^+e^-)}{Br(\tau^-\to e^-\mu^+\mu^-)}$	$1.3\ldots1.7$	~ 5	$0.3\ldots0.5$
$\frac{Br(\tau^-\to \mu^-\mu^+\mu^-)}{Br(\tau^-\to \mu^-e^+e^-)}$	$1.2\ldots1.6$	~ 0.2	$5\ldots10$
$\frac{R(\mu\mathrm{Ti}\to e\mathrm{Ti})}{Br(\mu\to e\gamma)}$	$10^{-2}\ldots10^{2}$	$\sim 5\cdot10^{-3}$	$0.08\ldots0.15$

Table 6.4: *Comparison of various ratios of branching ratios in the LHT model and in the MSSM without and with significant Higgs contributions.*

certain correlations between branching ratios that have been previously considered in the context of the MSSM. We find that the ratios in Table 6.4 could allow for a transparent distinction between the LHT model and the MSSM. In particular, the ratios involving $Br\left(\ell_i\to\ell_j\gamma\right)$ turn out to be of $\mathcal{O}\left(1\right)$ in the LHT model, while being $\mathcal{O}\left(\alpha\right)$ in the MSSM. Also the $\mu-e$ conversion rate in nuclei, normalized to $Br\left(\mu\to e\gamma\right)$, can be significantly enhanced in the LHT model, with respect to the MSSM without significant Higgs contributions. However, the distinction in this case is not as clear as in the case of $Br(\ell_i^-\to\ell_j^-\ell_j^+\ell_j^-)/Br(\ell_i\to\ell_j\gamma)$.

The significant difference in the pattern of the LFV branching ratios in the LHT model from the MSSM allows for a clear distinction of these two models. The origin for this difference is the fact, that in the MSSM the LFV rates are dominated by the dipole operator, while in the LHT the dipole contributions to the decays $\ell_i^-\to\ell_j^-\ell_j^+\ell_j^-$ and $\ell_i^-\to\ell_j^-\ell_k^+\ell_k^-$ can be neglected compared to the Z^0-penguin and box diagram contributions. The reason is that the neutral gauge boson (A_H, Z_H) contributions annihilate with the $W_H^\pm$ contributions to the dipole operator functions $\bar{D}'^{ij}_{\mathrm{odd}}$, but combine constructively in the case of the $\bar{Y}'^{ij}_{\mathrm{k,odd}}$, relevant for the Z^0-penguin and box contributions. Furthermore, the characteristic enhancement of dipole operators due to large $\tan\beta$ in the MSSM does exist in the LHT model.

However, in the presence of significant Higgs contributions this distinction between the MSSM and the LHT is less emphasized in τ decays with μ in the final state. This makes it difficult to distinguish between both models because of the parametric uncertainties in the relevant MSSM ratios, as seen in 6.4. In addition, the ratio $R(\mu Ti\to eTi)/Br(\mu\to e\gamma)$ is larger than α, making it harder to discriminate between the LHT model and the MSSM.

Chapter 7

Summary and Outlook

In this work we have presented a detailed analysis of several prominent FCNC processes as well as LFV observables in the context of the Littlest Higgs model without and with T-parity, whose basic structure is based on an idea by *Arkani-Hamed et al.* [4].

We started this thesis with a brief overview of the SM and its basic ingredients, where we have seen that it is extremely successful in describing the fundamental interactions of particles. However, we noticed that the SM suffers from a number of shortcomings and is therefore regarded as an effective theory. Among these problems one of the most striking questions is the unknown mechanism of electroweak symmetry breaking, which requires the introduction of a scalar Higgs boson. However, being not protected by any symmetry, the Higgs particle receives radiative corrections proportional to the square of the cut-off Λ, thus being the origin of the little hierarchy problem.

To overcome this problem many extensions of the SM have been developed of which the most prominent ones are supersymmetry or theories with extra space-time dimensions. Starting in Chapter 3 from deconstructed gauge field theories a further, very interesting alternative, denoted as the Little Higgs model, has been proposed in the last years by *Arkani-Hamed et al.* [47, 49]. Although Little Higgs models have not been worked out in the same detail as the MSSM, they nonetheless represent an interesting alternative in explaining why we have not yet seen any evidence of the mechanism behind EWSB in precision experiments.

In the present thesis we have studied the LH model with and without T-parity, which is based on the symmetry breaking pattern $SU(5)/SO(5)$ [4]. In such a framework the Higgs is realized as a pseudo-Goldstone boson and can be kept naturally light without fine-tuning. Moreover, it is necessary to introduce only a very small number of new, weakly coupled particles at the TeV scale to stabilize the Higgs mass. As discussed in Chapter 4 this includes one heavy copy each of the electroweak gauge bosons, the top quark and a new scalar triplet coupled to the Higgs. In view of the constraints on the new physics scale coming from EWPT we started to analyze the impact of this model on FCNC. After the correction of several Feynman rules, that have already been derived in [5], we were able to calculate the

relevant X and Y functions relevant for the phenomenology of the rare decays $K^+ \to \pi^0\nu\bar{\nu}$, $K_L \to \pi^0\nu\bar{\nu}$ and $B_{s,d} \to \mu^+\mu^-$. Finally one should always be aware of the fact that the LH model is an effective field theory with a cut-off in the range of 10 TeV, beyond which one has to construct a UV-completion [48]. This sensitivity to the UV completion, which is reflected by a logarithmic divergence on the cut-off, is also present in our calculation and thus lowers the model's ability to make precise predictions.

As already mentioned, it soon turned out that the original LH models is severely constrained by electroweak precision tests, which requires the scale f to be higher than 3 TeV. Such a scale however re-introduces a certain amount of fine-tuning in the theory and is against the spirit of the original construction. To evade these problems connected with EWPT *Cheng* and *Low* proposed to introduce a new, discrete symmetry, called T-parity [9]. Embedding this new symmetry into the LH model they were able to avoid the stringent experimental bounds since the new particles in the LHT are assigned to be odd under T-parity, which prevented them from contributing to electroweak precision observables at tree level. Thus, as seen in Chapter 5, the scale of new physics f can be lowered to values $f \gtrsim 500\,\text{GeV}$ while still being consistent with EWPT.

Having now at hand the LHT as a more viable scenario to describe physics beyond the SM we decided to extend our analysis of FCNC in the LH model to the LHT model. Together with a previous work [15] on quantities related to particle-antiparticle mixing and $B \to X_s\gamma$ the rare K and B decays in [17] provide a general description of FCNC processes in this model. In Chapter 6 of this thesis we focused on the calculation of the X_i, Y_i and Z_i, $i = K, d, s$, which are the responsible short distance functions for several rare decays. In contrast to models with minimal flavor violation the short distance functions X_i, Y_i and Z_i are complex quantities which depend on the index i and thus signal the breakdown of universality. With the help of these functions we could straightforwardly calculate several branching ratios of interesting rare decays like $K^+ \to \pi^0\nu\bar{\nu}$, $K_L \to \pi^0\nu\bar{\nu}$, $B_{s,d} \to \mu^+\mu^-$ and $K_L \to \pi^0\ell^+\ell^-$. The most evident departures from the SM predictions are found for CP-violating observables like the branching ratio $K_L \to \pi^0\nu\bar{\nu}$ but large deviations from the SM expectations are also possible for the branching ratios $Br\left(K^+ \to \pi^+\nu\bar{\nu}\right)$ and $Br\left(K_L \to \pi^0\ell^+\ell^-\right)$. In contrast to the large effects in the K system the branching ratios for $B_{s,d} \to \mu^+\mu^-$ are only moderately modified by at most $20\% - 30\%$. Finally, we have seen that universality of new physics effects can be largely broken, in particular between K and $B_{s,d}$ systems.

In contrast to rare K and B decays, where the SM contributions play an important role, in the LHT model the mirror fermion contributions to LFV processes play the by far dominant role, since in the SM LFV effects are suppressed by the smallness of the neutrino masses. Moreover, the absence of QCD corrections and hadronic matrix elements allow for predictions that are determined by perturbation theory. In this thesis we concentrated on the radiative decays $\ell_i \to \ell_j\gamma$, semileptonic τ decays like $\tau \to \ell P$, $P = \pi, \eta, \eta'$, $\mu^- \to e^-e^+e^-$, $\tau^- \to e^-e^+e^-$, $\tau^- \to \mu^-\mu^+\mu^-$, $\mu \to e$ conversion in nuclei, $\tau^- \to \mu^-e^+e^-$, $\tau^- \to e^-\mu^+\mu^-$

and finally $(g-2)_\mu$. As seen in Table 6.3 several branching ratios can reach the experimental upper bounds and are interesting in the view of new experiments. The contributions of mirror leptons to $(g-2)_\mu$ are negligible and thus the discrepancy between SM prediction and experimental data cannot be explained. The correlation between various branching ratios also allow for a clear distinction between the MSSM and the LHT, since in the MSSM without significant Higgs contributions the dipole operator plays the dominant role while in the LHT model penguin and box contributions are much more important. Although this distinction is less obvious in the case of the MSSM with significant Higgs contributions the ratios involving $\ell_i \to \ell_j\gamma$ and decays with electrons in the final state still offer an excellent opportunity to distinguish these two models.

We want to conclude this thesis with the message that both FCNC and LFV processes provide a formidable framework to test the LH and LHT model. As we have seen, in spite of the impressive agreement of the SM with the available data it is still possible to obtain large deviations form the Standard Model's predictions. In particular, the correlations between different LFV processes should turn out to be very useful to distinguish the LHT from various other models, like the MSSM and thus provide an interesting alternative in the search for new physics to the high-energy processes at the LHC. Apart from the MSSM, which is getting more and more under pressure by precision tests, these models represent one of the most promising candidates for extensions of the SM. Now, it is up to the next generation of experiments, like the LHC, to uncover the unknown pattern of EWSB.

Appendix A

Relevant Formulae and Feynman Rules

A.1 Classes of Diagrams in the LH Model

In this section, we show all the diagrams contributing to the rare decays $K_L \to \pi^0 \nu\bar{\nu}$ and $K^+ \to \pi^+ \nu\bar{\nu}$ in the Littlest Higgs model without T-parity. The different classes are arranged according to their contributions given in (4.3.84) – (4.3.89).

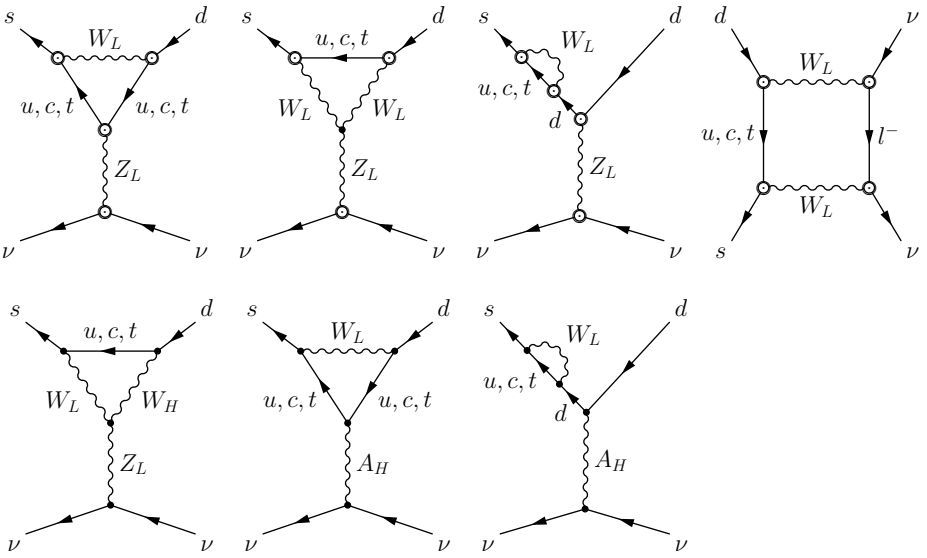

Figure A.1: Class 1. Penguin and box diagrams with SM particles and A_H contributing to $K \to \pi\nu\bar{\nu}$ in the LH model at $\mathcal{O}(v^2/f^2)$.

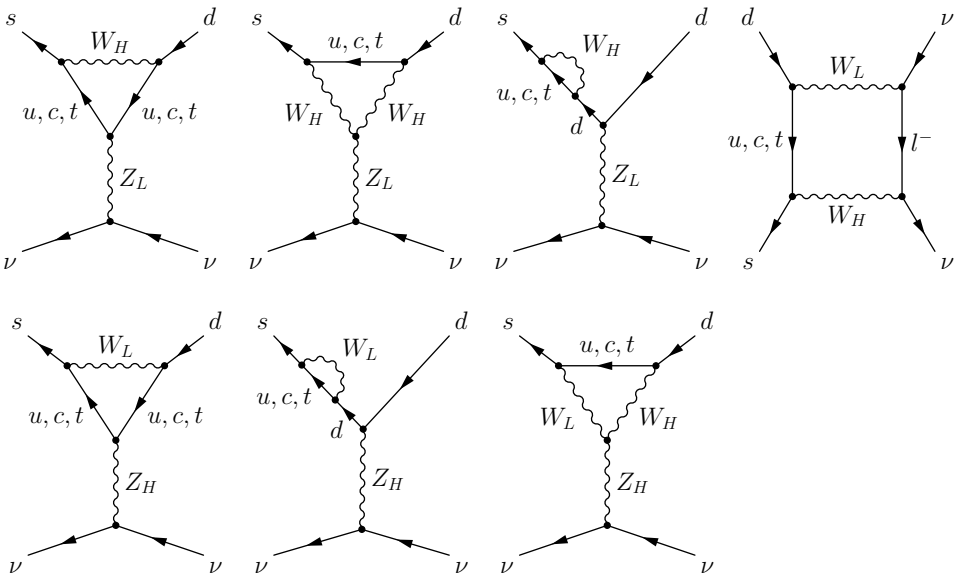

Figure A.2: Class 2. Penguin and box diagrams with W_H and Z_H contributing to $K \to \pi\nu\bar{\nu}$ in the LH model at $\mathcal{O}(v^2/f^2)$.

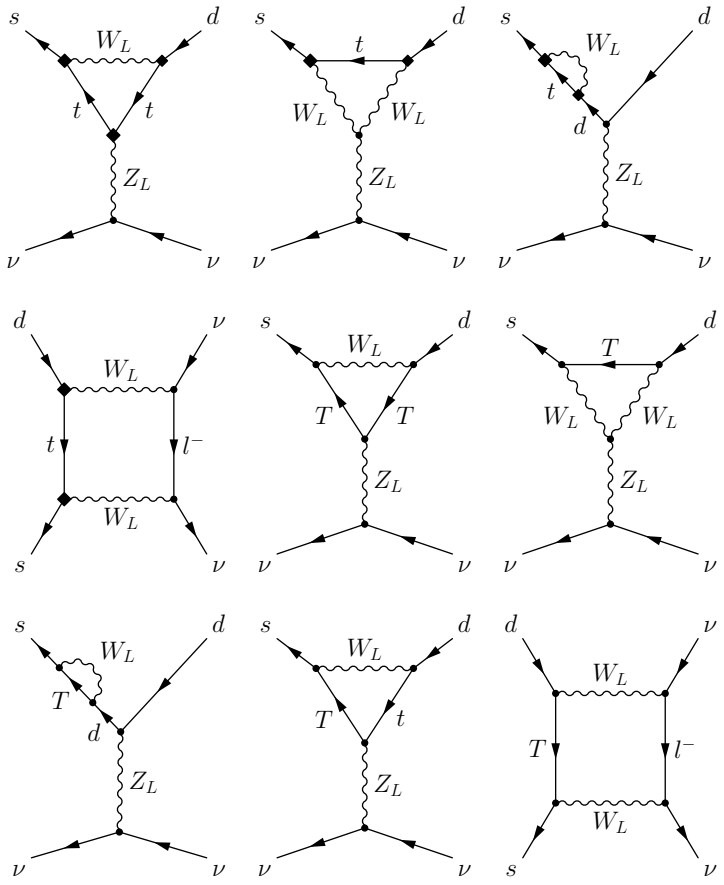

Figure A.3: Class 3. Top and heavy top quark contributions to $K \to \pi\nu\bar{\nu}$ in the LH model at $\mathcal{O}(v^2/f^2)$ which are proportional to x_L^2. The diamonds correspond to terms proportional to x_L^2, which were not considered in class 1.

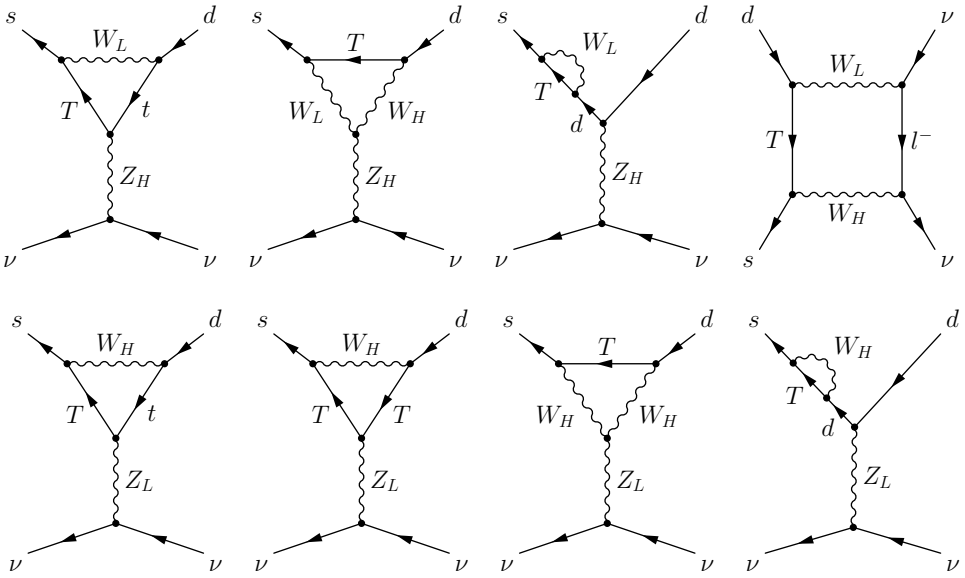

Figure A.4: Class 4. Penguin and box contributions to $K \to \pi\nu\bar{\nu}$ in the LH model at $\mathcal{O}(v^2/f^2)$ which are proportional to $v^4/f^4c^4x_L^2$.

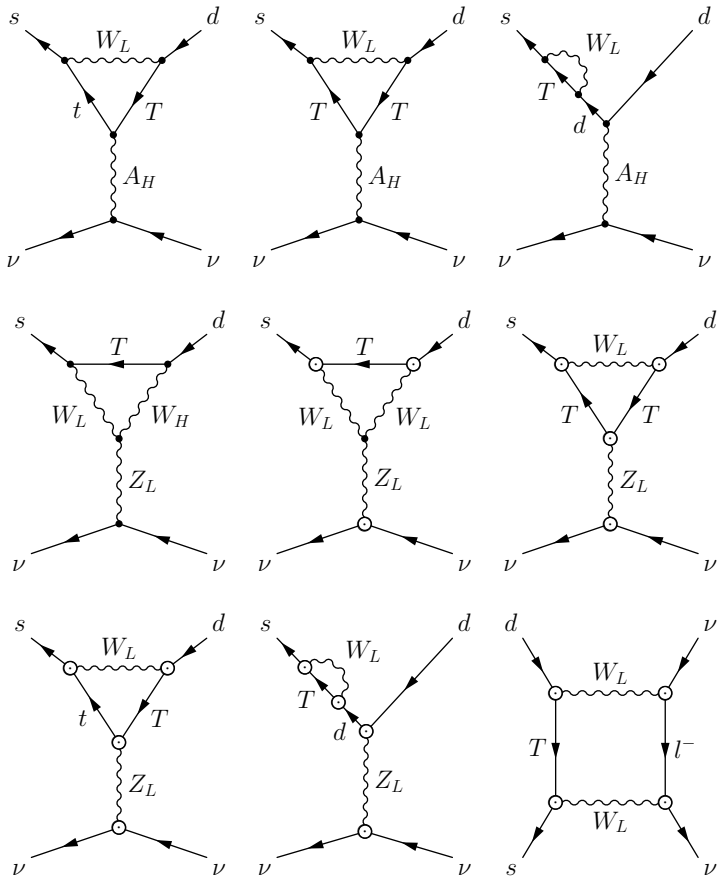

Figure A.5: Class 5. Penguin and box contributions to $K \to \pi\nu\bar{\nu}$ in the LH model at $\mathcal{O}(v^2/f^2)$ which are proportional to $v^4/f^4x_Tx_L^2$.

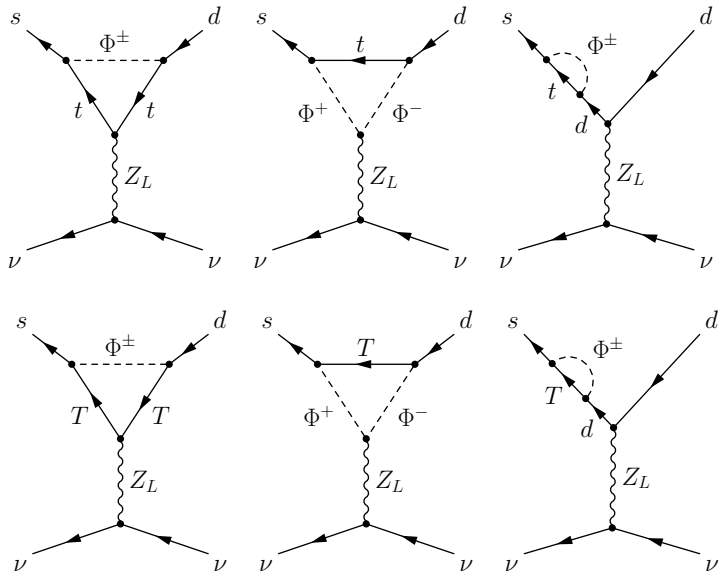

Figure A.6: Class 6. Penguin contributions to $K \to \pi\nu\bar{\nu}$ in the LH model at $\mathcal{O}(v^2/f^2)$ with internal charged scalars $\Phi^{\pm}$.

A.2 Feynman Rules in the LHT Model

A.2.1 Fermion–Goldstone Boson Couplings

In this section, we present the vertex rules concerning the interactions between the fermions and the Goldstone bosons that are needed for the calculation of the diagrams in the LHT. Further Feynman rules involving fermions and heavy/light gauge bosons are not repeated here and the reader is referred to [11, 16, 17].

Fermion couplings to SM Goldstone bosons	
$\bar{u}^i\pi^+ d^j$	$\frac{g}{\sqrt{2}M_{W_L}}\left(m_u^i P_L - m_d^j P_R\right)(V_{\rm CKM})_{ij}$
$\bar{t}\pi^+ d^j$	$\frac{g}{\sqrt{2}M_{W_L}}\left(1-\frac{x_L^2}{2}\frac{v^2}{f^2}\right)\left(m_t P_L - m_d^j P_R\right)(V_{\rm CKM})_{tj}$
$\bar{T}_+\pi^+ d^j$	$\frac{gx_L}{\sqrt{2}M_{W_L}}\frac{v}{f}\left[m_{T_+}\left(1+\frac{v^2}{f^2}d_2\right)P_L - m_d^j P_R\right](V_{\rm CKM})_{tj}$
$\bar{u}^i\pi^0 u^j$	$-\frac{gm_u^i}{2M_{Z_L}\cos\theta_W}\gamma_5\delta_{ij}$
$\bar{t}\pi^0 t$	$-\frac{gm_t}{2M_{Z_L}\cos\theta_W}\left(1-x_L^2\frac{v^2}{f^2}\right)\gamma_5$
$\bar{T}_+\pi^0 T_+$	$-\frac{gm_{T_+}}{2M_{Z_L}\cos\theta_W}x_L^2\frac{v^2}{f^2}\gamma_5$
$\bar{T}_+\pi^0 t$	$\frac{gx_L}{2M_{Z_L}\cos\theta_W}\frac{v}{f}\left[m_{T_+}\left(1+\frac{v^2}{f^2}\left(d_2-\frac{x_L^2}{2}\right)\right)P_L - m_t P_R\right]$
$\bar{d}^i\pi^0 d^j$	$\frac{gm_d^i}{2M_{Z_L}\cos\theta_W}\gamma_5\delta_{ij}$
$\bar{u}_H^i\pi^+ d_H^j$	$-\frac{g}{8\sqrt{2}M_{W_L}}\frac{v^2}{f^2}m_{Hi}^d\delta_{ij}$
$\bar{\nu}^i\pi^+\ell^j$	$\frac{g}{\sqrt{2}M_{W_L}}\left(m_\nu^i P_L - m_\ell^j P_R\right)(V_{\rm PMNS})_{ij}$
$\bar{\nu}^i\pi^0\nu^j$	$-\frac{gm_\nu^i}{2M_{Z_L}\cos\theta_W}\gamma_5\delta_{ij}$
$\bar{\ell}^i\pi^0\ell^j$	$\frac{gm_\ell^i}{2M_{Z_L}\cos\theta_W}\gamma_5\delta_{ij}$
$\bar{\nu}_H^i\pi^+\ell_H^j$	$-\frac{g}{8\sqrt{2}M_{W_L}}\frac{v^2}{f^2}m_{Hi}^\ell\delta_{ij}$

The leading order contributions to the couplings of fermions to the heavy Goldstone bosons have already been given in [16]. We included also $\mathcal{O}(v^2/f^2)$ corrections, necessary for the calculation of rare decays, and the contributions proportional to the SM fermion masses.

Fermion couplings to heavy Goldstone bosons	
$\bar{u}_H^i\omega^+ d^j$	$\frac{g}{\sqrt{2}M_{W_H}}\left(m_{Hi}^u P_L - m_d^j P_R\right)(V_{Hd})_{ij}$
$\bar{u}_H^i\omega^0 u^j$	$\frac{g}{2M_{Z_H}}\left[m_{Hi}^u\left(1+\frac{v^2}{f^2}\left(\frac{1}{8}-\frac{x_H}{\tan\theta_W}\right)\right)P_L - m_u^j P_R\right](V_{Hu})_{ij}$
$\bar{u}_H^i\omega^0 t$	$\frac{g}{2M_{Z_H}}\left[m_{Hi}^u\left(1+\frac{v^2}{f^2}\left(\frac{1}{8}-\frac{x_H}{\tan\theta_W}-\frac{x_L^2}{2}\right)\right)P_L - m_t P_R\right](V_{Hu})_{i3}$
$\bar{u}_H^i\omega^0 T_+$	$\frac{gx_L}{2M_{Z_H}}\frac{v}{f}\left(m_{Hi}^u P_L - m_{T_+}P_R\right)(V_{Hu})_{i3}$

$\bar{T}_-\omega^0 t$	$\frac{gm_t v}{2M_{Z_H} f} P_R$
$\bar{T}_-\omega^0 T_+$	$\frac{gm_{T_+} v^2}{2M_{Z_H} f^2}\left(1-\frac{4x_H}{\tan\theta_W}\right) P_R$
$\bar{u}^i_H \eta u^j$	$-\frac{g'}{10M_{A_H}}\left[m^u_{Hi}\left(1+\frac{v^2}{f^2}\left(\frac{5}{8}+x_H\tan\theta_W\right)\right)P_L - m^j_u P_R\right](V_{Hu})_{ij}$
$\bar{u}^i_H \eta t$	$-\frac{g'}{10M_{A_H}}\left[m^u_{Hi}\left(1+\frac{v^2}{f^2}\left(\frac{5}{8}+x_H\tan\theta_W-\frac{x_L^2}{2}\right)\right)P_L - m_t P_R\right](V_{Hu})_{i3}$
$\bar{u}^i_H \eta T_+$	$-\frac{g' x_L}{10M_{A_H}}\frac{v}{f}\left(m^u_{Hi}P_L - m_{T_+}P_R\right)(V_{Hu})_{i3}$
$\bar{T}_-\eta t$	$-\frac{2g' m_t}{5M_{A_H}}\frac{f}{v}\left(1-\frac{v^2}{f^2}\left(\frac{x_L^2}{2}+\frac{1}{6}\right)\right)P_R$
$\bar{T}_-\eta T_+$	$-\frac{2g' x_L m_{T_+}}{5M_{A_H}}\left(1-\frac{v^2}{f^2}\left(\frac{3}{2}x_L^2-2x_L+1\right)\right)P_R$
$\bar{d}^i_H \omega^- u^j$	$\frac{g}{\sqrt{2}M_{W_H}}\left[m^d_{Hi}\left(1-\frac{v^2}{8f^2}\right)P_L - m^j_u P_R\right](V_{Hu})_{ij}$
$\bar{d}^i_H \omega^- t$	$\frac{g}{\sqrt{2}M_{W_H}}\left[m^d_{Hi}\left(1-\frac{v^2}{f^2}\left(\frac{1}{8}+\frac{x_L^2}{2}\right)\right)P_L - m_t P_R\right](V_{Hu})_{i3}$
$\bar{d}^i_H \omega^- T_+$	$\frac{g}{\sqrt{2}M_{W_H}} x_L \frac{v}{f}\left(m^d_{Hi}P_L - m_{T_+}P_R\right)(V_{Hu})_{i3}$
$\bar{d}^i_H \omega^0 d^j$	$-\frac{g}{2M_{Z_H}}\left[m^d_{Hi}\left(1+\frac{v^2}{f^2}\left(-\frac{1}{4}+\frac{x_H}{\tan\theta_W}\right)\right)P_L - m^j_d P_R\right](V_{Hd})_{ij}$
$\bar{d}^i_H \eta d^j$	$-\frac{g'}{10M_{A_H}}\left[m^d_{Hi}\left(1-\frac{v^2}{f^2}\left(\frac{5}{4}+x_H\tan\theta_W\right)\right)P_L - m^j_d P_R\right](V_{Hd})_{ij}$
$\bar{\nu}^i_H \omega^+ \ell^j$	$\frac{g}{\sqrt{2}M_{W_H}}\left(m^\nu_{Hi}P_L - m^j_\ell P_R\right)(V_{H\ell})_{ij}$
$\bar{\nu}^i_H \omega^0 \nu^j$	$\frac{g}{2M_{Z_H}}\left[m^\nu_{Hi}\left(1+\frac{v^2}{f^2}\left(\frac{1}{8}-\frac{x_H}{\tan\theta_W}\right)\right)P_L - m^j_\nu P_R\right](V_{H\nu})_{ij}$
$\bar{\nu}^i_H \eta \nu^j$	$-\frac{g'}{10M_{A_H}}\left[m^\nu_{Hi}\left(1+\frac{v^2}{f^2}\left(\frac{5}{8}+x_H\tan\theta_W\right)\right)P_L - m^j_\nu P_R\right](V_{H\nu})_{ij}$
$\bar{\ell}^i_H \omega^- \nu^j$	$\frac{g}{\sqrt{2}M_{W_H}}\left[m^\ell_{Hi}\left(1-\frac{v^2}{8f^2}\right)P_L - m^j_\nu P_R\right](V_{H\nu})_{ij}$
$\bar{\ell}^i_H \omega^0 \ell^j$	$-\frac{g}{2M_{Z_H}}\left[m^\ell_{Hi}\left(1+\frac{v^2}{f^2}\left(-\frac{1}{4}+\frac{x_H}{\tan\theta_W}\right)\right)P_L - m^j_\ell P_R\right](V_{H\ell})_{ij}$
$\bar{\ell}^i_H \eta \ell^j$	$-\frac{g'}{10M_{A_H}}\left[m^\ell_{Hi}\left(1-\frac{v^2}{f^2}\left(\frac{5}{4}+x_H\tan\theta_W\right)\right)P_L - m^j_\ell P_R\right](V_{H\ell})_{ij}$

A.2.2 Triple Gauge Boson–Goldstone Boson Couplings

The kinetic term for the non-linear sigma model field Σ is given by

$$\mathcal{L} = \frac{f^2}{8}\mathrm{Tr}\left[\left(D_\mu\Sigma\right)^\dagger\left(D^\mu\Sigma\right)\right], \tag{A.2.1}$$

where the covariant derivative is defined through

$$D_\mu\Sigma = \partial_\mu\Sigma - \sqrt{2}i\sum_{j=1}^{2}\left[gW^a_{j\mu}\left(Q^a_j\Sigma+\Sigma Q^{aT}_j\right)+g'B_{j\mu}\left(Y_j\Sigma+\Sigma Y_j^T\right)\right]. \tag{A.2.2}$$

From this term, taking into account the mixing of the Goldstone boson and scalar fields, the interactions of the Goldstone boson fields with the SM and heavy gauge bosons can be obtained.

All momenta are defined to be incoming.

Gauge boson–Goldstone boson interactions	
$W_L^{+\mu} W_H^{-\nu} \eta$	$\frac{g}{4} M_{A_H} \left(\frac{5}{\tan\theta_W} + 4x_H \right) \frac{v^2}{f^2} g^{\mu\nu}$
$W_L^{+\mu} W_H^{-\nu} \omega^0$	$-g M_{Z_H} \left(1 - \frac{v^2}{4f^2} \right) g^{\mu\nu}$
$W_H^{+\mu} Z_L^{\nu} \omega^-$	$-g M_{W_H} \cos\theta_W \left(1 - \frac{v^2}{4f^2 \cos^2\theta_W} \right) g^{\mu\nu}$
$W_H^{+\mu} A_L^{\nu} \omega^-$	$-e M_{W_H} g^{\mu\nu}$
$W_L^{+\mu} Z_H^{\nu} \omega^-$	$g M_{W_H} \left(1 - \frac{v^2}{4f^2} \right) g^{\mu\nu}$
$W_L^{+\mu} A_H^{\nu} \omega^-$	$\frac{g M_{W_H} v^2}{f^2} \left(\frac{\tan\theta_W}{4} - x_H \right) g^{\mu\nu}$
$W_L^{+\mu} Z_L^{\nu} \pi^-$	$g M_{W_L} \frac{\sin^2\theta_W}{\cos\theta_W} g^{\mu\nu}$
$W_L^{+\mu} A_L^{\nu} \pi^-$	$-e M_{W_L} g^{\mu\nu}$
$W_H^{+\mu} A_H^{\nu} \pi^-$	$g' M_{W_L} g^{\mu\nu}$
$\omega^+(p) \omega^-(q) Z_L$	$ig \cos\theta_W \left(1 - \frac{v^2}{8f^2 \cos^2\theta_W} \right) (p-q)^{\mu}$
$\omega^+(p) \omega^-(q) A_L$	$ie\,(p-q)^{\mu}$
$\pi^+(p) \pi^-(q) Z_L$	$\frac{ig\left(1 - 2\sin^2\theta_W\right)}{2\cos\theta_W} (p-q)^{\mu}$
$\pi^+(p) \pi^-(q) A_L$	$ie\,(p-q)^{\mu}$
$\omega^+(p) \pi^-(q) A_H$	$-i\frac{g' v}{3f} (p-q)^{\mu}$
$\omega^+(p) \omega^0(q) W_L^{-\mu}$	$-ig \left(1 - \frac{v^2}{8f^2} \right) (p-q)^{\mu}$
$\omega^+(p) \eta(q) W_L^{-\mu}$	$i\frac{25g + 24g' x_H}{24\sqrt{5}} \frac{v^2}{f^2} (p-q)^{\mu}$
$\pi^+(p) \omega^0(q) W_H^{-\mu}$	$-i\frac{g}{2}\frac{v}{f} (p-q)^{\mu}$
$\pi^+(p) \eta(q) W_H^{-\mu}$	$-i\frac{\sqrt{5}g}{6}\frac{v}{f} (p-q)^{\mu}$
$\pi^+(p) \pi^0(q) W_L^{-\mu}$	$-i\frac{g}{2} (p-q)^{\mu}$

A.3 The Functions U_i and V_i

In the following we list the functions that enter the study of rare decays in the LH model, where $x_i = m_i^2/M_{W_L^\pm}^2$ and $y = M_{W_H^\pm}^2/M_{W_L^\pm}^2$. Both the results relevant for the X and Y function are collected.

$$\begin{aligned}
U_1(x_t,y) &= -\frac{(1+4x_L)\,x_t}{320}S_1 + \frac{(1+4x_L)\,(-7+x_t)\,x_t}{640\,(-1+x_t)} \\
&\quad + \frac{(1+4x_L)\,x_t\left(4-2x_t+x_t^2\right)\log x_t}{320\,(-1+x_t)^2} \\
&\quad - \frac{a x_t\,(11+4x_t)}{8\,(-1+x_t)} - \frac{3a x_t\left(-8+2x_t+x_t^2\right)\log x_t}{8\,(-1+x_t)^2} + \frac{3a x_t \log y}{8} \qquad \text{(A.3.1)} \\
U_2(x_t,y) &= -\frac{x_t\,(4-7x_t)}{16(-1+x_t)} - \frac{3x_t\left(8-6x_t-x_t^2\right)\log x_t}{16(-1+x_t)^2} - \frac{x_t\log y}{4} \qquad \text{(A.3.2)} \\
U_3(x_t,x_T) &= \frac{-3+2x_t-2x_t^2}{8(-1+x_t)} - \frac{x_t\left(-4-x_t+2x_t^2\right)\log x_t}{8(-1+x_t)^2} + \frac{(3+2x_t)\log x_T}{8} \qquad \text{(A.3.3)} \\
U_4(x_T,y) &= \frac{3x_T y}{16\,(-x_T+y)} + \frac{3x_T y^2\log x_T}{16(x_T-y)^2} - \frac{3x_T y^2\log y}{16(x_T-y)^2} - \frac{x_T\log y}{16} \qquad \text{(A.3.4)} \\
U_5(x_t,x_T) &= -\frac{(-3+4x_L)\,x_T}{320}S_1 + \frac{\left(-7-12x_L+80x_L^2\right)x_T}{640} + \frac{(-3+4x_L)\,x_T\log x_T}{320} \\
&\quad + \frac{3a x_T y\,(\log x_T-\log y)}{8\,(x_T-y)} \qquad \text{(A.3.5)} \\
U_6(\hat{x}_T) &= -\frac{S_2}{x_L} + \frac{\hat{x}_T}{(1-\hat{x}_T)} + \frac{\hat{x}_T^2\log\hat{x}_T}{(1-\hat{x}_T)^2} \qquad \text{(A.3.6)}
\end{aligned}$$

$$\begin{aligned}
V_1(x_t,y) &= -\frac{(1+4x_L)\,x_t}{320}S_1 + \frac{(1+4x_L)\,(-7+x_t)\,x_t}{640\,(-1+x_t)} \\
&\quad + \frac{(1+4x_L)\,x_t\left(4-2x_t+x_t^2\right)\log x_t}{320\,(-1+x_t)^2} \\
&\quad - \frac{a x_t\,(-13+4x_t)}{8\,(-1+x_t)} - \frac{3a x_t^2\,(2+x_t)\log x_t}{8\,(-1+x_t)^2} + \frac{3a x_t\log y}{8} \qquad \text{(A.3.7)} \\
V_2(x_t,y) &= -\frac{x_t\,(4-7x_t)}{16(-1+x_t)} - \frac{3x_t^2\,(2-x_t)\log x_t}{16(-1+x_t)^2} - \frac{x_t\log y}{4} \qquad \text{(A.3.8)} \\
V_3(x_t,x_T) &= \frac{\left(3+2x_t-2x_t^2\right)}{8(-1+x_t)} - \frac{x_t\left(2-x_t+2x_t^2\right)\log x_t}{8(-1+x_t)^2} + \frac{(3+2x_t)\log x_T}{8} \qquad \text{(A.3.9)} \\
V_4(x_T,y) &= \frac{3x_T y}{16\,(-x_T+y)} + \frac{3x_T y^2\log x_T}{16(x_T-y)^2} - \frac{3x_T y^2\log y}{16(x_T-y)^2} - \frac{x_T\log y}{16} \qquad \text{(A.3.10)} \\
V_5(x_t,x_T) &= -\frac{(-3+4x_L)\,x_T}{320}S_1 + \frac{\left(-7-12x_L+80x_L^2\right)x_T}{640} + \frac{(-3+4x_L)\,x_T\log x_T}{320} \\
&\quad + \frac{3a x_T y\,(\log x_T-\log y)}{8\,(x_T-y)} \qquad \text{(A.3.11)}
\end{aligned}$$

A.4 Functions Relevant for Rare Decays

In this appendix we list the functions that entered the present study of rare and CP-violating K and B decays in the LHT model. Both the SM contributions and the new physics contributions coming from the T-even and T-odd sectors are collected. The variables are defined as follows:

$$x_q = \frac{m_q^2}{M_{W_L}^2}\,, \qquad x_T = \frac{m_{T_+}^2}{M_{W_L}^2} \qquad (q = c, t)\,, \tag{A.4.1}$$

$$z_i = \frac{m_{Hi}^2}{M_{W_H}^2}\,, \quad z_i' = \frac{m_{Hi}^2}{M_{A_H}^2} = z_i\, a \quad \text{with} \quad a = \frac{5}{\tan^2\theta_W}\,, \qquad (i = 1, 2, 3)\,, \tag{A.4.2}$$

$$y = \frac{m_{H\ell}^2}{M_{W_H}^2} = \frac{m_{H\ell}^2}{M_{Z_H}^2}\,, \qquad y' = ya\,, \qquad \eta = \frac{1}{a}\,. \tag{A.4.3}$$

$$X_{\rm SM}(x_t) = \frac{x_t}{8}\left[\frac{x_t+2}{x_t-1} + \frac{3x_t-6}{(x_t-1)^2}\,\log x_t\right] \tag{A.4.4}$$

$$Y_{\rm SM}(x_t) = \frac{x_t}{8}\left[\frac{x_t-4}{x_t-1} + \frac{3x_t}{(x_t-1)^2}\log x_t\right] \tag{A.4.5}$$

$$\begin{aligned} Z_{\rm SM}(x_t) &= -\frac{1}{9}\log x_t + \frac{18x_t^4 - 163x_t^3 + 259x_t^2 - 108x_t}{144(x_t-1)^3} \\ &\quad + \frac{32x_t^4 - 38x_t^3 - 15x_t^2 + 18x_t}{72(x_t-1)^4}\log x_t \end{aligned} \tag{A.4.6}$$

$$C_0(y) = \frac{y}{8}\left[\frac{y-6}{y-1} + \frac{3y+2}{(y-1)^2}\log y\right] \tag{A.4.7}$$

$$D_0(y) = -\frac{4}{9}\log y + \frac{-19y^3+25y^2}{36(y-1)^3} + \frac{y^2(5y^2-2y-6)}{18(y-1)^4}\log y \tag{A.4.8}$$

$$E_0(y) = -\frac{2}{3}\log y + \frac{y^2(15-16y+4y^2)}{6(y-1)^4}\log y + \frac{y(18-11y-y^2)}{12(1-y)^3} \tag{A.4.9}$$

$$D_0'(y) = -\frac{(3y^3-2y^2)}{2(y-1)^4}\log y + \frac{(8y^3+5y^2-7y)}{12(y-1)^3} \tag{A.4.10}$$

$$E_0'(y) = \frac{3y^2}{2(y-1)^4}\log y + \frac{(y^3-5y^2-2y)}{4(y-1)^3} \tag{A.4.11}$$

$$U_3(x_t, x_T) = \frac{-3+2x_t-2x_t^2}{8(-1+x_t)} - \frac{x_t\left(-4-x_t+2x_t^2\right)\log x_t}{8(-1+x_t)^2} + \frac{(3+2x_t)\log x_T}{8} \tag{A.4.12}$$

$$V_3(x_t, x_T) = \frac{\left(3+2x_t-2x_t^2\right)}{8(-1+x_t)} - \frac{x_t\left(2-x_t+2x_t^2\right)\log x_t}{8(-1+x_t)^2} + \frac{(3+2x_t)\log x_T}{8} \tag{A.4.13}$$

$$(D')_{\rm SM} = D'_0(x_t) \tag{A.4.14}$$

$$(D')_{\rm LHT} = (D')_{\rm even} + \frac{1}{\lambda_t^{(s)}} T_{D'}^{\rm odd} \tag{A.4.15}$$

$$(D')_{\rm even} = D'_0(x_t) + \frac{v^2}{f^2} x_L^2 \Big[D'_0(x_T) - D'_0(x_t) \Big] \tag{A.4.16}$$

$$T_{D'}^{\rm odd} = \frac{1}{4}\frac{v^2}{f^2} \left[\xi_2^{(s)} \big(D'_{\rm odd}(z_2) - D'_{\rm odd}(z_1) \big) + \xi_3^{(s)} \big(D'_{\rm odd}(z_3) - D'_{\rm odd}(z_1) \big) \right] \tag{A.4.17}$$

$$D'_{\rm odd}(z_i) = D'_0(z_i) - \frac{1}{6} E'_0(z_i) - \frac{1}{30} E'_0(z'_i) \tag{A.4.18}$$

$$R_2(z_i) = -\left[\frac{z_i \log z_i}{(1-z_i)^2} + \frac{1}{1-z_i} \right] \tag{A.4.19}$$

$$F_2(z_i) = -\frac{1}{2} \left[\frac{z_i^2 \log z_i}{(1-z_i)^2} + \frac{1}{1-z_i} \right] \tag{A.4.20}$$

$$F^{\nu\bar{\nu}}(z_i, y; W_H) = \frac{3}{2} z_i - F_5(z_i, y) - 7F_6(z_i, y) - 9U(z_i, y) \tag{A.4.21}$$

$$F^{\mu\bar{\mu}}(z_i, y; W_H) = \frac{3}{2} z_i - F_5(z_i, y) - 7F_6(z_i, y) + 3U(z_i, y) \tag{A.4.22}$$

$$F_5(z_i, y) = \frac{z_i^3 \log z_i}{(1-z_i)(y-z_i)} + \frac{y^3 \log y}{(1-y)(z_i-y)} \tag{A.4.23}$$

$$F_6(z_i, y) = -\left[\frac{z_i^2 \log z_i}{(1-z_i)(y-z_i)} + \frac{y^2 \log y}{(1-y)(z_i-y)} \right] \tag{A.4.24}$$

$$U(z_i, y) = \frac{z_i^2 \log z_i}{(z_i-y)(1-z_i)^2} + \frac{y^2 \log y}{(y-z_i)(1-y)^2} + \frac{1}{(1-z_i)(1-y)} \tag{A.4.25}$$

$$G(z_i, y; Z_H) = -\frac{3}{4} U(z, y) \tag{A.4.26}$$

$$G_1\left(z'_i, y'_i; A_H\right) = \frac{1}{25a} G\left(z'_i, y'_i; Z_H\right) \tag{A.4.27}$$

$$G_2(z_i, y; \eta) = -\frac{3}{10a} \left[\frac{z_i^2 \log z_i}{(1-z_i)(\eta-z_i)(z_i-y)} + \frac{y^2 \log y}{(1-y)(\eta-y)(y-z_i)} + \frac{\eta^2 \log \eta}{(1-\eta)(z_i-\eta)(\eta-y)} \right] \tag{A.4.28}$$

A.5 Functions Relevant for Lepton Flavor Violating Decays

Finally, in this appendix we list the functions relevant for the study of LFV decays with the variables being defined in Appendix A.4.

$$D_0(x) = -\frac{4}{9}\log x + \frac{-19x^3+25x^2}{36(x-1)^3} + \frac{x^2(5x^2-2x-6)}{18(x-1)^4}\log x \tag{A.5.29}$$

$$E_0(x) = -\frac{2}{3}\log x + \frac{x^2(15-16x+4x^2)}{6(1-x)^4}\log x + \frac{x(18-11x-x^2)}{12(1-x)^3} \tag{A.5.30}$$

$$D_0'(x) = -\frac{3x^3-2x^2}{2(x-1)^4}\log x + \frac{8x^3+5x^2-7x}{12(x-1)^3} \tag{A.5.31}$$

$$E_0'(x) = \frac{3x^2}{2(x-1)^4}\log x + \frac{x^3-5x^2-2x}{4(x-1)^3} \tag{A.5.32}$$

$$H(y_i) = D_0'(y_i) - \frac{2}{3}E_0'(y_i) \tag{A.5.33}$$

$$R_2(y_i) = -\left[\frac{y_i\log y_i}{(1-y_i)^2} + \frac{1}{1-y_i}\right] \tag{A.5.34}$$

$$F_2(y_i) = -\frac{1}{2}\left[\frac{y_i^2\log y_i}{(1-y_i)^2} + \frac{1}{1-y_i}\right] \tag{A.5.35}$$

$$F^{u\bar{u}}(y_i,z;W_H) = \frac{3}{2}y_i - F_5(y_i,z) - 7F_6(y_i,z) - 9U(y_i,z) \tag{A.5.36}$$

$$F^{d\bar{d}}(y_i,z;W_H) = \frac{3}{2}y_i - F_5(y_i,z) - 7F_6(y_i,z) + 3U(y_i,z) \tag{A.5.37}$$

$$F_5(y_i,z) = \frac{y_i^3\log y_i}{(1-y_i)(z-y_i)} + \frac{z^3\log z}{(1-z)(y_i-z)} \tag{A.5.38}$$

$$F_6(y_i,z) = -\left[\frac{y_i^2\log y_i}{(1-y_i)(z-y_i)} + \frac{z^2\log z}{(1-z)(y_i-z)}\right] \tag{A.5.39}$$

$$U(y_i,z) = \frac{y_i^2\log y_i}{(y_i-z)(1-y_i)^2} + \frac{z^2\log z}{(z-y_i)(1-z)^2} + \frac{1}{(1-y_i)(1-z)} \tag{A.5.40}$$

$$G(y_i,z;Z_H) = -\frac{3}{4}U(y_i,z) \tag{A.5.41}$$

$$G_1(y_i',z';A_H) = \frac{1}{25a}G(y_i',z';Z_H) \tag{A.5.42}$$

$$G_2(y_i,z;\eta) = -\frac{3}{10a}\left[\frac{y_i^2\log y_i}{(1-y_i)(\eta-y_i)(y_i-z)} + \frac{z^2\log z}{(1-z)(\eta-z)(z-y_i)} + \frac{\eta^2\log\eta}{(1-\eta)(y_i-\eta)(\eta-z)}\right] \tag{A.5.43}$$

$$C_{\rm odd}(y_i) = \frac{1}{64}\frac{v^2}{f^2}\left[y_i S_{\rm odd} - 8y_i R_2(y_i) + \frac{3}{2}y_i + 2y_i F_2(y_i)\right] \quad \text{(A.5.44)}$$

$$D_{\rm odd}(y_i) = \frac{1}{4}\frac{v^2}{f^2}\left[D_0(y_i) - \frac{7}{6}E_0(y_i) - \frac{1}{10}E_0(y_i')\right] \quad \text{(A.5.45)}$$

$$S_{\rm odd} = \frac{1}{\varepsilon} + \log\frac{\mu^2}{M_{W_H}^2} \longrightarrow \log\frac{(4\pi f)^2}{M_{W_H}^2} \quad \text{(A.5.46)}$$

$$F(z_i, y_j; W_H) = \frac{1}{(1-z_i)(1-y_j)}\left(1 - \frac{7}{4}z_i y_j\right) + \frac{z_i^2 \log z_i}{(z_i - y_j)(1-z_i)^2}\left(1 - 2y_j + \frac{z_i y_j}{4}\right) - \frac{y_j^2 \log y_j}{(z_i - y_j)(1-y_j)^2}\left(1 - 2z_i + \frac{z_i y_j}{4}\right) \quad \text{(A.5.47)}$$

$$A_1(z_i, y_j; Z_H) = -\frac{3}{100a}\left[\frac{1}{(1-z_i')(1-y_j')} + \frac{z_i' z_i \log z_i'}{(z_i - y_j)(1-z_i')^2} - \frac{y_j' y_j \log y_j'}{(z_i - y_j)(1-y_j')^2}\right] \quad \text{(A.5.48)}$$

$$A_2(z_i, y_j; Z_H) = -\frac{3}{10}\left[\frac{\log a}{(a-1)(1-z_i')(1-y_j')} + \frac{z_i^2 \log z_i}{(z_i - y_j)(1-z_i)(1-z_i')} - \frac{y_j^2 \log y_j}{(z_i - y_j)(1-y_j)(1-y_j')}\right] \quad \text{(A.5.49)}$$

$$L_1(y_i) = \frac{1}{12(1-y_i)^4}\left[-8 + 38y_i - 39y_i^2 + 14y_i^3 - 5y_i^4 + 18y_i^2 \log y_i\right] \quad \text{(A.5.50)}$$

$$L_2(y_i) = \frac{1}{6(1-y_i)^4}\left[-10 + 43y_i - 78y_i^2 + 49y_i^3 - 4y_i^4 - 18y_i^3 \log y_i\right] \quad \text{(A.5.51)}$$

Bibliography

[1] N. Arkani-Hamed, A. G. Cohen, and H. Georgi, (De)constructing dimensions, *Phys. Rev. Lett.* **86** (2001) 4757.

[2] N. Arkani-Hamed, A. G. Cohen, and H. Georgi, Electroweak symmetry breaking from dimensional deconstruction, *Phys. Lett.* **B513** (2001) 232.

[3] M. Schmaltz and D. Tucker-Smith, Little Higgs review, *Ann. Rev. Nucl. Part. Sci.* **55** (2005) 229.

M. Perelstein, Little Higgs models and their phenomenology, *Prog. Part. Nucl. Phys.* **58** (2007) 247.

[4] N. Arkani-Hamed, A. G. Cohen, E. Katz, and A. E. Nelson, The Littlest Higgs, *JHEP* **07** (2002) 034.

[5] T. Han, H. E. Logan, B. McElrath, and L.-T. Wang, Phenomenology of the little Higgs model, *Phys. Rev.* **D67** (2003) 095004.

[6] A. J. Buras, A. Poschenrieder, and S. Uhlig, Particle-antiparticle mixing, ε_K and the unitarity triangle in the Littlest Higgs model, *Nucl. Phys.* **B716** (2005) 173.

[7] A. J. Buras, A. Poschenrieder, S. Uhlig, and W. A. Bardeen, Rare K and B decays in the Littlest Higgs model without T-parity, *JHEP* **11** (2006) 062.

[8] C. Csaki, J. Hubisz, G. D. Kribs, P. Meade, and J. Terning, Big corrections from a little Higgs, *Phys. Rev.* **D67** (2003) 115002.

J. L. Hewett, F. J. Petriello, and T. G. Rizzo, Constraining the Littlest Higgs, *JHEP* **10** (2003) 062.

M.-C. Chen and S. Dawson, One-loop radiative corrections to the ρ parameter in the Littlest Higgs model, *Phys. Rev.* **D70** (2004) 015003.

[9] H.-C. Cheng and I. Low, TeV symmetry and the little hierarchy problem, *JHEP* **09** (2003) 051.

H.-C. Cheng and I. Low, Little hierarchy, little Higgses, and a little symmetry, *JHEP* **08** (2004) 061.

[10] J. Hubisz, P. Meade, A. Noble, and M. Perelstein, Electroweak precision constraints on the Littlest Higgs model with T-parity, *JHEP* **01** (2006) 135.

[11] J. Hubisz and P. Meade, Phenomenology of the Littlest Higgs with T-parity, *Phys. Rev.* **D71** (2005) 035016.

[12] S. R. Choudhury, N. Gaur, A. Goyal, and N. Mahajan, $B_d - \bar{B}_d$ mass difference in little Higgs model, *Phys. Lett.* **B601** (2004) 164.

[13] A. J. Buras, A. Poschenrieder, and S. Uhlig, Non-decoupling effects of the heavy T in the $B^0_{d,s} - \bar{B}^0_{d,s}$ mixing and rare K and B decays, (2005).

[14] W.-j. Huo and S.-h. Zhu, $b \to s\gamma$ in Littlest Higgs model, *Phys. Rev.* **D68** (2003) 097301.

[15] M. Blanke *et al.*, Particle antiparticle mixing, ε_K, $\Delta\Gamma_q$, A^q_{SL}, $A_{CP}(B_d \to \psi K_S)$, $A_{CP}(B_s \to \psi\phi)$ and $B \to X_{s,d}\gamma$ in the Littlest Higgs model with T-parity, *JHEP* **12** (2006) 003.

[16] J. Hubisz, S. J. Lee, and G. Paz, The flavor of a little Higgs with T-parity, *JHEP* **06** (2006) 041.

[17] M. Blanke *et al.*, Rare and CP-violating K and B decays in the Littlest Higgs model with T-parity, *JHEP* **01** (2007) 066.

[18] A. Goyal, Lepton flavor violation in little Higgs model with T-parity, (2006).

[19] S. R. Choudhury, A. S. Cornell, A. Deandrea, N. Gaur, and A. Goyal, Lepton flavour violation in the little Higgs model, *Phys. Rev.* **D75** (2007) 055011.

[20] J. R. Ellis, J. Hisano, M. Raidal, and Y. Shimizu, A new parametrization of the seesaw mechanism and applications in supersymmetric models, *Phys. Rev.* **D66** (2002) 115013.

[21] A. Brignole and A. Rossi, Anatomy and phenomenology of μ-τ lepton flavour violation in the MSSM, *Nucl. Phys.* **B701** (2004) 3.

[22] E. Arganda and M. J. Herrero, Testing supersymmetry with lepton flavor violating τ and μ decays, *Phys. Rev.* **D73** (2006) 055003.

[23] P. Paradisi, Constraints on SUSY lepton flavour violation by rare processes, *JHEP* **10** (2005) 006.

[24] P. Paradisi, Higgs-mediated $\tau \to \mu$ and $\tau \to e$ transitions in II Higgs doublet model and supersymmetry, *JHEP* **02** (2006) 050.

[25] P. Paradisi, Higgs-mediated $e \to \mu$ transitions in II Higgs doublet model and supersymmetry, *JHEP* **08** (2006) 047.

[26] M. Gell-Mann, A schematic model of baryons and mesons, *Phys. Lett.* **8** (1964) 214.

O. W. Greenberg, Spin and unitary spin independence in a paraquark model of baryons and mesons, *Phys. Rev. Lett.* **13** (1964) 598.

G. Zweig, An $SU(3)$ model for strong interaction symmetry and its breaking. 2, CERN-TH-412.

M. Y. Han and Y. Nambu, Three-triplet model with double $SU(3)$ symmetry, *Phys. Rev.* **139** (1965) B1006.

H. Fritzsch, M. Gell-Mann, and H. Leutwyler, Advantages of the color octet gluon picture, *Phys. Lett.* **B47** (1973) 365.

[27] S. L. Glashow, Partial symmetries of weak interactions, *Nucl. Phys.* **22** (1961) 579.

[28] S. Weinberg, A model of leptons, *Phys. Rev. Lett.* **19** (1967) 1264.

[29] S. L. Glashow, J. Iliopoulos, and L. Maiani, Weak interactions with lepton-hadron symmetry, *Phys. Rev.* **D2** (1970) 1285.

[30] D. J. Gross and F. Wilczek, Asymptotically free gauge theories. 1, *Phys. Rev.* **D8** (1973) 3633.

H. D. Politzer, Reliable perturbative results for strong interactions?, *Phys. Rev. Lett.* **30** (1973) 1346.

D. J. Gross and F. Wilczek, Asymptotically free gauge theories. 2, *Phys. Rev.* **D9** (1974) 980.

[31] J. Goldstone, Field theories with superconductor solutions, *Nuovo Cim.* **19** (1961) 154.

[32] B. W. Lee, C. Quigg, and H. B. Thacker, The strength of weak interactions at very high-energies and the Higgs boson mass, *Phys. Rev. Lett.* **38** (1977) 883.

B. W. Lee, C. Quigg, and H. B. Thacker, Weak interactions at very high-energies: The role of the Higgs boson mass, *Phys. Rev.* **D16** (1977) 1519.

M. S. Chanowitz and M. K. Gaillard, The TeV physics of strongly interacting W's and Z's, *Nucl. Phys.* **B261** (1985) 379.

[33] R. F. Dashen and H. Neuberger, How to get an upper bound on the Higgs mass, *Phys. Rev. Lett.* **50** (1983) 1897.

M. Luscher and P. Weisz, Scaling laws and triviality bounds in the lattice ϕ^4 theory. 1. One component model in the symmetric phase, *Nucl. Phys.* **B290** (1987) 25.

M. Luscher and P. Weisz, Scaling laws and triviality bounds in the lattice ϕ^4 theory. 2. One component model in the phase with spontaneous symmetry breaking, *Nucl. Phys.* **B295** (1988) 65.

[34] G. 't Hooft, Naturalness, chiral symmetry, and spontaneous chiral symmetry breaking, *NATO Adv. Study Inst. Ser. B Phys.* **59** (1980) 135.

[35] R. Barbieri and A. Strumia, The 'LEP paradox', (2000).

[36] L. Randall and R. Sundrum, A large mass hierarchy from a small extra dimension, *Phys. Rev. Lett.* **83** (1999) 3370.

[37] L. Randall and R. Sundrum, An alternative to compactification, *Phys. Rev. Lett.* **83** (1999) 4690.

[38] C. T. Hill, S. Pokorski, and J. Wang, Gauge invariant effective Lagrangian for Kaluza-Klein modes, *Phys. Rev.* **D64** (2001) 105005.

[39] H. Georgi, A tool kit for builders of composite models, *Nucl. Phys.* **B266** (1986) 274.

[40] M. R. Douglas and G. W. Moore, D-branes, Quivers, and ALE Instantons, (1996).

[41] S. Weinberg, Phenomenological Lagrangians, *Physica* **A96** (1979) 327.

A. Manohar and H. Georgi, Chiral quarks and the nonrelativistic quark model, *Nucl. Phys.* **B234** (1984) 189.

[42] W. A. Bardeen and R. B. Pearson, Local gauge invariance and the bound state nature of hadrons, *Phys. Rev.* **D14** (1976) 547.

[43] I. Montvay and G. Munster, Quantum fields on a lattice, Cambridge, UK: Univ. Pr. (1994) 491 p. (Cambridge monographs on mathematical physics).

[44] A. Pich, Chiral perturbation theory, *Rept. Prog. Phys.* **58** (1995) 563.

[45] J. Gasser and H. Leutwyler, Chiral perturbation theory to one loop, *Ann. Phys.* **158** (1984) 142.

[46] J. Gasser and H. Leutwyler, Chiral perturbation theory: Expansions in the mass of the strange quark, *Nucl. Phys.* **B250** (1985) 465.

[47] N. Arkani-Hamed *et al.*, The minimal moose for a little Higgs, *JHEP* **08** (2002) 021.

[48] E. Katz, J.-y. Lee, A. E. Nelson, and D. G. E. Walker, A composite little Higgs model, *JHEP* **10** (2005) 088.

[49] N. Arkani-Hamed, A. G. Cohen, T. Gregoire, and J. G. Wacker, Phenomenology of electroweak symmetry breaking from theory space, *JHEP* **08** (2002) 020.

[50] I. Low, W. Skiba, and D. Smith, Little Higgses from an antisymmetric condensate, *Phys. Rev.* **D66** (2002) 072001.

[51] M. Schmaltz, Physics beyond the standard model (Theory): Introducing the little Higgs, *Nucl. Phys. Proc. Suppl.* **117** (2003) 40.

C. Csaki, J. Hubisz, G. D. Kribs, P. Meade, and J. Terning, Variations of little Higgs models and their electroweak constraints, *Phys. Rev.* **D68** (2003) 035009.

G. Burdman, M. Perelstein, and A. Pierce, Collider tests of the little Higgs model, *Phys. Rev. Lett.* **90** (2003) 241802.

C. Dib, R. Rosenfeld, and A. Zerwekh, Higgs production and decay in the little Higgs model, (2003).

M.-C. Chen and S. Dawson, The Littlest Higgs model and one-loop electroweak precision constraints, (0900).

C.-x. Yue and W. Wang, The branching ratio R_b in the Littlest Higgs model, *Nucl. Phys.* **B683** (2004) 48.

W. Kilian and J. Reuter, The low-energy structure of little Higgs models, *Phys. Rev.* **D70** (2004) 015004.

T. Han, H. E. Logan, B. McElrath, and L.-T. Wang, Loop induced decays of the little Higgs: $H \to gg, \gamma\gamma$, *Phys. Lett.* **B563** (2003) 191.

S. Chang and J. G. Wacker, Little Higgs and custodial SU(2), *Phys. Rev.* **D69** (2004) 035002.

G. D. Kribs, Electroweak precision tests of little Higgs theories, (2003).

[52] H. Georgi, D. B. Kaplan, and P. Galison, Calculation of the composite Higgs mass, *Phys. Lett.* **B143** (1984) 152.

H. Georgi and D. B. Kaplan, Composite Higgs and custodial SU(2), *Phys. Lett.* **B145** (1984) 216.

[53] S. R. Coleman and E. Weinberg, Radiative corrections as the origin of spontaneous symmetry breaking, *Phys. Rev.* **D7** (1973) 1888.

[54] S. Peris, g_A in the constituent quark model, *Phys. Lett.* **B268** (1991) 415.

[55] G. D'Ambrosio, G. F. Giudice, G. Isidori, and A. Strumia, Minimal flavour violation: An effective field theory approach, *Nucl. Phys.* **B645** (2002) 155.

[56] A. J. Buras, P. Gambino, M. Gorbahn, S. Jager, and L. Silvestrini, Universal unitarity triangle and physics beyond the standard model, *Phys. Lett.* **B500** (2001) 161.

A. J. Buras, Minimal flavor violation, *Acta Phys. Polon.* **B34** (2003) 5615.

[57] A. Abulencia *et al.*, Measurement of the B_s^0 - $\bar{B}_s^0$ Oscillation Frequency, *Phys. Rev. Lett.* **97** (2006) 062003.

[58] V. M. Abazov *et al.*, First direct two-sided bound on the B_s^0 oscillation frequency, *Phys. Rev. Lett.* **97** (2006) 021802.

[59] HFAG, http://www.slac.stanford.edu/xorg/hfag/.

[60] E. Blucher *et al.*, Status of the Cabibbo angle (CKM2005 - WG 1), (2005).

[61] M. Bona *et al.*, The UTfit collaboration report on the status of the unitarity triangle beyond the standard model. I: Model-independent analysis and minimal flavour violation, *JHEP* **03** (2006) 080.

M. Bona *et al.*, The UTfit collaboration report on the unitarity triangle beyond the standard model: Spring 2006, *Phys. Rev. Lett.* **97** (2006) 151803.

[62] I. Low, T-parity and the Littlest Higgs, *JHEP* **10** (2004) 067.

[63] S. R. Coleman, J. Wess, and B. Zumino, Structure of phenomenological Lagrangians. 1, *Phys. Rev.* **177** (1969) 2239.

J. Callan, Curtis G., S. R. Coleman, J. Wess, and B. Zumino, Structure of phenomenological Lagrangians. 2, *Phys. Rev.* **177** (1969) 2247.

[64] G. F. Giudice and A. Strumia, Constraints on extra-dimensional theories from virtual- graviton exchange, *Nucl. Phys.* **B663** (2003) 377.

[65] M. Blanke *et al.*, Another look at the flavour structure of the Littlest Higgs model with T-parity, *Phys. Lett.* **B646** (2007) 253.

[66] M. Blanke, A. J. Buras, B. Duling, A. Poschenrieder, and C. Tarantino, Charged lepton flavour violation and $(g-2)_\mu$ in the Littlest Higgs model with T-parity: A clear distinction from supersymmetry, (2007).

[67] M. Blanke, A. J. Buras, D. Guadagnoli, and C. Tarantino, Minimal flavour violation waiting for precise measurements of ΔM_s, $S_{\psi\phi}$, A_{SL}^s, $|V_{ub}|$, γ and $B_{s,d}^0 \to \mu^+\mu^-$, *JHEP* **10** (2006) 003.

[68] A. J. Buras, R. Fleischer, S. Recksiegel, and F. Schwab, Anatomy of prominent B and K decays and signatures of CP- violating new physics in the electroweak penguin sector, *Nucl. Phys.* **B697** (2004) 133.

A. J. Buras, R. Fleischer, S. Recksiegel, and F. Schwab, New aspects of $B \to \pi\pi, \pi K$ and their implications for rare decays, *Eur. Phys. J.* **C45** (2006) 701.

[69] A. J. Buras, M. Gorbahn, U. Haisch, and U. Nierste, The rare decay $K^+ \to \pi^+ \nu\bar{\nu}$ at the next-to-next- to-leading order in QCD, *Phys. Rev. Lett.* **95** (2005) 261805.

A. J. Buras, M. Gorbahn, U. Haisch, and U. Nierste, Charm quark contribution to $K^+ \to \pi^+ \nu\bar{\nu}$ at next-to-next-to-leading order, *JHEP* **11** (2006) 002.

[70] G. Isidori, F. Mescia, and C. Smith, Light-quark loops in $K \to \pi\nu\bar{\nu}$, *Nucl. Phys.* **B718** (2005) 319.

[71] G. Buchalla and A. J. Buras, $\sin 2\beta$ from $K \to \pi\nu\bar{\nu}$, *Phys. Lett.* **B333** (1994) 221.

[72] A. J. Buras and R. Fleischer, Bounds on the unitarity triangle, $\sin 2\beta$ and $K \to \pi\nu\bar{\nu}$ decays in models with minimal flavor violation, *Phys. Rev.* **D64** (2001) 115010.

[73] S. Adler *et al.*, Further evidence for the decay $K^+ \to \pi^+ \nu\bar{\nu}$, *Phys. Rev. Lett.* **88** (2002) 041803.

V. V. Anisimovsky *et al.*, Further study of the decay $K^+ \to \pi^+ \nu\bar{\nu}$, *Phys. Rev. Lett.* **93** (2004) 031801.

[74] J. K. Ahn *et al.*, New limit for the $K_L^0 \to \pi^0 \nu\bar{\nu}$, *Phys. Rev.* **D74** (2006) 051105.

[75] A. J. Buras, F. Schwab, and S. Uhlig, Waiting for precise measurements of $K^+ \to \pi^+ \nu\bar{\nu}$ and $K_L \to \pi^0 \nu\bar{\nu}$, (2004).

[76] G. Isidori, Flavor physics with light quarks and leptons, (2006).

C. Smith, Theory review on rare K decays: Standard model and beyond, (2006).

[77] A. J. Buras, Relations between $\Delta M_{s,d}$ and $B_{s,d} \to \mu\bar{\mu}$ in models with minimal flavour violation, *Phys. Lett.* **B566** (2003) 115.

[78] CDF, http://www-cdf.fnal.gov/physics/new/bottom/060316.blessed-bsmumu3/.

[79] G. D'Ambrosio, G. Ecker, G. Isidori, and J. Portoles, The decays $K \to \pi l^+ l^-$ beyond leading order in the chiral expansion, *JHEP* **08** (1998) 004.

[80] G. Buchalla, G. D'Ambrosio, and G. Isidori, Extracting short-distance physics from $K_{L,S} \to \pi^0 e^+ e^-$ decays, *Nucl. Phys.* **B672** (2003) 387.

[81] G. Isidori, C. Smith, and R. Unterdorfer, The rare decay $K_L \to \pi^0 \mu^+ \mu^-$ within the SM, *Eur. Phys. J.* **C36** (2004) 57.

[82] S. Friot, D. Greynat, and E. De Rafael, Rare kaon decays revisited, *Phys. Lett.* **B595** (2004) 301.

[83] F. Mescia, C. Smith, and S. Trine, $K_L \to \pi^0 e^+ e^-$ and $K_L \to \pi^0 \mu^+ \mu^-$: A binary star on the stage of flavor physics, *JHEP* **08** (2006) 088.

[84] A. J. Buras, M. E. Lautenbacher, M. Misiak, and M. Munz, Direct CP violation in $K_L \to \pi^0 e^+ e^-$ beyond leading logarithms, *Nucl. Phys.* **B423** (1994) 349.

[85] A. Alavi-Harati *et al.*, Search for the rare decay $K_L \to \pi^0 e^+ e^-$, *Phys. Rev. Lett.* **93** (2004) 021805.

[86] A. Alavi-Harati *et al.*, Search for the decay $K_L \to \pi^0 \mu^+ \mu^-$, *Phys. Rev. Lett.* **84** (2000) 5279.

[87] M. Bona *et al.*, The unitarity triangle fit in the standard model and hadronic parameters from lattice QCD: A reappraisal after the measurements of ΔM_s and $Br(B \to \tau \nu_\tau)$, *JHEP* **10** (2006) 081.

J. Charles *et al.*, CP violation and the CKM matrix: Assessing the impact of the asymmetric B factories, *Eur. Phys. J.* **C41** (2005) 1.

[88] S. Eidelman *et al.*, Review of particle physics, *Phys. Lett.* **B592** (2004) 1.

[89] S. Hashimoto, Recent results from lattice calculations, *Int. J. Mod. Phys.* **A20** (2005) 5133.

[90] Y. Grossman and Y. Nir, $K_L \to \pi^0 \nu \bar{\nu}$ beyond the standard model, *Phys. Lett.* **B398** (1997) 163.

[91] M. L. Brooks *et al.*, New limit for the family-number non-conserving decay $\mu^+ \to e^+ \gamma$, *Phys. Rev. Lett.* **83** (1999) 1521.

[92] S. Banerjee, Searches for lepton flavor violating decays $\tau^\pm \to \ell^\pm \gamma$, $\tau^\pm \to \ell^\pm P^0$ (where $\ell^- = e^-, \mu^-$, and $P^0 = \pi^0, \eta, \eta'$) at B-factories: Status and combinations, (2007).

[93] K. Abe *et al.*, A new search for $\tau \to \mu\gamma$ and $\tau \to e\gamma$ decays at Belle, (2006).

[94] B. Aubert *et al.*, Search for lepton flavor violation in the decay $\tau^\pm \to e^\pm \gamma$, *Phys. Rev. Lett.* **96** (2006) 041801.

[95] Y. Enari *et al.*, Search for lepton flavor violating decays $\tau^- \to l^- \pi^0, \ell^- \eta, \ell^- \eta'$, *Phys. Lett.* **B622** (2005) 218.

[96] B. Aubert *et al.*, Search for lepton flavor violating decays $\tau^\pm \to \ell^\pm \pi^0, \ell^\pm \eta, \ell^\pm \eta'$, (2006).

[97] U. Bellgardt *et al.*, Search for the decay $\mu^+ \to e^+ e^+ e^-$, *Nucl. Phys.* **B299** (1988) 1.

[98] J. Hisano, T. Moroi, K. Tobe, and M. Yamaguchi, Lepton flavor violation via right-handed neutrino Yukawa couplings in supersymmetric Standard Model, *Phys. Rev.* **D53** (1996) 2442.

[99] C. Dohmen *et al.*, Test of lepton flavor conservation in $\mu - e$ conversion on titanium, *Phys. Lett.* **B317** (1993) 631.

[100] Y. Mori *et al.*, LOI at J-PARC 50-GeV PS, LOI-25, http://psux1.kek.jp/ ~jhf-np/LOIlist/LOIlist.html.

[101] R. Kitano, M. Koike, and Y. Okada, Detailed calculation of lepton flavor violating muon electron conversion rate for various nuclei, *Phys. Rev.* **D66** (2002) 096002.

[102] A. Czarnecki, W. J. Marciano, and K. Melnikov, Coherent muon electron conversion in muonic atoms, *AIP Conf. Proc.* **435** (1998) 409.

[103] J. C. Sens, Capture of negative muons by nuclei, *Phys. Rev.* **113** (1959) 679 .

K. W. Ford and J. G. Wills, Calculated properties of μ-mesonic atoms, *Nucl. Phys.* **35** (1962) 295.

H. C. Chiang, E. Oset, T. S. Kosmas, A. Faessler, and J. D. Vergados, Coherent and incoherent $\mu^- - e^-$ conversion in nuclei, *Nucl. Phys.* **A559** (1993) 526.

[104] J. Bernabeu, E. Nardi, and D. Tommasini, $\mu - e$ conversion in nuclei and Z-prime physics, *Nucl. Phys.* **B409** (1993) 69.

[105] T. Suzuki, D. F. Measday, and J. P. Roalsvig, Total nuclear capture rates for negative muons, *Phys. Rev.* **C35** (1987) 2212.

[106] G. Buchalla, A. J. Buras, and M. E. Lautenbacher, Weak decays beyond leading logarithms, *Rev. Mod. Phys.* **68** (1996) 1125.

[107] G. W. Bennett *et al.*, Final report of the muon E821 anomalous magnetic moment measurement at BNL, *Phys. Rev.* **D73** (2006) 072003.

[108] K. Hagiwara, A. D. Martin, D. Nomura, and T. Teubner, Predictions for $g-2$ of the muon and $\alpha_{\rm QED}(M_Z^2)$, *Phys. Rev.* **D69** (2004) 093003.

[109] T. Kinoshita and M. Nio, Improved α^4 term of the muon anomalous magnetic moment, *Phys. Rev.* **D70** (2004) 113001.

M. Passera, Precise mass-dependent QED contributions to leptonic $g-2$ at order α^2 and α^3, *Phys. Rev.* **D75** (2007) 013002.

[110] A. Czarnecki, W. J. Marciano, and A. Vainshtein, Refinements in electroweak contributions to the muon anomalous magnetic moment, *Phys. Rev.* **D67** (2003) 073006.

A. Czarnecki, A finer constant, *Nature* **442** (2006) 516.

[111] M. Davier, The hadronic contribution to $(g-2)_\mu$, (2007).

[112] J. F. de Troconiz and F. J. Yndurain, The hadronic contributions to the anomalous magnetic moment of the muon, *Phys. Rev.* **D71** (2005) 073008.

[113] M. Knecht and A. Nyffeler, Hadronic light-by-light corrections to the muon $g-2$: The pion-pole contribution, *Phys. Rev.* **D65** (2002) 073034.

M. Knecht, A. Nyffeler, M. Perrottet, and E. De Rafael, Hadronic light-by-light scattering contribution to the muon $g-2$: An effective field theory approach, *Phys. Rev. Lett.* **88** (2002) 071802.

M. Ramsey-Musolf and M. B. Wise, Hadronic light-by-light contribution to muon $g-2$ in chiral perturbation theory, *Phys. Rev. Lett.* **89** (2002) 041601.

J. H. Kuhn, A. I. Onishchenko, A. A. Pivovarov, and O. L. Veretin, Heavy mass expansion, light-by-light scattering and the anomalous magnetic moment of the muon, *Phys. Rev.* **D68** (2003) 033018.

K. Melnikov and A. Vainshtein, Hadronic light-by-light scattering contribution to the muon anomalous magnetic moment revisited, *Phys. Rev.* **D70** (2004) 113006.

M. Hayakawa, T. Kinoshita, and A. I. Sanda, Hadronic light by light scattering effect on muon $g-2$, *Phys. Rev. Lett.* **75** (1995) 790.

M. Hayakawa and T. Kinoshita, Pseudoscalar pole terms in the hadronic light-by-light scattering contribution to muon $g-2$, *Phys. Rev.* **D57** (1998) 465.

J. Bijnens, E. Pallante, and J. Prades, Hadronic light by light contributions to the muon $g-2$ in the large N_c limit, *Phys. Rev. Lett.* **75** (1995) 1447.

J. Bijnens, E. Pallante, and J. Prades, Analysis of the hadronic light-by-light contributions to the muon $g-2$, *Nucl. Phys.* **B474** (1996) 379.

J. Bijnens, E. Pallante, and J. Prades, Comment on the pion pole part of the light-by-light contribution to the muon $g-2$, *Nucl. Phys.* **B626** (2002) 410.

J. Bijnens and J. Prades, The hadronic light-by-light contribution to the muon anomalous magnetic moment: Where do we stand?, *Mod. Phys. Lett.* **A22** (2007) 767.

[114] J. P. Leveille, The second order weak correction to $(g-2)_\mu$ of the muon in arbitrary gauge models, *Nucl. Phys.* **B137** (1978) 63.

[115] O. Mena and S. J. Parke, Unified graphical summary of neutrino mixing parameters, *Phys. Rev.* **D69** (2004) 117301.

R. N. Mohapatra *et al.*, Theory of neutrinos: A white paper, (2005).

G. Ahuja, M. Gupta, and M. Randhawa, Constructing the CKM and PMNS matrices from mixing data, (2006).

[116] B. Aubert *et al.*, Search for lepton flavor violation in the decay $\tau^- \to \ell^-\ell^+\ell^-$, *Phys. Rev. Lett.* **92** (2004) 121801.

[117] Y. Yusa *et al.*, Search for neutrinoless decays $\tau \to 3\ell$, *Phys. Lett.* **B589** (2004) 103.

Danksagung

- An erster Stelle gilt mein Dank Andrzej Buras, der mir die Möglichkeit gab, an seinem Lehrstuhl diese Doktorarbeit anfertigen zu können und der mir immer mit Ratschlägen hilfreich zur Seite stand. Insbesondere möchte ich mich für die angenehme Zusammenarbeit und die Unterstützung bei der Erstellung aller Veröffentlichungen bedanken. Vielen Dank auch für seinen Beistand in physikalischen Fragen, in schweren privaten Momenten und seine offene Art, über viele Dinge reden zu können.

- Weiterhin möchte ich mich bei Monika Blanke für die produktive und erfolgreiche Zusammenarbeit der letzten Jahre bedanken, sowie die kritische Durchsicht dieser Arbeit. Danke für die zahlreichen und hilfreichen Diskussionen über verschiedene physikalische Probleme.

- Als nächstes möchte ich Selma Uhlig meinen Dank aussprechen für die sehr ergiebige Zusammenarbeit mit ihr, viele Diskussionen und immer wieder lustige Weihnachtsfeiern. Sie werden mir immer in Erinnerung bleiben.

- Herzlichen Dank auch an Björn Duling alias Dr. Duling, mit dem ich aufgrund seiner reifen und besonnenen Art zu vielen Einsichten gelangte. Vielen Dank auch für die erhellenden Gespräche über Physik, die sehr gute Zusammenarbeit während unser gemeinsamen Arbeit und die aufmerksame Lektüre dieser Arbeit.

- Ferner möchte ich mich recht herzlich auch bei allen anderen Kollegen William Bardeen, Pham Hung, Stefan Recksiegel, Michael Spranger, Cecilia Tarantino, Andreas Weiler und Elmar Wyszomirski bedanken. Ich bin mir bewusst, daß ohne ihre Mithilfe, Geduld und Einsatzbereitschaft die Vielzahl an wissenschaftlichen Publikationen nicht möglich gewesen wäre. Herzlichen Dank auch für ihre Geduld meine Fragen zu beantworten, ich konnte viel von euch allen lernen.

- Dank auch an allen anderen Mitgliedern des Lehrstuhls T31 Michaela Albrecht, Wolfgang Altmannshofer, Dominik Bauer, Christoph Bobeth, Thorsten Ewerth, Katrin Gemmler, Martin Gorbahn, Diego Guadagnoli, Ulrich Haisch, Sebastian Jäger, Elke Krüger, Christoph Promberger, Sebastian Schatt, David Straub, Andreas Weinberger, Michael Wick für die Hilfsbereitschaft bei aller Art von Fragen und die sehr angenehme Atmosphäre am Lehrstuhl.

- Felix Schwab, Björn Duling und Sebastian Jäger für die freundliche Atmosphäre im gemeinsamen Arbeitszimmer und die Diskussionen über Gott, Physik und das Leben.

- Explizit sei auch meinen Mitstreitern Marc-Thomas Eisele, Marc Rolinec und Felix Schwab gedankt, mit denen ich viele angenehme und vielseitige Diskussionen über alle

erdenklichen Probleme der Physik und des Lebens hatte. Für mich war es eine unvergessliche Zeit, da ich dadurch viel über Menschen und mich selbst lernen durfte.

- Weiterhin auch vielen Dank an Roman Zwicky für einen sehr angenehmen Aufenthalt in Durham.

- Vor allem möchte ich auch meinen Eltern für ihre liebevolle moralische und finanzielle Unterstützung während der Zeit des gesamten Studiums und der Doktorarbeit danken. Ohne ihren Beistand wäre das Studium gar nicht möglich gewesen.

- Weiterhin möchte ich mich bei meiner Freundin Michaela Albrecht bedanken, die mir in der Phase des Aufschreibens der Doktorarbeit immer zur Seite gestanden hat und für die ich viel zu wenig Zeit hatte. Vielen Dank für die schönen gemeinsamen Stunden, ihre Geduld und die endlosen Gespräche.

- Zum Schluß gilt mein Dank auch meinen Freunden, die mir oft gezeigt haben, dass man mit beiden Beinen am Boden und im Leben stehen muss und die ich ebenfalls während der letzten Monate oft vernachlässigt habe.